

**UCSF**

**UC San Francisco Electronic Theses and Dissertations**

**Title**

An analysis of candidate ionotropic receptors mutations that block synaptic homeostasis: PPK11 and PPK16 drive homeostatic synaptic plasticity.

**Permalink**

<https://escholarship.org/uc/item/373592q3>

**Author**

Younger, Meg A.

**Publication Date**

2013

Peer reviewed|Thesis/dissertation

An analysis of candidate ionotropic receptor mutations that block synaptic homeostasis: PPK11 and PPK16 drive homeostatic synaptic plasticity.

by

Meg A. Younger

DISSERTATION

Submitted in partial satisfaction of the requirements for the degree of

DOCTOR OF PHILOSOPHY

in

Neuroscience



in the

GRADUATE DIVISION

of the

UNIVERSITY OF CALIFORNIA, SAN FRANCISCO

Copyright 2013

by

Meg A. Younger

## **Acknowledgements**

I am incredibly grateful for all the support I have received during my time in graduate school. Any success I have had reflects the wonderful people who have helped me along the way. I would especially like to thank Grae Davis for his excellent mentorship throughout the entire span of graduate school. Grae's endless excitement for experimental science and his positive encouragement were instrumental in the completion of my PhD.

I would also like to thank the current and former members of the Davis lab, who created a workplace that was both intellectually stimulating and. I would especially like to thank Martin Müller, Catherine O'Hare, Sharon Bergquist, Ed Pym, Lani Keller and Amy Tong.

I feel fortunate to have attended UCSF, as I have benefitted from interactions with so many people here. I am grateful for the continuous advice of my graduate committee, Robert Edwards, Peter Sargent, Lily Jan, and Diana Bautista, as well as the other faculty and students who have helped me along the way.

I would especially like to thank my friends and my family who have provided me with love and encouragement throughout my time in graduate school. I couldn't have done it without you.



## **Preface**

Chapter 1 contains general background information.

Chapter 2 has been published in *Neuron* (2012) 79, 1183-1196 (Younger et al., 2013). The genetic screen that identified *ppk11* was conducted by Edward Pym (Figure 1a and Table 1). The sequencing of possible *ppk11<sup>Mi</sup>* and *ppk16<sup>Mi</sup>* excision mutants, and the PCR reaction in Figure 6D was done together with Amy Tong. The calcium imaging was done by Martin Müller (Figure 8a-c). All other experiments in this chapter were done by Meg Younger.

In Chapter 3 all experiments were done by Meg Younger.

In Chapter 4 the genetic screen that identified *Puny* was done by Edward Pym. The sequencing of possible *IR75c<sup>Mi</sup>* excision mutants to generate *IR75c<sup>114</sup>* was done together with Amy Tong. All other experiments were done by Meg Younger. Chapter 5 is general discussion and conclusions.

**An analysis of candidate ionotropic receptors mutations that block synaptic homeostasis: PPK11 and PPK16 drive homeostatic synaptic plasticity.**

**by  
Meg A Younger**

Robert Edwards  
Chair, Thesis Committee

## ABSTRACT

Homeostatic plasticity restricts changes in neural activity to allow for a stable yet plastic nervous system. At the synapse, homeostatic regulation maintains synaptic efficacy when there is a disruption of postsynaptic neurotransmitter sensitivity or excitability (Turrigiano, 2012; Davis, 2006). At the *Drosophila* neuromuscular junction (NMJ), when glutamate receptor sensitivity is decreased, either genetically or pharmacologically, the motoneuron potentiates neurotransmitter release to precisely offset changes in receptor sensitivity. This restores muscle excitation within minutes. The molecular mechanisms that underlie this form of synaptic homeostasis are beginning to be discovered, in large part due to an ongoing forward genetic screen for mutations that block synaptic homeostasis (Dickman and Davis, 2009; Müller et al., 2011). This thesis work focuses on the examination of two candidate mutations identified by this genetic screen. These were chosen for study because they completely blocked synaptic homeostasis and were likely to disrupt genes encoding ion channel subunits.

In chapter 2 we provide evidence that two Degenerin/Epithelial Sodium Channel (DEG/ENaC) subunits, *pickpocket11* (*ppk11*) and *pickpocket16* (*ppk16*), are necessary for synaptic homeostasis. These genes are required for both the rapid induction and sustained expression of synaptic homeostasis. Mutations in *ppk11* and *ppk16* do not disrupt baseline synaptic transmission or NMJ development. *ppk11* and *ppk16* reside in a single locus and are coregulated as

an operon-like genetic unit, with increased transcription accompanying prolonged expression of synaptic homeostasis. We use pharmacology to show that DEG/ENaC channel conductance is continuously required for the potentiation of release during homeostasis. Lastly we show that DEG/ENaC channel function is necessary to enhance action-potential evoked presynaptic calcium influx specifically during synaptic homeostasis, but not baseline release. Taken together this identifies PPK11 and PPK16 as components of the molecular pathway that potentiates release during synaptic homeostasis and we present a model for how PPK11 and PPK16 enhance calcium influx during synaptic homeostasis.

In chapter 3 we examine a third gene encoding a DEG/ENaC channel subunit, *pickpocket 18* (*ppk18*), which is in the same genetic locus as *ppk11* and *ppk16*. We found that despite the proximity to *ppk11* and *ppk16*, *ppk18* is transcribed independently from the other two genes, and the quantity of *ppk18* transcript is unchanged during the sustained expression of synaptic homeostasis. Furthermore, mutations in *ppk18* do not block the rapid induction of synaptic homeostasis, indicating that it does not act in concert with *ppk11* and *ppk16* to potentiate release during synaptic homeostasis.

In chapter 4 we examine a separate mutation that was identified in the same forward genetic screen for mutations that block synaptic homeostasis. This mutation resides in a complicated locus containing four genes: *Ionotropic Receptor 75a* (*IR75a*), *Ionotropic Receptor 75b* (*IR75b*), *Ionotropic Receptor 75c*

(*IR75c*), and *GABA and glycine-like receptor of Drosophila (GRD)*. We use a combination of electrophysiology, quantitative PCR, immunostaining and genetics to examine the requirement of different genes in this locus for the homeostatic potentiation of release. We show that multiple mutations within this genomic region block synaptic homeostasis, and that the distribution of postsynaptic glutamate receptors is altered by a mutation within this locus, which may be an underlying cause. We are unable to identify the responsible gene, although our data points to *GRD* as the most promising candidate. This work provides a basis for future investigation into this locus.

## TABLE OF CONTENTS

<b>ACKNOWLEDGEMENTS</b> .....	<b>iii</b>
<b>PREFACE</b> .....	<b>iv</b>
<b>ABSTRACT</b> .....	<b>vi</b>
<b>TABLE OF CONTENTS</b> .....	<b>ix</b>
<b>LIST OF FIGURES AND TABLES</b> .....	<b>x</b>
<b>Chapter 1: General Introduction</b> .....	<b>1</b>
Homeostatic Plasticity in the Nervous System.....	2
Mechanisms of presynaptic homeostasis at the <i>Drosophila</i> NMJ. ....	5
An ongoing forward genetic screen to identify mutations that block synaptic homeostasis .....	9
<b>Chapter 2: Pickpocket11 and Pickpocket16 drive synaptic homeostasis. .</b>	<b>11</b>
SUMMARY .....	12
INTRODUCTION.....	13
RESULTS .....	15
DISCUSSION.....	35
FIGURES AND TABLES.....	40
<b>Chapter 3: Pickpocket18 does not contribute to NMJ growth or function..</b>	<b>71</b>
SUMMARY .....	72
INTRODUCTION.....	73
RESULTS .....	75
DISCUSSION.....	79
FIGURES AND TABLES .....	83
<b>Chapter 4: The <i>IR75/GRD</i> locus is required for synaptic homeostasis.....</b>	<b>90</b>
SUMMARY .....	91
INTRODUCTION.....	92
RESULTS .....	95
DISCUSSION.....	105
FIGURES AND TABLES.....	110
<b>Chapter 5: General Discussion</b> .....	<b>127</b>
Gene Identification: From Screen to Function. ....	128
ENaCs as homeostatic effector proteins .....	129
<b>EXPERIMENTAL PROCEDURES</b> .....	<b>137</b>

## LIST OF FIGURES AND TABLES

Figure 2-1: <i>ppk11</i> is necessary for the homeostatic modulation of presynaptic neurotransmitter release. ....	40
Figure 2-2: Analysis of baseline neurotransmission in <i>ppk11</i> mutants.....	43
Figure 2-3: <i>ppk11</i> is required in motoneurons for synaptic homeostasis..	45
Figure 2-4: <i>ppk16</i> is necessary in motoneurons for the homeostatic modulation of presynaptic release. ....	47
Figure 2-5: Normal NMJ morphology in <i>ppk11</i> and <i>ppk16</i> mutants. ....	50
Figure 2-6: Pickpocket function and regulation during the long-term expression of synaptic homeostasis.....	52
Figure 2-7: Pharmacological inhibition of PPK channels erases the expression of homeostatic plasticity.....	55
Figure 2-8: A Model for PPK11/16 function during synaptic homeostasis.	58
Figure 2-9: Analysis of baseline neurotransmission of two <i>ppk11</i> mutations <i>in trans</i> . ....	60
Figure 2-10: The organization of the <i>ppk11/16</i> locus is conserved across multiple <i>Drosophila</i> species. ....	62
Figure 2-11: Benzamil has separable effects on mEPSP amplitude and synaptic transmission. ....	64
Figure 2-12: EIPA blocks synaptic homeostasis. ....	66
Table 2-1. Specific mutations screened .....	68
Table 2-2. Non-normalized values for electrophysiology measurements. .	69
Figure 3-1: Conservation of the <i>ppk11/16/18</i> gene locus across multiple <i>Drosophila</i> species.....	83
Figure 3-2: <i>ppk18</i> mutations do not disrupt synaptic homeostasis. ....	85
Figure 3-3: <i>PPK18<sup>Mi</sup></i> does not alter synapse gross morphology.....	87
Table 3-1: Non-normalized values for electrophysiology measurements. .	89
Figure 4-1: Mutations in <i>GRD</i> disrupt synaptic homeostasis.....	110
Figure 4-2: <i>Puny</i> mutations disrupt synaptic homeostasis in a background dependent manner.....	112

**Figure 4-3: Puny mutations do not alter NMJ size or active zone density. 115**

**Figure 4-4: *Puny* mutations have altered glutamate receptor distribution. .... 117**

**Figure 4-5: Mutations in *IR75c* block synaptic homeostasis..... 119**

**Figure 4-6: *IR75c*<sup>114</sup> mutations do not alter synapse morphology..... 121**

**Figure 4-7: *IR75a* mutations do not block synaptic homeostasis..... 123**

**Table 4-1: Non-normalized values for electrophysiology measurements. 125**



## **Chapter 1:**

### **General Introduction**

## Homeostatic Plasticity in the Nervous System

Organisms exist in a world that is constantly changing and, yet, are somehow able to maintain stability within their internal environment. Homeostatic systems exist throughout the body to stabilize varied physiological processes at levels of organization ranging from cellular to organism-wide. Diverse biological factors are under homeostatic control including blood pressure, systemic salt balance, body temperature and circulating blood sugar, among others where instability would cause pathological consequences. While the factor under regulation differs in every system, homeostatic systems theoretically share certain components: sensors, error signals, feedback, effectors, and an optimal set point (Schneck, 1987; Davis, 2006).

The nervous system is incredibly dynamic, responding to ever-changing input and altering neuronal connections accordingly, to ultimately modify behavior. Homeostatic signaling systems are believed to interface with the mechanisms of learning-related plasticity to achieve stable, yet flexible, neural function and animal behavior. Experimental evidence from organisms as diverse as *Drosophila*, lobster, mouse and humans, demonstrates that homeostatic signaling systems stabilize neural function through the modulation of synaptic transmission, ion channel abundance and neurotransmitter receptor trafficking (Petersen et al., 1997; Davis, 2006; Marder and Goaillard, 2006; Turrigiano, 2008; Thiagarajan et al., 2007; Kim and Ryan, 2010; Gonzalez-Islas et al., 2010).

In each experiment, the cells respond to an experimental perturbation by modulating ion channel abundance or synaptic transmission to counteract the perturbation and re-establish baseline function. The cellular mechanisms that stabilize neural function can be grouped into three categories: 1) homeostasis of intrinsic excitability, 2) synaptic scaling, and 3) presynaptic homeostasis.

Homeostasis of intrinsic excitability reestablishes the firing properties of a neuron by adjusting ion channel conductances and synaptic weights (Marder and Goaillard, 2006). This form of homeostatic plasticity is likely engaged when the firing rate of a neuron is vital to its role within a network. The most striking evidence for this form of regulation is the finding that when certain neurons are removed from a network, they will reconstruct their intrinsic firing properties in isolation. This has been demonstrated in crustacean stomatogastric ganglion cells and in mouse cerebellar Purkinje cells, among others (Turrigiano et al., 1994; Khorkova and Golowasch, 2007; Swensen and Bean, 2005). The homeostatic regulation of intrinsic excitability is also seen in neurons with ion channel mutations (Swensen and Bean, 2005; Nerbonne et al., 2008). Somehow these cells are able to alter ion channel conductances to establish the firing properties typical of their cell type despite the absence of an ion channel gene.

Synaptic scaling employs a change in postsynaptic receptor abundance to counteract a decrease or increase in neuronal activity (Turrigiano, 2008; Marder and Goaillard, 2006). Synaptic scaling was first discovered in mammalian neurons. It was termed synaptic scaling because, in response to a decrease or

an increase in activity, receptors are added or removed, respectively, at every postsynaptic site within a neuron. The change in receptor abundance is proportional to the basal synaptic strength resulting in synaptic responses that are "scaled" up or down across the entire cell in a multiplicative manner (Turrigiano et al., 1998; O'Brien et al., 1998; Turrigiano, 2012). This form of homeostatic plasticity likely retains the information contained in the relative weight of different synaptic connections, while restoring the overall activity of the neuron. Synaptic scaling has been seen in many organisms, from zebrafish to mammals and recent evidence has highlighted a role for synaptic scaling in the mouse visual system *in vivo* (Deeg and Aizenman, 2011; Keck et al., 2013).

Presynaptic homeostasis utilizes a change in neurotransmitter release to counteract changes in the activity of a postsynaptic neuron or muscle. Presynaptic homeostasis has been observed at mammalian central synapses in culture and in slices (Piedras-Renteria et al., 2004; Kim and Ryan, 2010; Zhao et al., 2011; Branco et al., 2008), however, the majority of work on this process has been conducted at the neuromuscular junction (NMJ). At the NMJ, when postsynaptic receptor sensitivity is decreased, there is an increase in presynaptic release to precisely offset the change in postsynaptic receptor sensitivity, thereby restoring muscle excitability. A similar phenomenon is seen at the human NMJ in patients with myasthenia gravis, a disorder in which the immune system targets postsynaptic acetylcholine receptors, decreasing their function. There is an increase in acetylcholine release from the motoneuron to compensate for the

decreased receptor sensitivity (Cull-candy et al, 1980). Presynaptic homeostasis has been seen at the rat NMJ as well, where there is an increase in release after postsynaptic acetylcholine receptor blockade with the antagonist alpha-bungarotoxin (Plomp et al., 1992; Plomp et al., 1994). The molecular mechanisms that underlie presynaptic homeostasis have been studied most thoroughly at the *Drosophila* NMJ. Since presynaptic homeostasis will be the topic for the remainder of this thesis, it will simply be referred to as "synaptic" homeostasis.

### **Mechanisms of presynaptic homeostasis at the *Drosophila* NMJ.**

The *Drosophila* NMJ can be viewed as a powerful "model" synapse, as it has been widely used to identify genes that underlie synaptic transmission and synapse development, many of which are highly conserved in other organisms (Keshishian, et al., 1996). The *Drosophila* NMJ is a glutamatergic synapse (Jan and Jan, 1976), with an ultrastructure that is similar to mammalian central synapses (Menon et al., 2013). The postsynaptic receptors are the ionotropic glutamate receptors, GluRIIA, B, C, D, and E, which are AMPA/kainate-type receptors (DiAntonio et al., 1999; Petersen et al., 1997; Marrus et al., 2004; Featherstone et al., 2005; Qin et al., 2005). One of the greatest technical advantages of the *Drosophila* NMJ is that it is an isopotential synapse and can therefore be used to accurately measure quantal size, including measurements from every postsynaptic site without spatial filtering of quantal amplitude (Jan and

Jan, 1976). This makes it possible to accurately determine quantal content, which is ideal when studying homeostatic changes in presynaptic release.

The homeostatic potentiation of release at the *Drosophila* NMJ is seen in animals containing a mutation in the postsynaptic glutamate receptor subunit *GluRIIA*. These mutants are less sensitive to glutamate (Petersen et al., 1997; DiAntonio et al., 1999). Despite a profound decrease in quantal size, there is little change in the amplitude of the evoked response, due to an increase in presynaptic release. Synaptic homeostasis is bidirectional at the NMJ; overexpression of the vesicular glutamate transporter (VGLUT) increases quantal size, inducing a homeostatic reduction in quantal content that leaves the amplitude of the evoked response similar to the wild type (Daniels et al., 2004).

*Drosophila* glutamate receptors can be rapidly inhibited with the antagonist Philanthotoxin-433 (PhTx), which inhibits *GluRIIA* containing glutamate receptors, causing a reduction in quantal size (Frank et al., 2006). Amazingly, within 10 minutes the presynaptic terminal increases release to precisely offset the change in receptor sensitivity. The rapid increase in release is both transcription and translation independent (Frank et al, 2006).

Genetic data combined with experiments probing synapse function during synaptic homeostasis suggests a model. In response to inhibition of postsynaptic glutamate receptor function, a retrograde signal acts upon the presynaptic nerve terminal to enhance the number of synaptic vesicles released per action potential to precisely offset the severity of glutamate receptor inhibition. Two components

of the presynaptic release mechanism are necessary for the execution of synaptic homeostasis, increased calcium influx through presynaptic calcium channels (Müller and Davis, 2012) and an increase in the readily releasable pool of synaptic vesicles (Müller et al., 2012; Weyhersmüller et al, 2011). Mutations in the voltage-gated calcium channel orthologue *cacophony* (*cac*; Frank et al, 2006) block synaptic homeostasis by preventing the modulation of presynaptic calcium influx during synaptic homeostasis (Müller and Davis, 2012). Mutations in the gene encoding the *Rab3 interacting molecule* (*RIM*) do not prevent the modulation of presynaptic calcium influx during synaptic homeostasis, but rather, *RIM* mutations prevent a modulation of the readily releasable pool of synaptic vesicles, thereby blocking synaptic homeostasis (Müller et al., 2012).

Mutations in other synaptic vesicle associated proteins block synaptic homeostasis, including the schizophrenia susceptibility gene *dysbindin* (*dys*; Dickman and Davis, 2009) and its binding partner, *snapin* (Dickman et al., 2012). These might act to modulate the readily releasable pool in a pathway with RIM. However, there is no direct evidence to support a specific role in the homeostat for either *dys* or *snapin*. The presynaptic small GTPase Rab3 represses synaptic homeostasis, preventing aberrant excitation, and this repression is relieved by the Rab3 GTPase-activating protein (Rab3-GAP; Müller et al., 2011). This provides a level of regulation constructed around the core molecules that drive synaptic homeostasis.

There are a number of genes that are necessary for the establishment of a homeostasis-competent synapse, but do not actively participate in synaptic homeostasis. These genes are necessary during development and can be considered permissive cues for homeostatic potentiation. These include the Bone Morphogenic Protein ligand *glass bottom boat (gbb)* and its receptor *wishful thinking (wit)* (Goold and Davis, 2007). Lastly, a subset of genes are specifically required for the sustained expression of synaptic homeostasis seen in the *GluRIIA* mutant background, but not the rapid induction of synaptic homeostasis caused by PhTx application. These include *Ephexin* and the *Eph receptor* (Frank et al., 2009), *Gooseberry* (Marie et al., 2010), the *miR-10* cluster (Tsurudome et al., 2010) and the *TOR/S6 Kinase* pathway (Penney et al., 2012). The specific requirement of genes in the long-term expression of synaptic homeostasis, but not the short-term, indicates that this process is not identical throughout its progression. In particular, transcription and translation are likely engaged over time.

Many questions remain unanswered regarding how these, and as-yet-unknown genes, fit together and how they interface with the synaptic transmission apparatus to create a synapse capable of undergoing synaptic homeostasis. It is unknown how activity is sensed postsynaptically. Evoked transmission is not required, indicating that spontaneous release might be the relevant signal. The identity of the retrograde signal is also unknown, as is its presynaptic receptor. It is unclear how a change in presynaptic calcium influx is



induced and sustained during synaptic homeostasis. Additionally, it is not known if the homeostatic potentiation of release is achieved through the same mechanisms as the homeostatic reduction of release.

### **An ongoing forward genetic screen to identify mutations that block synaptic homeostasis**

The identification of genes involved in synaptic homeostasis has been particularly challenging. The rapid induction of synaptic homeostasis is transcription independent, making transcription-based strategies, such as microarray analysis, unlikely to yield a comprehensive set of genes required for synaptic homeostasis. Studying candidate genes with known synaptic function led to the identification of *cac*, however, this approach will not isolate any genes that have not been previously implicated in synaptic transmission. In order to identify new molecules that are components of the homeostatic signaling machinery at the *Drosophila* NMJ, an electrophysiology-based forward genetic screen was conducted (Dickman and Davis, 2009; Müller et al., 2011). The rationale for this screen is that mutations in genes that function as components of the homeostat should block the rapid induction of synaptic homeostasis.

Screening genes expressed in neurons and muscle would enable the identification of novel homeostasis genes. It is possible that some mutations that block synaptic homeostasis could do so indirectly, however, some fraction of the identified mutations should participate as the core machinery that drives synaptic

homeostasis. To this end, approximately 1000 mutations have been screened by electrophysiology, successfully identifying many genes that are necessary for synaptic homeostasis, including *Dys* (Dickman and Davis, 2009), *Rab3-GAP* (Müller et al., 2011), and the voltage-activated potassium channel subunit *Shal* (Bergquist et al., 2010).

This screen identified two mutations that will be the subject of this thesis. Both mutations completely blocked the rapid induction of synaptic homeostasis and were predicted to disrupt the expression of ligand-gated ion channel subunits. The first sits in the gene *pickpocket 11(ppk11)*. The second resides in a locus containing four genes: *Ionotropic Receptor 75a (IR75a)*, *Ionotropic Receptor 75b (IR75b)*, *Ionotropic Receptor 75c (IR75c)* and *GABA and glycine-like receptor of Drosophila (GRD)*. At the onset of this thesis work the only genes identified that blocked synaptic homeostasis were *cac* (Frank et al., 2006) and the homeostasis-permissive BMP signaling pathway (Goold and Davis., 2007). Ligand gated ion channels were chosen for study because they were attractive candidates as receptors for the retrograde signal or as components of the sensor of muscle activity. We were surprised to find a novel presynaptic role for *ppk11* in synaptic homeostasis, highlighting the power of forward genetic screening (see chapter 2).

## **Chapter 2:**

**Pickpocket11 and Pickpocket16 drive synaptic homeostasis.**

## SUMMARY

An electrophysiology-based forward genetic screen led to the identification of two genes, *pickpocket11* (*ppk11*) and *pickpocket16* (*ppk16*), as being necessary for the homeostatic modulation of presynaptic neurotransmitter release at the *Drosophila* neuromuscular junction (NMJ). Pickpocket genes encode Degenerin/Epithelial Sodium channel subunits (DEG/ENaC). We demonstrate that *ppk11* and *ppk16* are necessary in presynaptic motoneurons for both the acute induction and long-term maintenance of synaptic homeostasis. We show that *ppk11* and *ppk16* are co-transcribed as a single mRNA that is upregulated during homeostatic plasticity. Acute pharmacological inhibition of a PPK11 and PPK16 containing channel abolishes the expression of short and long-term homeostatic plasticity without altering baseline presynaptic neurotransmitter release, indicating remarkable specificity for homeostatic plasticity rather than NMJ development. Finally, presynaptic calcium imaging experiments support a model in which a PPK11 and PPK16 containing DEG/ENaC channel modulates presynaptic membrane voltage and, thereby, controls calcium channel activity to homeostatically regulate neurotransmitter release.

## INTRODUCTION

An electrophysiology based forward genetic screen led to the identification of two genes, *pickpocket16* (*ppk16*) and *pickpocket11* (*ppk11*) that, when mutated, block homeostatic plasticity. *Drosophila* pickpocket genes encode Degenerin/ Epithelial Sodium channel (DEG/ENaC) subunits (Adams et al., 1998; Liu et al., 2003a; Bianchi and Driscoll, 2002). Channels in this superfamily are voltage insensitive and are assembled as either homomeric or heteromeric trimers (Bianchi and Driscoll, 2002; Benson et al., 2002; Jasti et al., 2007). Each channel subunit has two transmembrane domains with short cytoplasmic N and C-termini, and a large extracellular loop implicated in responding to diverse extracellular stimuli.

Little is known regarding the function of pH insensitive DEG/ENaC channels in the nervous system. DEG/ENaC channels have been implicated as part of the mechanotransduction machinery (Chalfie, 2009), and in taste perception in both invertebrate and vertebrate systems (Liu et al, 2003b; Chandrashenkar, 2010). In *Drosophila*, PPK11 has been shown to function as an ENaC channel subunit that is required for the perception of salt-taste (Liu et al, 2003b) and fluid clearance in the tracheal system, a function that may be considered analogous to ENaC channel activity in the mammalian lung (Liu et al., 2003a).

We demonstrate that *ppk11* and *ppk16*, are co-regulated during homeostatic synaptic plasticity and that homeostatic plasticity is blocked when

either gene is genetically deleted, when gene expression is disrupted in motoneurons, or when pickpocket channel function is pharmacologically inhibited. We then take advantage of the fact that presynaptic homeostasis can be blocked pharmacologically to demonstrate that the persistent induction of homeostatic plasticity does not interfere with synapse growth and development. We show that homeostatic plasticity can be acutely and rapidly erased, leaving behind otherwise normal synaptic transmission. Finally, we demonstrate that pharmacological inhibition of this pickpocket channel abolishes the homeostatic modulation of presynaptic calcium influx that was previously shown to be necessary for the homeostatic increase in neurotransmitter release (Müller and Davis, 2012).

A model for DEG/ENaC channel function can be based on the well-established regulation of ENaC channel trafficking in the kidney during the homeostatic control of salt balance. Enhanced sodium reabsorption in the principle cells of the cortical collecting duct of the kidney is achieved by increased ENaC channel transcription and trafficking to the apical cell surface, which enhances sodium influx. Sodium is then pumped out of the basolateral side of the cell, accomplishing sodium reabsorption (Schild, 2010). By analogy, we propose a model for synaptic homeostasis in which the trafficking of DEG/ENaC channels to the neuronal membrane, at or near the NMJ, modulates presynaptic membrane potential to potentiate presynaptic calcium channel activity and thereby achieve precise homeostatic modulation of neurotransmitter release.

## RESULTS

We are pursuing an ongoing electrophysiology-based forward genetic screen for mutations that block the rapid induction of synaptic homeostasis. In brief, we record from the NMJ of annotated transposon-insertion mutations in the presence of the glutamate receptor antagonist philanthotoxin-433 (PhTx; 10 $\mu$ M) according to published methods (Dickman and Davis, 2009; Müller et al., 2011). For each NMJ, we quantify mEPSP amplitude, EPSP amplitude, quantal content (calculated by dividing the EPSP amplitude /mEPSP amplitude), mEPSP frequency, muscle input resistance and muscle resting membrane potential. In wild type, the application of PhTx induces a homeostatic increase in presynaptic release that restores EPSP amplitudes to wild-type levels (0.5mM Ca<sup>2+</sup>). We are then able to identify mutations that have a reduced EPSP amplitude in the presence of PhTx, and therefore appear to disrupt homeostatic plasticity. To further validate our screen, a subset of mutations was analyzed in the presence and absence of PhTx, regardless of whether or not they appeared to block synaptic homeostasis. In Figure 1A we present previously unpublished data for a sample of 22 transposon insertion lines in which synaptic transmission was assayed both in the absence and in the presence of PhTx (mutation annotations are listed in Table 1; sample sizes are 3-14 muscles for each genotype in each condition). For each genotype, we present the percent change in mEPSP amplitude as an indication of the severity of glutamate receptor inhibition (black

bars), as well as the percent change in quantal content (grey bars), which indicates the magnitude of the homeostatic increase in presynaptic release. In all cases mEPSP amplitude is reduced and most mutants are capable of robust homeostatic plasticity (Dickman and Davis, 2009; Müller et al., 2011). Notably, the transposon insertion lines that we screened showed a wide range of baseline evoked responses in the absence of PhTx (Figure 1B) with EPSP amplitudes ranging between  $18.0 \pm 2.5$  mV (*CcapR*, n=6) and  $43.0 \pm 2.3$  mV (nAChR $\alpha$ -18C, n=4). Despite the considerable span in baseline release, most transposon insertion lines were capable of synaptic homeostasis, as indicated by a PhTx-dependent increase in quantal content (Figure 1A). However, a few lines showed virtually no PhTx-dependent change in quantal content, indicating impaired homeostatic compensation. The mutation in *rab3-GAP* has been previously published and is a confirmed homeostatic plasticity gene (Figure 1A, green bars; Müller et al., 2011). Another line that showed a decrease in mEPSP amplitude, but no increase in presynaptic release, resides within the *ppk11* gene locus (Figure 1A, blue bars). *ppk11* was, therefore, selected as a candidate homeostatic plasticity gene.

In order to pursue a formal genetic analysis of *ppk11*, we acquired additional genetic and transgenic reagents (Figure 1C). These reagents include: 1) an independently derived Minos transposable element insertion (*ppk11*<sup>Mi</sup>) that resides within a coding exon of the *ppk11* gene and is predicted to be a strong loss-of-function or null mutation, 2) a previously published *UAS-ppk11-RNAi*



transgenic line (Liu et al., 2003b), 3) a previously published dominant-negative transgene (*UAS-dnPPK11*; Liu et al., 2003b) targeting the PPK11 trimerization domain that disrupts channel assembly and 4) a deficiency chromosome that uncovers the entire *ppk11* gene locus.

The *ppk11* gene terminates in close proximity (63 bp upstream) to the predicted start of a previously uncharacterized member of the DEG/ENaC channel family, *pickpocket16* (*ppk16*) (Figure 1C, red). The close proximity of these two genes suggested that they might both contribute to the same DEG/ENaC channel. Therefore, we assembled genetic reagents to test the hypothesis that PPK16 might function with PPK11 during synaptic homeostasis. These reagents include: 1) a Minos transposon insertion that resides within the *ppk16* gene (*ppk16<sup>Mi</sup>*), 2) a newly generated small deficiency (*ppk16<sup>166</sup>*) that removes two coding exons of the *ppk16* gene and is predicted to be a strong loss-of-function or null mutation and 3) a *UAS-ppk16-RNAi* transgenic line. Together, these reagents allow us to test the involvement of both *ppk11* and *ppk16* during synaptic homeostasis.

### **Loss of *ppk11* Blocks the Rapid Induction of Synaptic Homeostasis**

To examine the rapid induction of synaptic homeostasis, PhTx (10-20 $\mu$ M) is applied to the dissected NMJ for 10 minutes (see methods) and recordings are made from muscle 6 in abdominal segments A2 and A3. For purposes of display, data for a given mutant background are presented as normalized to the same

genotype recorded in the absence of PhTx, as done previously (Frank et al., 2006; Frank et al., 2009; Bergquist et al., 2010). All of our data are also presented as non-normalized values (Table 2). In wild type, application of PhTx causes a significant decrease in mEPSP amplitude compared to baseline and we observe a homeostatic increase in presynaptic neurotransmitter release (Figure 1E). However, in mutations that disrupt the *ppk11* gene, we find that synaptic homeostasis is completely and consistently blocked. Specifically, in every mutation that we have analyzed, including the homozygous *ppk11<sup>Mi</sup>* mutation, the homozygous *ppk11<sup>PBac</sup>* mutation, and *ppk11<sup>PBac</sup>/Df*, there is no statistically significant increase in presynaptic neurotransmitter release following PhTx-dependent inhibition of mEPSP amplitudes. We also generated a precise excision of the *ppk11<sup>Mi</sup>* transposon that restores the *ppk11* gene locus, assessed by sequence analysis. After the addition of PhTx to the precise excision background (*ppk11<sup>Precise</sup>*), the EPSP amplitude is returned to the size it was in the absence of PhTx (*ppk11<sup>Precise</sup>*, Figure 1D), and the homeostatic enhancement of presynaptic neurotransmitter release is restored to wild-type levels (Figure 1E). Taken together, these data support the conclusion that disruption of the *ppk11* gene blocks the rapid induction of synaptic homeostasis.

Despite observing a complete block of synaptic homeostasis, there is no consistent alteration in baseline synaptic transmission caused by the loss of *ppk11*. First, we compare wild type (Figure 2B, black bars) with the *ppk11<sup>Pbac</sup>* mutation (Figure 2B, dark blue bars) and find no significant change in presynaptic

release and only a minor change in mEPSP amplitude. Second, we compare the *ppk11<sup>Mi</sup>* mutation (Figure 2B, light blue bars) with its appropriate genetic control, the precise excision of the *ppk11<sup>Mi</sup>* transposon (*ppk11<sup>Precise</sup>*; Figure 2B, open bars). There is no change in baseline release when this comparison is made. We note that there is a significant ( $p < 0.01$ ) difference in baseline release when we compare wild type with either *ppk11<sup>Mi</sup>* or the *ppk11<sup>Precise</sup>* control line, and we attribute this to differences in genetic background. Third, we analyzed a trans-heterozygous combination of independently derived *ppk11* mutations (*ppk11<sup>Mi</sup>/ppk11<sup>Pbac</sup>*) and find no change in quantal content compared to wild type (Figure 9). In this trans-heterozygous combination there is a decrease in mEPSP amplitude that correlates with a decrease in postsynaptic muscle input resistance (WT = 8.1M $\Omega$  compared to *ppk11<sup>Mi</sup>/ppk11<sup>Pbac</sup>* = 3.9M $\Omega$ ;  $p < 0.01$ ). From these data we conclude that disruption of *ppk11* blocks synaptic homeostasis without altering baseline release, specifically when mutations are compared to their appropriate genetic control. This conclusion is supported by several additional experiments, presented below.

We next examined synaptic homeostasis and baseline transmission at elevated external calcium (1mM) that is within the range of what is thought to be physiological calcium (Figure 2C-E). We first quantified mEPSP amplitudes in current clamp mode, where the signal-to-noise ratio is excellent, and then switched into two-electrode voltage clamp mode to measure evoked synaptic currents. We observe a decrease in mEPSP amplitude when PhTx is applied to

the wild-type NMJ at 1mM calcium and we find that EPSC amplitudes are unchanged in the presence of PhTx, as expected for precise homeostatic compensation. However, in the *ppk11<sup>Mi</sup>* mutant, a similar decrease in mEPSP amplitude is achieved following PhTx application, but the average EPSC amplitude remains significantly smaller than the average baseline EPSC recorded in the absence of PhTx. Thus, homeostatic compensation is disrupted in the *ppk11<sup>Mi</sup>* mutant at physiological calcium without a parallel deficit in baseline transmission. Taken together with our results from Figure 1, these data show that synaptic homeostasis is blocked at two different extracellular calcium concentrations (0.3mM and 1mM). Finally, it is also worth noting that we observed a significant decrease in muscle input resistance in the *ppk11<sup>PBac</sup>*, the *ppk11<sup>Mi</sup>* mutant and the *ppk11<sup>Precise</sup>* control compared to wild type, indicating an effect in the muscle cell, although the persistence of this effect in the *ppk11<sup>Precise</sup>* control suggests that it is also not linked to this genetic locus and can not account for a change in homeostatic plasticity (Supplemental Table 2).

### ***ppk11* is Necessary in Motoneurons for the Rapid Induction of Synaptic Homeostasis**

To confirm that *ppk11* is necessary for the rapid induction of synaptic homeostasis, and to determine whether PPK11 functions in motoneurons or muscle (or both), we took advantage of both a previously published *UAS-ppk11-RNAi* line and a previously published dominant negative transgene that targets

PPK11 (Liu et al., 2003b). First, we demonstrate that expression of *UAS-ppk11-RNAi* selectively in motoneurons (*OK371-GAL4*) completely blocks the homeostatic increase in presynaptic release following PhTx-dependent inhibition of postsynaptic glutamate receptors (Figure 3A,B). By contrast, expression of *UAS-ppk11-RNAi* in muscle (*MHC-GAL4*) does not (Figure 3B). These data indicate that *ppk11* is required in motoneurons for synaptic homeostasis.

Because *ppk11* is expressed in *Drosophila* trachea, where it has been implicated in fluid clearance, we visually confirmed that *OK371-GAL4* does not express in trachea by driving *UAS-CD8-GFP* (data not shown). Next, we attained independent confirmation that PPK11 functions in motoneurons during homeostatic plasticity by expressing the *UAS-dnPPK11* transgene in motoneurons with *OK37-GAL4*. Again, we observe a complete block of homeostatic compensation (Figure 3B). Notably, the motoneuron-specific expression of *UAS-ppk11-RNAi* blocks synaptic homeostasis without altering any aspect of synaptic transmission in the absence of PhTx (Figure 3C). When the *UAS-dnPPK11* transgene is expressed in motoneurons there is a small decrease in mEPSP amplitude and a small increase in quantal content, neither of which are of a magnitude that is expected to interfere with homeostatic plasticity.

Based on these data we conclude that *ppk11* is necessary in motoneurons for synaptic homeostasis, and that the blockade of synaptic homeostasis is independent of any effect of PPK11 on baseline synaptic transmission.

***ppk16* is necessary for the rapid induction of synaptic homeostasis.**

To determine if *ppk16* is required for synaptic homeostasis, we examined a Minos transposon insertion that resides within an intron of the *ppk16* gene (*ppk16<sup>Mi</sup>*; Figure 1C). After the addition of PhTx, we observed a complete block in synaptic homeostasis (Figure 4A,B). To confirm this finding, we utilized imprecise excision of the *ppk16<sup>Mi</sup>* element to generate a deletion mutation that removes 767 base pairs of the *ppk16* gene, encompassing a large portion of the predicted extracellular domain (Figure 1C). This deletion mutation, termed *ppk16<sup>166</sup>*, is expected to be a strong loss-of-function or null allele. We find that the *ppk16<sup>166</sup>* mutation also blocks synaptic homeostasis (Figure 4B). Finally, significant synaptic homeostasis is restored in animals with a precise excision of the *ppk16<sup>Mi</sup>* transposon (158% increase in release;  $p < 0.05$  compared to the same genotype in the absence of PhTx), indicating that the block in synaptic homeostasis is derived from this genetic locus.

To confirm that *ppk16* is necessary for synaptic homeostasis, and to determine whether it is required in motoneurons along with *ppk11*, we expressed *UAS-ppk16-RNAi* in either motoneurons or muscle. When expressed in motoneurons, *UAS-ppk16-RNAi* completely blocks synaptic homeostasis (Figure 4D,E). However, muscle specific expression does not (Figure 4E). Furthermore, expression of *UAS-ppk16-RNAi* blocks synaptic homeostasis without altering baseline EPSP amplitude or presynaptic vesicle release (quantal content; Figure 4F). Although there is a small but statistically significant change in mEPSP

amplitude, this minor deficit is unlikely to account for the complete block of the homeostatic modulation of quantal content. Taken together, these data support the conclusion that *ppk16* is necessary in motoneurons for homeostatic plasticity and could function with PPK11 in a novel DEG/ENaC channel that is required for synaptic homeostasis.

We performed an additional experiment to explore the potential subunit composition of the putative motoneuron DEG/ENaC channel. Pickpocket19 (PPK19) has been previously implicated in acting with PPK11 in the taste cells of the terminal organ (Liu et al., 2003b). A *UAS-ppk19-RNAi* was previously shown to inhibit sodium preference when expressed in sensory neurons (Liu et al., 2003b). However, when this RNAi is expressed in motoneurons, homeostasis remains normal (Figure 4E). These data suggest that PPK19 is unlikely to be a third subunit of the putative DEG/ENaC channel required for synaptic homeostasis.

As observed in *ppk11* mutants, loss of *ppk16* has a relatively minor effect on baseline synaptic transmission. Although we observe a significant decrease in EPSP amplitude and quantal content in the homozygous *ppk16<sup>Mi</sup>* transposon mutant, we find that baseline transmission is unaltered when compared to the *ppk16* precise excision mutant, which is the appropriate genetic control ( $20.1 \pm 1.9$  and  $26.2 \pm 3.3$  quanta, respectively  $p=0.11$ ). Consistent with this conclusion, the deletion mutation (*ppk16<sup>166</sup>*) shows a wild type EPSP amplitude, composed of a mEPSP that is slightly larger than wild type and a quantal content that is slightly

smaller than wild type (Figure 4C). Finally, motoneuron-specific expression of *UAS-ppk16-RNAi* does not alter quantal content, but blocks homeostatic plasticity (Figure 4F). The emerging picture is that loss of *ppk16* does not cause a consistent or dramatic defect in presynaptic release, but synaptic homeostasis is severely perturbed.

***ppk11* and *ppk16* mutations do not alter NMJ growth or morphology.**

To determine if either *ppk11* or *ppk16* participate in anatomical NMJ development we quantified the number of synaptic boutons at muscle 6/7, the NMJ at which all of our electrophysiological recordings were performed. In abdominal segment 2, no changes were observed in *ppk11*<sup>*PBac*</sup> and a small increase was observed in *ppk16*<sup>*Mi*</sup> compared to wild type (120.3% ±9.9 of wild type, p<0.05; Figure 5B).

We also quantified morphology at abdominal segment 3 and found no significant differences in either *ppk11* or *ppk16* mutants (data not shown). Next, we examined the NMJ of muscle 4, which is situated in the middle of the muscle, making it ideal for visualizing all active zones within each NMJ by staining for the presynaptic active-zone associated protein Bruchpilot (Brp; Davis et al., 1997; Wagh et al., 2006). Mutations in *ppk11* or *ppk16* had no significant effect on NMJ area, determined by staining for the PSD-95 homologue Discs Large (DLG), and no significant change in the number of active zones per NMJ (Figure 5C,D).

When we calculated active zone density by dividing active zone number by NMJ area, we find no change in *ppk11*<sup>*PBac*</sup> and a small (8.4%±2.4, p<0.05 compared to



wild type) decrease in *ppk16*<sup>Mi</sup> (Figure 5E). Since there were no major changes in NMJ appearance, size or organization, we conclude that neither *ppk11* nor *ppk16* plays a prominent role in NMJ growth.

***ppk11* is required for the sustained expression of synaptic homeostasis.**

Genetic deletion of the muscle-specific glutamate receptor subunit GluRIIA (*GluRIIA*<sup>SP16</sup>) has been shown to decrease mEPSP amplitudes by ~50% and induce a homeostatic increase in presynaptic release that restores EPSP amplitudes to wild-type levels (Petersen et al., 1997; DiAntonio et al., 1999; Frank et al., 2006; Figure 6A,B). Since the *GluRIIA* mutation is present throughout larval development, this experiment reflects the sustained expression of synaptic homeostasis for several days. To test if *ppk11* is necessary for the sustained expression of synaptic homeostasis we generated a *GluRIIA*<sup>SP16</sup>, *ppk11*<sup>PBac</sup> double mutant. The double mutant shows a decrease in mEPSP amplitude without a homeostatic increase in presynaptic release (Figure 6A,B), demonstrating that *ppk11* is necessary for both the rapid induction and the sustained expression of synaptic homeostasis.

***ppk11* and *ppk16* are co-regulated and required for the sustained expression of synaptic homeostasis.**

In *GluRIIA* mutant animals, synaptic homeostasis persists over several days of larval development. We reasoned that if *ppk11* and *ppk16* are instructive for

synaptic homeostasis, their transcription might be increased in *GluRIIA* mutants compared to wild type animals. Indeed, we found that the expression of both *ppk11* and *ppk16* mRNA are increased ~4-fold in the *GluRIIA* mutant background compared to wild type, as assessed by qPCR (Figure 6C; see methods). PPK11 and PPK16 are the first motoneuron proteins, necessary for homeostatic plasticity, that show a regulated change in gene expression that correlates with homeostatic plasticity.

We also noted that these genes show an identical increase in expression in the *GluRIIA* mutant. Since the *ppk11* and *ppk16* genes are separated by only 63 base pairs, we considered the possibility that these genes might be co-transcribed. To test this idea we generated PCR primers that could specifically amplify either full-length *ppk11*, *ppk16*, or both genes together as part of a single transcript. We find that we are able to isolate full-length cDNAs for *ppk11*, *ppk16* and a cDNA that spans the coding regions of both *ppk11* and *ppk16* and is of the expected size for a transcript containing both *ppk11* and *ppk16* (Figure 6D). The identity of the joint *ppk11-ppk16* transcript was confirmed by sequencing the junction between the *ppk11* and *ppk16* genes. A stop codon is present in the joint cDNA following the *ppk11* coding sequence suggesting that the two genes are co-transcribed and translated as independent proteins. This result is reproducible across three independently derived cDNA libraries (data not shown). These data indicate that *ppk11* and *ppk16* are co-transcribed and co-regulated during synaptic homeostasis, further suggesting that they could be subunits of a single

channel that is up-regulated during the sustained expression of synaptic homeostasis.

***ppk11* and *ppk16* represent a single functional genetic unit with respect to synaptic homeostasis.**

We next asked whether *ppk11* and *ppk16* are not only co-transcribed and co-regulated during synaptic homeostasis, but whether they function as part of a single genetic unit during synaptic homeostasis. If two genes function as part of a single genetic unit, then disrupting the expression of one gene will also affect the other gene. To test this, we performed a series of complementation experiments, diagrammed in Figure 6F. First, we show that heterozygous mutations in either the *ppk11* (+,*ppk11*<sup>Pbac</sup>/+,+) or the *ppk16* genes (*ppk16*<sup>Mi</sup>,+/,+) do not alter synaptic homeostasis (Figure 6E, F). Next, we demonstrate that a heterozygous deficiency that encompasses both *ppk11* and *ppk16* (*ppk16*<sup>Df</sup>,*ppk11*<sup>Df</sup>/+,+) also does not alter synaptic homeostasis (Figure 6E, F). Therefore, animals that harbor one functional copy of *ppk11* and one functional copy of *ppk16* can express normal synaptic homeostasis. However, when the heterozygous +,*ppk11*<sup>Pbac</sup>/+,+ mutation is placed *in trans* to the heterozygous *ppk16*<sup>Mi</sup>,+/,+ mutation (+,*ppk11*<sup>PBac</sup>/*ppk16*<sup>Mi</sup>,+), then we find that synaptic homeostasis is completely blocked (Figure 6E, F). Although each mutation is heterozygous, they are resident on different chromosomes. As such, the heterozygous mutation in *ppk11* could disrupt the remaining functional copy

of *ppk16* and vice versa (Figure 6F). Since homeostasis is blocked when heterozygous mutations are placed *in trans* but not when they are placed *in cis*, we conclude that one or both of the mutations must affect both *ppk11* and *ppk16*. These data argue that *ppk11* and *ppk16* are not only co-transcribed, but function as a single, operon-like genetic unit, further supporting the possibility that these genes function together during synaptic homeostasis. This is further supported by our finding that the organization of the *ppk11/16* locus is conserved across multiple species of *Drosophila* (Figure 10), representing approximately 30 million years of evolutionary divergence, suggesting that the tandem placement of these genes is relevant to their regulation.

Although the *ppk11/16* locus is transcribed as a single RNA, we do not know whether these two could also be transcribed independently. This is important to consider when interpreting the results of transgenic RNAi. Specifically, this concerns whether *UAS-ppk11-RNAi* targets only the *ppk11* gene or whether it will also affect expression of co-transcribed *ppk16*, and vice versa (Figures 3 and 4). One further observation is worth considering in the *trans*-heterozygous data set. When mutations in *ppk11* and *ppk16* are placed *in trans*, synaptic homeostasis is blocked but baseline synaptic transmission (in the absence of PhTx) is not statistically different from wild type (Figure 6G). The only significant change observed is a minor decrease in mEPSP amplitude in *trans*-heterozygous mutants. These data confirm, again, that homeostatic synaptic

plasticity can be blocked by disruption of the *ppk11/16* locus without a parallel change in baseline synaptic transmission.

### **PPK11/16 channel function drives the expression of synaptic homeostasis.**

We hypothesize that PPK11/16 containing DEG/ENaC channels are inserted into the presynaptic plasma membrane to cause a homeostatic increase in presynaptic release and that these channels must be maintained on the plasma membrane in order to sustain the expression of synaptic homeostasis over several days. If this is correct, then pharmacological blockade of the PPK11/16 channel conductance should erase homeostatic potentiation that was previously induced by either PhTx application or by the presence of the *GluRIIA* mutation. This appears to be the case.

DEG/ENaC channels are blocked by amiloride and its derivatives (Kleyman and Cragoe, 1988). In *Drosophila*, Benzamil has been shown to be a potent inhibitor of ENaC channel function (Liu et al, 2003a). In our first set of experiments, wild type NMJs were co-incubated in 50 $\mu$ M Benzamil and 10 $\mu$ M PhTx. After a ten-minute incubation, recordings were made in the presence of 50 $\mu$ M Benzamil. Ten minutes is normally sufficient to induce potent homeostatic compensation (Figure 7B). However, in the presence of 50 $\mu$ M Benzamil, we saw a complete block in synaptic homeostasis (Figure 7A,B). Next, we tested whether this effect could be washed out. Benzamil reversibly blocks DEG/ENaC channels, while PhTx irreversibly antagonizes *Drosophila* glutamate

receptors (Drummond et al., 1998; Frank et al., 2006). Therefore, we were able to incubate larvae in PhTx and 50 $\mu$ M Benzamil for 10 minutes, and then wash out only Benzamil, limiting its action to the time when synaptic homeostasis was induced. We saw a complete restoration of synaptic homeostasis after Benzamil was washed out. The half maximal effective concentration for disruption of synaptic homeostasis is 32 $\mu$ M (Figure 11), which is within the range expected for amiloride derivatives to act on *Drosophila* pickpocket channels (Chen et al., 2010; Boiko et al., 2012). We have also confirmed a block of synaptic homeostasis with a second amiloride derivative EIPA (5-(n-ethyl-n-isopropyl)amiloride) at 20 $\mu$ M (Figure 12). From these data we can make several conclusions. First, these data demonstrate that the conductance of the pickpocket channel is required for synaptic homeostasis, since functional blockade is sufficient to erase homeostatic plasticity. Second, since homeostasis is restored upon washout, it demonstrates that the induction process remains intact, but expression is blocked by inhibition of the DEG/ENaC channel. Third, this is the first time that a pharmacological reagent has been available to block homeostatic plasticity. Since synaptic transmission reverts to the levels seen in an uncompensated synapse when Benzamil is applied (Figure 7C), it demonstrates that synaptic homeostasis is, at least initially, a process that is layered on top of normal synaptic transmission. Finally, in our assay, the axon is cut and only ~200 $\mu$ M of axon exists between our stimulation electrode and the

NMJ. Therefore, the DEG/ENaC channel must function within these 200 $\mu$ M of axon or within the NMJ itself.

We next asked whether the PPK channel conductance is continuously required for the expression of synaptic homeostasis. First, Benzamil was applied following a ten-minute incubation in PhTx and synaptic homeostasis was blocked (Figure 7D). Thus, ENaC channel function is necessary for the expression of synaptic homeostasis, not during the induction of the process. Next, Benzamil was applied to the *GluRIIA* mutant and, again, synaptic homeostasis was completely blocked (Figure 7E). Remarkably, quantal content in the *GluRIIA* mutant in the presence of Benzamil was identical to that observed for a wild type NMJ in the presence of Benzamil (Figure 7F). Thus, even when synaptic homeostasis has been persistently engaged for the life of the synapse, it can be erased by blocking the function of the Benzamil-sensitive DEG/ENaC channel.

Several controls were performed. It is well established that Benzamil acts to inhibit DEG/ENaC channels (Kleyman and Cragoe, 1988; Garty and Palmer, 1997; Cuthbert and Fanelli, 1978). However, we sought additional evidence that Benzamil acts on a *Drosophila* PPK11/PPK16 containing channel. To do so we tested whether animals that are doubly heterozygous for the *ppk11* and *ppk16* mutations (*in cis*) might have increased sensitivity to Benzamil. The double heterozygote has normal synaptic homeostasis (Figure 7G). When a low concentration of Benzamil (25 $\mu$ M) is applied to a wild type NMJ, synaptic homeostasis is also normal (Figure 7G). However, when 25 $\mu$ M Benzamil is

applied to the double heterozygote, synaptic homeostasis is blocked (Figure 7G). These data strongly suggest that Benzamil is acting on a DEG/ENaC channel containing PPK11 and PPK16 subunits, and that inhibition of this channel is the cause of impaired synaptic homeostasis.

Finally, we note that acute application of Benzamil to the wild type NMJ does not impair presynaptic quantal content (Figure 7B,11). We observe a modest decrease in mEPSP amplitude, but no change in quantal content. We further demonstrate that the reduction in mEPSP amplitude is an action of Benzamil that is independent of PPK11 or PPK16, and can be separated from the effect on synaptic homeostasis (Figure 11). Thus, Benzamil blocks PhTx-induced synaptic homeostasis at the wild type NMJ without impairing baseline presynaptic release. We conclude from these data, as well as our genetic analyses, that synaptic homeostasis requires a Benzamil sensitive DEG/ENaC channel, which is likely to include both the PPK11 and PPK16 subunits, and this channel has little or no role during baseline synaptic release in the absence of a homeostatic perturbation.

### **Pickpocket channel blockade prevents the homeostatic modulation of presynaptic calcium influx.**

It was previously demonstrated that the homeostatic modulation of presynaptic release is achieved, in part, through an increase in presynaptic calcium influx via the CaV2.1 calcium channel orthologue *cacophony* (Müller and



Davis, 2012). Since Benzamil does not alter baseline presynaptic release, it is unlikely to alter calcium channel function directly. However, DEG/ENaC channels are non-voltage activated cation channels that show a strong preference for sodium. As such, increased DEG/ENaC channel function could depolarize the presynaptic membrane and indirectly enhance calcium channel activity, thereby increasing neurotransmitter release. This possibility is consistent with evidence that subthreshold presynaptic depolarization enhances neurotransmitter release at the NMJ (Wojtowicz and Atwood, 1983, 1984) and enhances both presynaptic calcium influx and release at central synapses (Awatramani et al., 2005).

To determine whether the PPK11/16 containing DEG/ENaC channel might influence presynaptic calcium influx through the CaV2.1 calcium channel, we imaged presynaptic spatially averaged calcium signal after single action potential stimulation with the calcium indicator Oregon Green Bapta-1 (OGB-1), as previously described (Müller and Davis 2012). First, we find that calcium influx is increased in *GluRIIA* mutant animals compared to wild type, confirming our previously published results (Figure 8A, B;  $p < 0.05$ ; see also Müller and Davis, 2012). Next, we demonstrate that application of Benzamil to the wild type NMJ has no effect on the amplitude of the evoked calcium transient (Figure 8A,B).

This is consistent with our conclusion based on electrophysiology that Benzamil does not alter steady state neurotransmitter release. Finally, we show that Benzamil application to the *GluRIIA* mutant causes a pronounced decrease in the amplitude of the evoked calcium transient that could entirely account for the

observed Benzamil-dependent block of synaptic homeostasis (Figure 8B,  $p < 0.001$ ).

It should be noted that, in both wild type and *GluRIIA* mutant animals, Benzamil causes a drop in baseline OGB-1 fluorescence ( $F_{\text{base}}$ ) that is significant in wild type, and approaches significance in *GluRIIA* (Figure 8C;  $p < 0.01$  and  $p = 0.55$ , respectively). It is likely that photobleaching during sequential acquisition of calcium transients prior to and following Benzamil application contributes to the drop in  $F_{\text{base}}$ . It remains formally possible that Benzamil influences the  $F_{\text{base}}$  measurement and we cannot rule out the possibility that baseline calcium is decreased. However, since a drop in  $F_{\text{base}}$  should, if anything, increase calcium transient amplitudes (measured as  $\Delta F/F_{\text{base}}$ , see methods), this effect cannot account for the large decrease in the amplitude of the evoked calcium transients when Benzamil is applied to the *GluRIIA* mutant. These data support the conclusion that Benzamil-dependent inhibition of the PPK11/16 containing DEG/ENaC channel blocks synaptic homeostasis by indirectly preventing the modulation of calcium influx through presynaptic CaV2.1 calcium channels. These data are consistent with a new model for homeostatic synaptic plasticity in which the induction of synaptic homeostasis drives an increase in pickpocket channel function at or near the presynaptic membrane, possibly through the insertion of new channels (Figure 8D; see discussion).

## DISCUSSION

We provide evidence that a novel presynaptic DEG/ENaC channel composed of PPK11 and PPK16 is required for the rapid induction, expression and continued maintenance of homeostatic synaptic plasticity at the *Drosophila* NMJ.

Remarkably, *ppk11* and *ppk16* genes are not only required for homeostatic plasticity, but are among the first homeostatic plasticity genes shown to be differentially regulated during homeostatic plasticity. Specifically, we show that expression of both *ppk11* and *ppk16* is increased 4-fold in the *GluRIIA* mutant background. We also demonstrate that *ppk11* and *ppk16* are transcribed together in a single transcript and behave genetically as an operon-like, single genetic unit. This molecular organization suggests a model in which *ppk11* and *ppk16* are co-transcribed to generate DEG/ENaC channels with an equal stoichiometric ratio of PPK11 and PPK16 subunits. This is consistent with previous models for gene regulation in *Drosophila* (Blumenthal, 2004). However, we cannot rule out the possibility that two independent DEG/ENaC channels are up-regulated, one containing PPK11 and one containing PPK16. The upregulation of *ppk11* and *ppk16* together with the necessity of DEG/ENaC channel function during the time when synaptic homeostasis is assayed, indicates that these genes are likely part of the homeostat, and not merely necessary for the expression of synaptic homeostasis.

**A model for DEG/ENaC channel function during homeostatic plasticity.**

DEG/ENaC channels are voltage-insensitive cation channels that are primarily permeable to sodium (Ben-Shahar, 2011; Bianchi and Driscoll, 2002) and can carry a sodium leak current. A model for DEG/ENaC channel function during synaptic homeostasis can be based on the well-established regulation of ENaC channel trafficking in the kidney during the homeostatic control of salt balance. Enhanced sodium reabsorption in the principle cells of the cortical collecting duct of the kidney is triggered by aldosterone binding to the mineralocorticoid receptor. This increases ENaC channel transcription and trafficking to the apical cell surface, which enhances sodium influx. Sodium is then pumped out of the basolateral side of the cell, accomplishing sodium reabsorption (Schild, 2010).

We speculate that a retrograde, homeostatic signal from muscle triggers increased trafficking of a PPK11/16 containing DEG/ENaC channel to the neuronal plasma membrane, at or near the NMJ. Since the rapid induction of synaptic homeostasis is protein synthesis independent (Goold et al., 2007), we hypothesize the existence of a resting pool of PPK11/16 channels that are inserted in the membrane in response to postsynaptic glutamate receptor inhibition. If postsynaptic glutamate receptor inhibition is sustained, as in the *GluRIIA* mutant, then increased transcription of *ppk11/16* supports a persistent requirement for this channel at the developing NMJ. Once on the plasma membrane, the PPK11/16 channel would induce a sodium leak and cause a moderate depolarization of the nerve terminal. This subthreshold depolarization

would lead, indirectly, to an increase in action potential-induced presynaptic calcium influx through the CaV2.1 calcium channel and subsequent neurotransmitter release (Figure 8D).

There are two major possibilities for how ENaC-dependent depolarization of the nerve terminal could potentiate calcium influx and evoked neurotransmitter release. One possibility, based on work in the ferret prefrontal cortex and *Aplysia* central synapses (Shu et al., 2006; Shapiro et al., 1980), is that presynaptic membrane depolarization causes action potential broadening through potassium channel inactivation, thereby enhancing both calcium influx and release. A second possibility is that sub-threshold depolarization of the nerve terminal causes an increase in resting calcium that leads to calcium-dependent calcium channel facilitation (Cuttle et al., 1998; Borst and Sakmann, 1998). Consistent with this model, it has been shown at several mammalian synapses that sub-threshold depolarization of the presynaptic nerve terminal increases resting calcium and neurotransmitter release through low voltage modulation of presynaptic P/Q type calcium channels (Awatramani et al., 2005; Alle and Geiger, 2006; Christie et al., 2010). However, at these mammalian synapses the change in resting calcium does not lead to an increase in action potential evoked calcium influx, highlighting a difference between the mechanisms of homeostatic potentiation and the type of presynaptic modulation observed at these other synapses (Awatramani et al., 2005; Alle and Geiger, 2006; Christie et al., 2011). The mechanism by which elevated basal calcium potentiates release at these

mammalian synapses remains under debate (Bouhours et al., 2011; Chu et al., 2012). It should be noted that small, sub-threshold depolarization of the presynaptic resting potential, as small as 5mV, are sufficient to cause a 2-fold increase in release at both neuromuscular (Wojtowicz and Atwood, 1983) and mammalian central synapses (Awatrimani et al., 2005; Christie et al., 2011). This is within a reasonable range for modulation of presynaptic membrane potential by pickpocket channel insertion. Unfortunately, it is not technically feasible to record directly from the presynaptic terminal at the *Drosophila* NMJ. Finally, we note that it remains formally possible that a PPK11/16 containing DEG/ENaC channel passes calcium, based upon the ability of mammalian ASIC channels to flux calcium (Waldmann et al., 1997).

This model might ~~also~~ provide insight regarding how accurate tuning of presynaptic neurotransmitter release can be achieved (Frank et al., 2006). There is a supralinear relationship between calcium influx and release (Katz and Miledi, 1970; Bollmann et al., 2000; Schneggenburger and Neher, 2000). Therefore, if changing calcium channel number is the mechanism by which synaptic homeostasis is achieved, then there must be very tight and tunable control of calcium channel number within each presynaptic active zone. By contrast, if homeostatic plasticity is achieved by ENaC-dependent modulation of membrane voltage, then variable insertion of ENaC channels could uniformly modulate calcium channel activity, simultaneously across all of the active zones of the presynaptic nerve terminal. Furthermore, if the ENaC channel sodium leak is

small, and if presynaptic calcium channels are moderately influenced by small changes in resting membrane potential, then relatively coarse modulation of ENaC channel trafficking could be used to achieve precise, homeostatic control of calcium influx and neurotransmitter release. Again, these are testable hypotheses that will be addressed in the future.

## FIGURES AND TABLES

### Figure 1: *ppk11* is necessary for the homeostatic modulation of presynaptic neurotransmitter release.

**A)** The percent change in mEPSP amplitude (black bars) and quantal content (QC; grey bars) in the presence of PhTx relative to baseline for each genotype in the absence of PhTx. The *ppk11*<sup>PBac</sup> mutation is shown in blue and the *rab3-GAP* mutation is shown in green. All changes in mEPSP are significant ( $p < 0.01$ ) as are change in EPSP amplitude ( $p \leq 0.05$ ) unless indicated otherwise. **B)** Average EPSP amplitude is plotted for each genotype shown in (A) in the absence of PhTx. **C)** Schematic showing the genetic locus that includes *ppk11* (blue) and *ppk16* (red). Indicated are: transposon insertion sites (black arrowheads), regions targeted by RNAi (black lines) the *dnPPK11* construct (dotted line), the *ppk16*<sup>166</sup> deletion (open red bar), and a deficiency spanning the locus is shown as a grey arrow. **D)** Representative traces showing EPSPs and mEPSPs from *ppk11*<sup>Precise</sup> (top), *ppk11*<sup>Mi</sup> (bottom). All genotypes are shown without and with PhTx (left and right, respectively). **E)** The percent change in mEPSP (solid bars) and quantal content (QC; open bars) in the presence of PhTx relative to baseline for each genotype recorded in the absence of PhTx. All conditions show a significant decrease in mEPSP amplitude ( $p < 0.001$ ). Only wild type (WT) and the precise excision (*ppk11*<sup>Precise</sup>) show an increase in quantal content ( $p < 0.001$ ). All data are



recorded in 0.3-0.35mM extracellular calcium (see Table 1). Data are presented as average  $\pm$  SEM. Comparisons are made according to a Student's t-test.

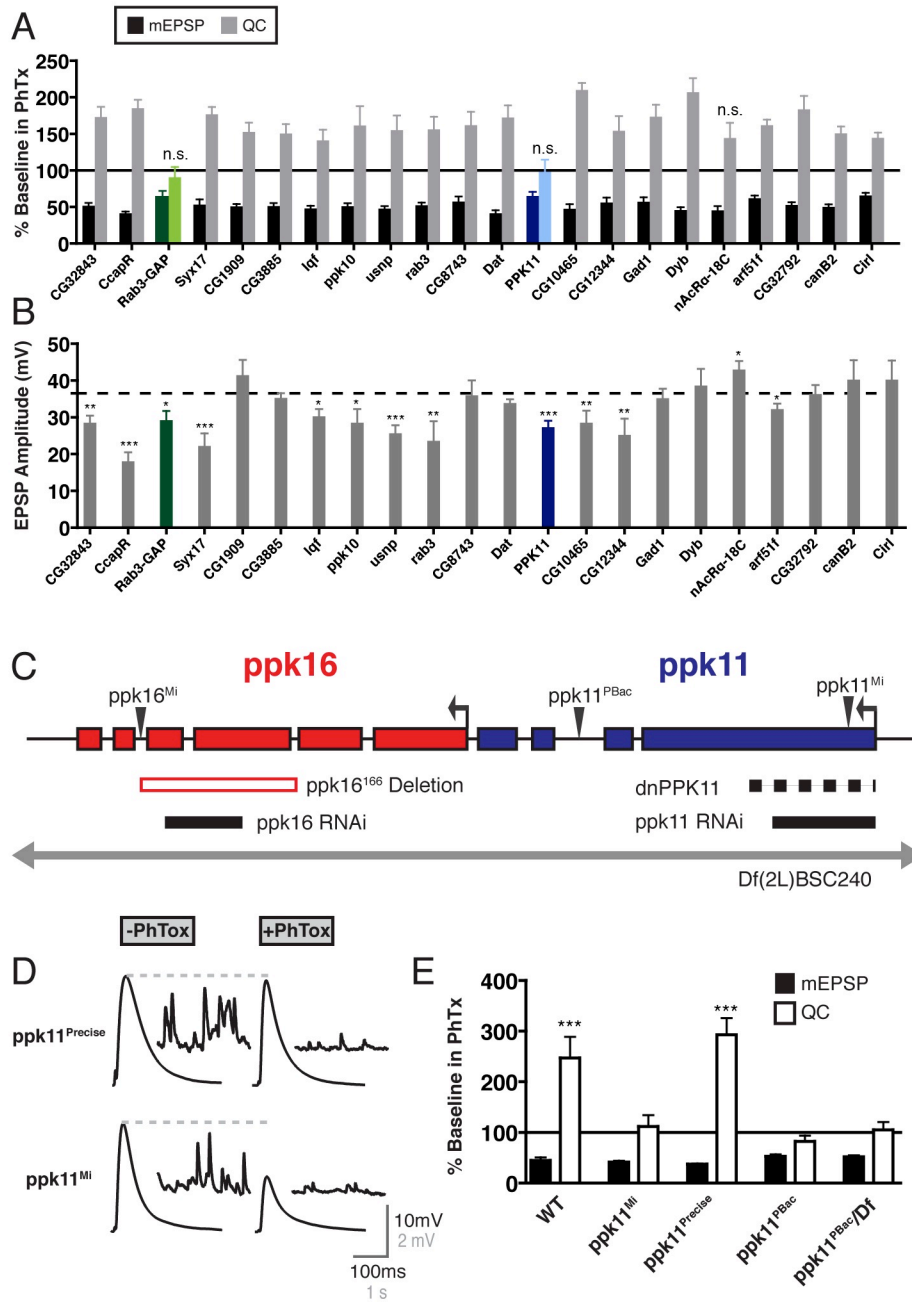


**Figure 2: Analysis of baseline neurotransmission in *ppk11* mutants.**

**A)** Sample traces for the indicated genotypes. **B)** mEPSP amplitude, EPSP amplitude, and quantal content for wild type (WT), *ppk11<sup>PBac</sup>*, *ppk11<sup>Mi</sup>* and *ppk11<sup>Precise</sup>* at 0.35mM extracellular calcium. **C)** Representative examples of EPSCs from wild type (WT; top) and *ppk11<sup>Mi</sup>* (bottom) in the absence of PhTx (left) and presence of PhTx (right) at 1mM extracellular calcium. **D)** Percent change in mEPSP amplitude and EPSC amplitude in the presence of PhTx compared to baseline in the absence of PhTx for each genotype. EPSC amplitude is not altered in WT after the addition of PhTx ( $p=0.39$ ) demonstrating homeostatic compensation ( $102.3\pm 9.2\text{nA}$ ,  $n=5$  without PhTx and  $112.8\pm 5.8\text{nA}$ ,  $n=4$  with PhTx). EPSC amplitude is significantly reduced in *ppk11<sup>Mi</sup>* after the addition of PhTx ( $p<0.05$ ) demonstrating impaired homeostatic compensation ( $101.0\pm 13.9\text{nA}$ ,  $n=8$  without PhTx and  $62.4\pm 5.9\text{nA}$ ,  $n=9$  with PhTx). **E)** In the absence of PhTx, neither EPSC amplitude nor EPSC 20-80% rise time are different compared to WT ( $p=0.95$  and  $p=0.48$ , respectively).

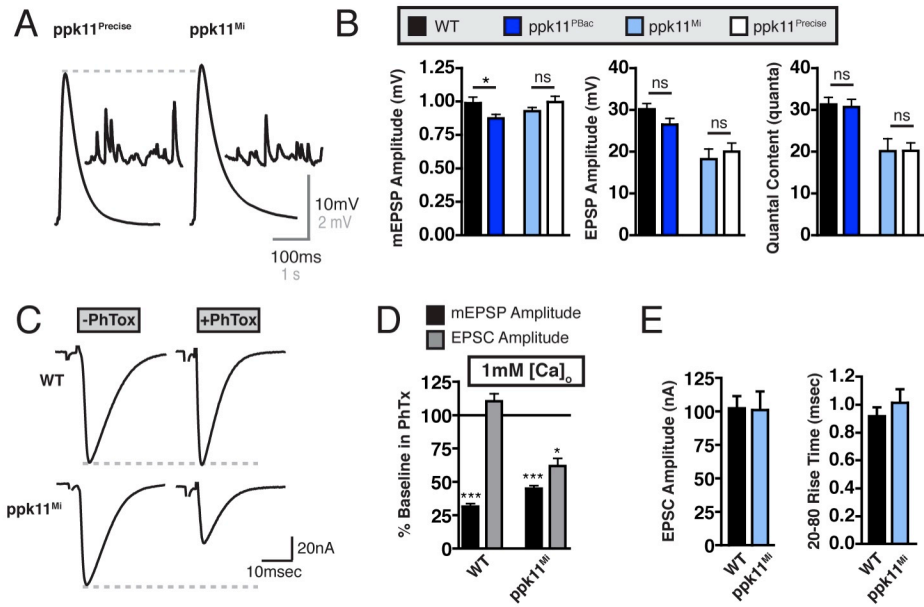


**Figure 3: *ppk11* is required in motoneurons for synaptic homeostasis.**

**A)** Sample traces for the indicated genotypes. **B)** Percent change in mEPSP (filled bars) and QC (open bars) as in Figure 1E. mEPSP amplitude is decreased after the addition of PhTx in all conditions ( $p < 0.001$ ). WT and *UAS-ppk11-RNAi* driven in muscle (*MHC-GAL4*) show a significant increase in quantal content (QC;  $p < 0.001$ ). *UAS-ppk11-RNAi* and *UAS-dnPPK11*, driven in motoneurons (*OK371-GAL4*) show no significant increase in QC after PhTx treatment ( $p = 0.69$  and  $p = 0.09$  respectively) demonstrating impaired synaptic homeostasis. **C)** mEPSP amplitude, EPSP amplitude, and quantal content are shown. mEPSP amplitude is unchanged in the *UAS-ppk11-RNAi* driven in motoneurons, and reduced in the *UAS-dnPPK11* driven in motoneurons ( $p < 0.01$ ). There is no decrease in EPSP amplitude or quantal content when either transgenic condition is compared to wild type. There is a small but significant increase in EPSP amplitude ( $p < 0.05$ ) and quantal content ( $p < 0.01$ ) when *UAS-dnPPK11* is driven in motoneurons.

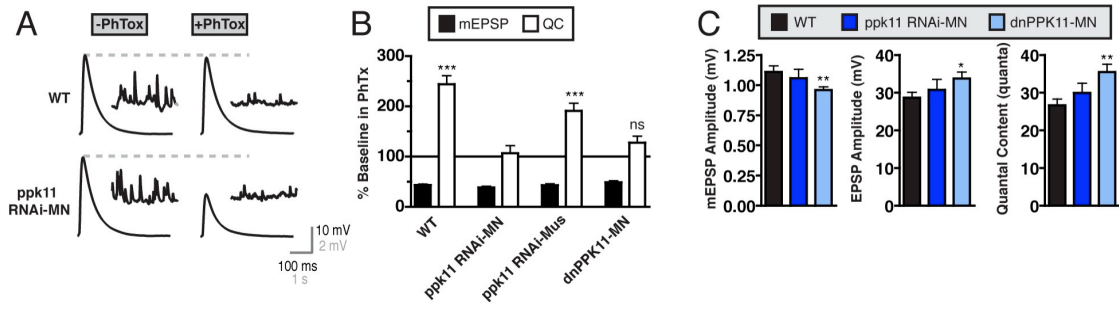


**Figure 4: *ppk16* is necessary in motoneurons for the homeostatic modulation of presynaptic release.**

**A)** Sample traces for the indicated genotypes. **B)** Percent change in mEPSP (filled bars), and quantal content (QC; open bars) as in Figure 1D. mEPSP amplitude is decreased after the addition of PhTx in all conditions ( $p < 0.001$ ). WT shows an increase in QC ( $p < 0.001$ ), while *ppk16<sup>Mi</sup>* and *ppk16<sup>166</sup>* do not ( $p = 0.68$  and  $p = 0.24$ , respectively). **C)** mEPSP amplitude, EPSP amplitude, and QC are shown. *ppk16<sup>166</sup>* has an increased mEPSP amplitude ( $p < 0.01$ ) compared to WT. *ppk16<sup>Mi</sup>* and has decreased EPSP amplitude compared to WT ( $p < 0.001$ ). *ppk16<sup>Mi</sup>* and *ppk16<sup>166</sup>* show reduced QC ( $p < 0.001$  and  $p < 0.05$  respectively) compared to WT. **D)** Sample traces for the indicated genotypes. **E)** Data as in B. mEPSP amplitude is decreased after the addition of PhTx in all conditions ( $p < 0.001$ ). WT, *UAS-ppk16-RNAi* driven in the muscle (*MHC-GAL4*), and *UAS-ppk19-RNAi* driven in motoneurons (*OK371-GAL4*) show an increase in QC ( $p < 0.001$ ) demonstrating normal synaptic homeostasis. *UAS-ppk16-RNAi* driven in motoneurons (*OK371-GAL4*) does not show an increase in QC, demonstrating a block of synaptic homeostasis ( $p = 0.19$ ). **F)** Data as in C. mEPSP amplitude is decreased when the *UAS-ppk16-RNAi* is expressed in motoneurons ( $p < 0.001$ ) while EPSP amplitude and quantal content remain unchanged ( $p = 0.30$  and  $p = 0.44$ , respectively). There is an increase in EPSP amplitude and quantal content ( $p < 0.05$ ) when *UAS-PPK19-RNAi* is expressed in motoneurons.





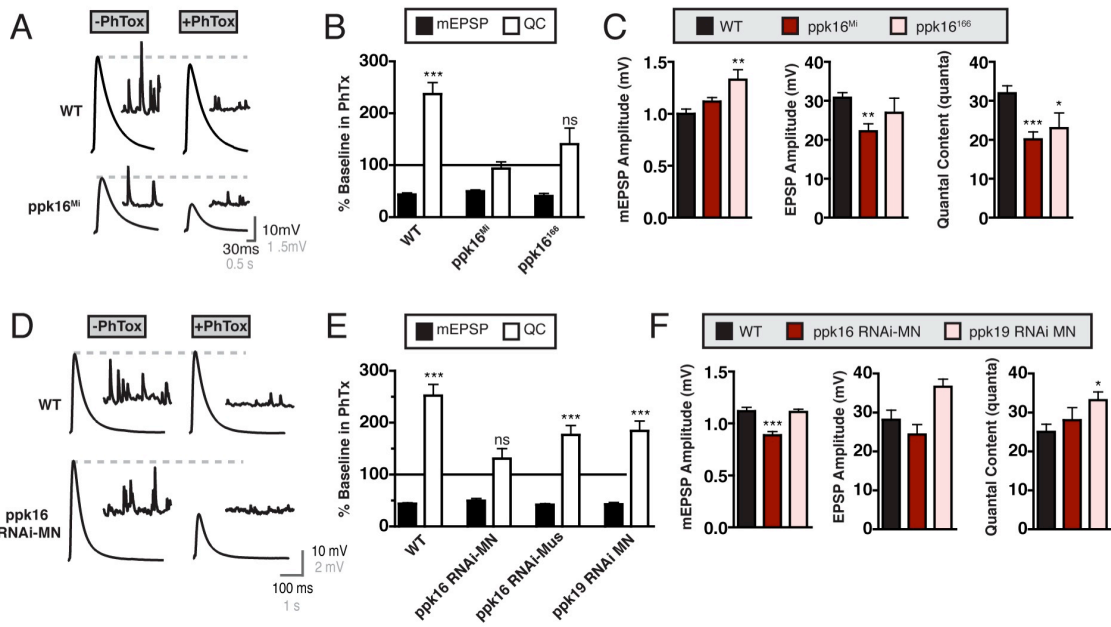


**Figure 5: Normal NMJ morphology in *ppk11* and *ppk16* mutants.**

**A)** Representative images of from muscle 4 of wild type (WT), *ppk11*<sup>PBac</sup> and *ppk16*<sup>Mi</sup> mutant animals stained for BRP (green), the DLG (red), and HRP (blue).

The bottom panel shows boutons enlarged 5X. **B)** The number of boutons per

NMJ at muscles 6/7 in segment 2 is expressed as percent wild type (% WT)

bouton number. No significant changes were observed. **C)** The area of the NMJ

at muscle 4 is shown as %WT area, as measured by DLG staining. It is not

significantly different from wild type in either genotype. **D)** The number of active

zones per NMJ at muscle 4 is shown as the % WT active zones (measured as

individual Brp puncta). Active zone number is not different from WT in either

genotype. **E)** The active zone density at muscle 4 is shown as % WT active zone

density. There is no significant difference in *ppk11*<sup>PBac</sup>, and a small decrease is

observed in *ppk16*<sup>Mi</sup> ( $p < 0.05$ ).

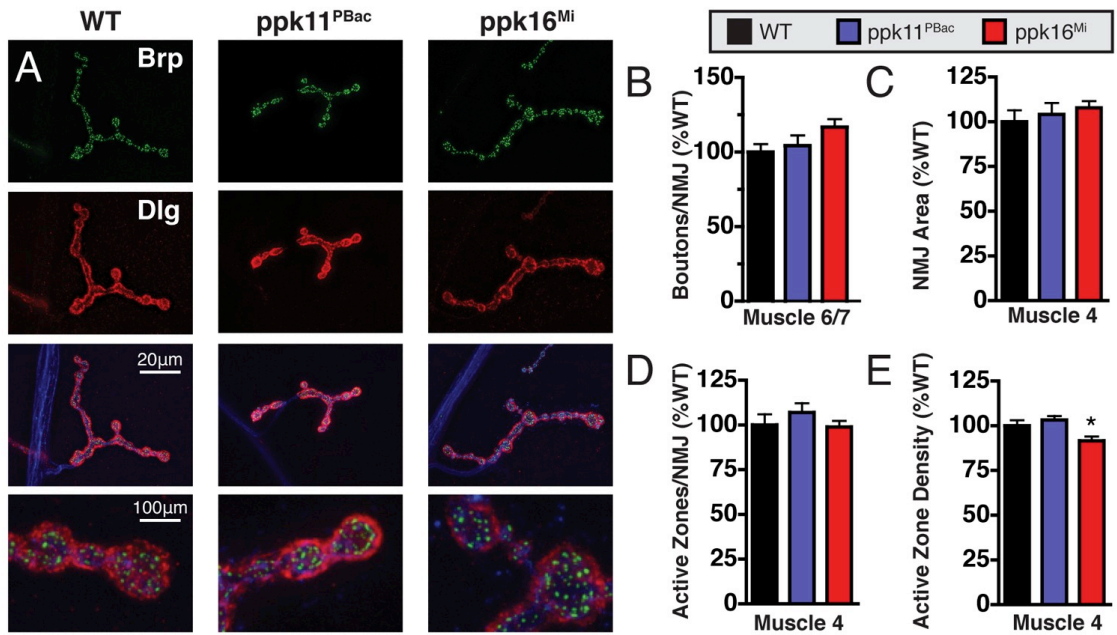


**Figure 6: Pickpocket function and regulation during the long-term expression of synaptic homeostasis.**

**A)** Representative traces for indicated genotypes. **B)** mEPSP amplitude and quantal content (QC) are shown as percent baseline for each genotype. *GluRIIA<sup>SP16</sup>* is shown as percent change relative to wild type. The *ppk11<sup>PBac</sup>*, *GluRIIA<sup>SP16</sup>* double mutant is normalized to *ppk11<sup>PBac</sup>* alone. mEPSP amplitudes are decreased ( $p < 0.001$ ) in genotypes that include the *GluRIIA<sup>SP16</sup>* mutation. *GluRIIA<sup>SP16</sup>* shows an increase in QC ( $p < 0.01$ ), while the *ppk11<sup>PBac</sup>*, *GluRIIA<sup>SP16</sup>* double mutant does not. **C)** *ppk11* and *ppk16* mRNA are increased ~4-fold in the *GluRIIA<sup>SP16</sup>* mutant. Experiment was performed in triplicate. **D)** Ethidium bromide gel showing PCR products generated from a wild-type cDNA library. cDNAs of the expected size could be isolated with primers targeting *ppk11*, *ppk16*, or using primers that span the full length of both genes (*ppk11-16*). **E)** mEPSP amplitude (filled bars) and QC (open bars) are expressed as the percent change in the absence of PhTx as in Figure 1D. mEPSP amplitude is decreased after the addition of PhTx in all conditions ( $p < 0.001$ ). QC is increased for WT ( $p < 0.001$ ), *+, PPK11/+, +* ( $p < 0.001$ ), *PPK16, +/+, +* ( $p < 0.05$ ), and *PPK16<sup>Df</sup>, PPK11<sup>Df</sup>/+, +* ( $p < 0.001$ ). There is no change in QC in *+, PPK11<sup>PBac</sup>/PPK16<sup>Mi</sup>, +* ( $p = 0.29$ ). **F)** Schematic diagram of genetic epistasis experiment quantified below. The *ppk11* and *ppk16* locus is shown. A red rectangle and a blue rectangle represent a functional copy of the *ppk16* and *ppk11* genes, respectively. Gray represents a

loss-of-function mutation in either gene, and stripes represent the unknown consequence of a transposon insertion. **G)** mEPSP amplitude, EPSP amplitude and QC are shown as % of WT. There are no significant differences from wild type in any condition except a small decrease in mEPSP amplitude in  $+,PPK11^{PBac}/PPK16^{Mi},+$  ( $p<0.05$ ).

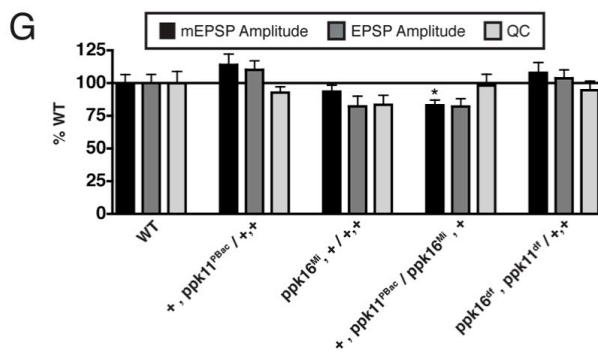
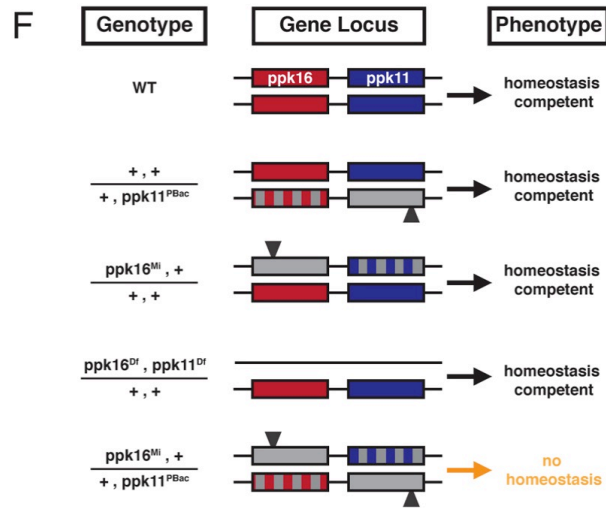
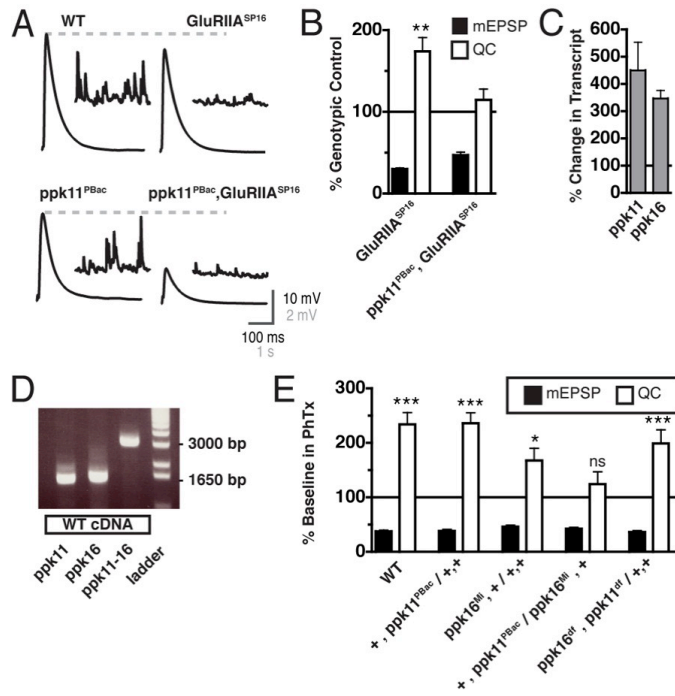


**Figure 7: Pharmacological inhibition of PPK channels erases the expression of homeostatic plasticity.**

**A)** Representative traces for the indicated genotypes with PhTx (right) and without PhTx (left). **B)** Percent change of mEPSP amplitude and quantal content (QC). mEPSP amplitude is decreased by PhTx in all conditions ( $p < 0.001$ ). QC is increased in WT ( $p < 0.001$ ) but not in the presence of 50 $\mu$ M Benzamil (Benz;  $p = 0.17$ ). QC is increased when Benzamil is washed out ( $p < 0.01$ ). **C)** Quantal content in the absence of PhTx for each genotype in B. Benzamil does not decrease quantal content ( $p = 0.63$ ) and there is a slight but significant increase after Benzamil washout ( $p < 0.05$ ). **D)** Data are represented as in A. mEPSP amplitude is decreased by PhTx ( $p < 0.001$ ). QC is increased in WT in the presence of PhTx ( $p < 0.001$ ), but not when the PhTx treatment is followed by incubation in 50 $\mu$ M Benzamil ( $p = 0.59$ ). **E)** Percent change in mEPSP amplitude (filled bars) and QC (corrected for non-linear summation; see Frank et al., 2006; open bars) in the presence of PhTx. 50 $\mu$ M Benzamil prevents the increase in QC observed in *GluRIIA*<sup>SP16</sup> alone ( $p < 0.001$  without Benzamil and  $p = 0.82$  with Benzamil). Recordings were made at 0.5mM extracellular calcium. **F)** QC is shown for wild WT and *GluRIIA*<sup>SP16</sup> in the absence and presence of Benzamil. There is an increase in QC in *GluRIIA*<sup>SP16</sup> compared to WT ( $p < 0.001$ ), and there is no significant difference between WT and *GluRIIA*<sup>SP16</sup> in the presence of Benzamil ( $p = 0.82$ ). **G)** Data are shown as in B. mEPSP amplitude is decreased

after the addition of PhTx in all conditions ( $p < 0.001$ ). The PPK11-PPK16 double heterozygous (PPK het) condition in the presence of 25 $\mu$ M Benzamil shows no increase in QC ( $p = 0.65$ ). For purposes of data comparison in this panel, data for 'ppk het' are identical to that presented in figure 6E (*ppk16<sup>df</sup>*, *ppk11<sup>df</sup>/+,+*).



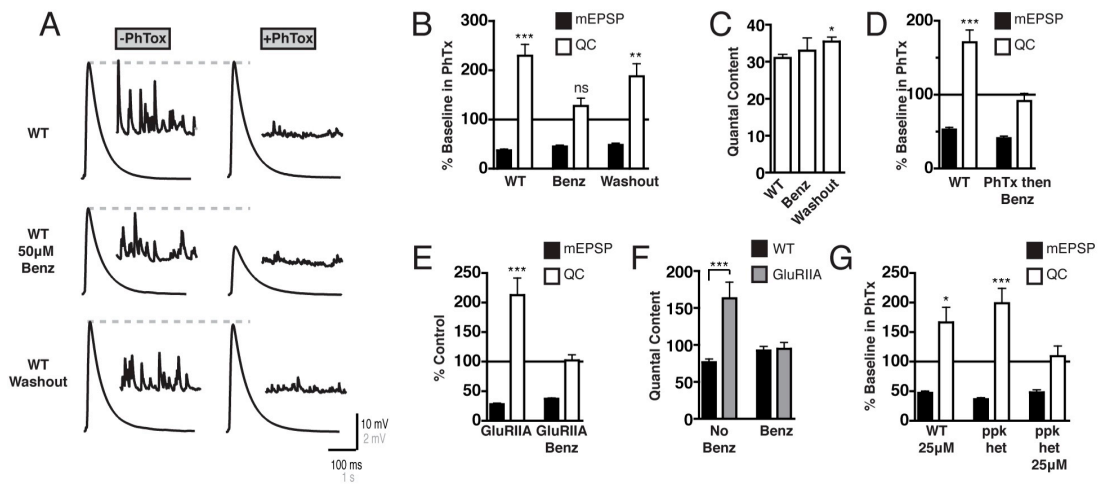


**Figure 8: A Model for PPK11/16 function during synaptic homeostasis.**

**A)** Representative traces of single action potential-evoked spatially averaged calcium transients (average of 8-10 scans each) for the indicated genotypes with and without Benzamil (right and left, respectively). **B)**  $\Delta F/F$  calcium transient peak amplitudes for individual boutons imaged before and after 75 $\mu$ M Benzamil application (n=8 and n=11 boutons for wild type (WT) and the *GluRIIA* mutant, respectively). There is no significant change in  $\Delta F/F$  in WT after Benzamil treatment (p=0.07), and there is a significant decrease in the *GluRIIA* mutant after Benzamil treatment (p<0.001). **C)** Average baseline fluorescence ( $F_{\text{base}}$ ) for WT and *GluRIIA* in the presence and absence of Benzamil. There is a statistically significant decrease in WT after Benzamil treatment (p<0.01), and a non-significant trend towards a decrease in *GluRIIA* treated with Benzamil (p=0.055). **D)** Our data support a model whereby PPK11 and PPK16 containing channels (purple) are inserted into the presynaptic membrane during synaptic homeostasis, to cause an increase in sodium influx and a resulting change in presynaptic resting potential  $\Delta V_m$  (right). The change in presynaptic resting potential directly or indirectly leads to increased presynaptic calcium influx (red).

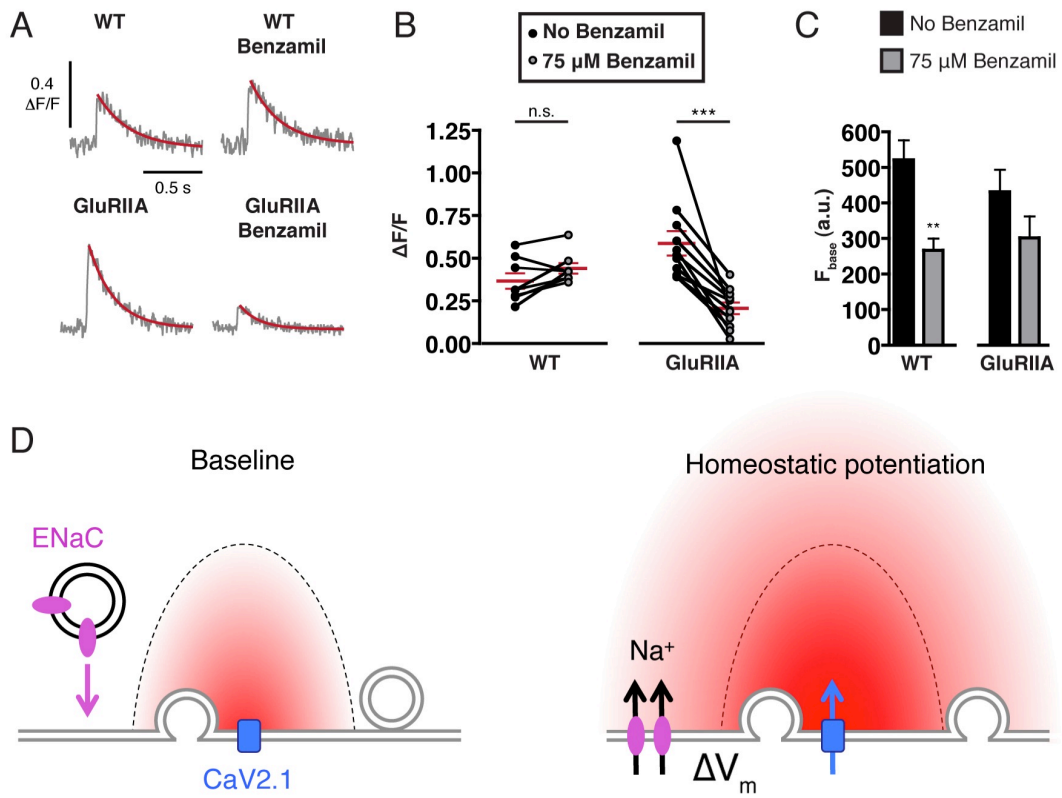


**Figure 9: Analysis of baseline neurotransmission of two *ppk11* mutations *in trans*.**

mEPSP amplitude, EPSP amplitude, quantal content, and muscle input resistance for wild type (WT), *ppk11<sup>Mi</sup>/ppk11<sup>PBac</sup>*, *ppk11<sup>Mi</sup>/+* and *ppk11<sup>PBac</sup>/+* at 0.35mM extracellular calcium. *ppk11<sup>Mi</sup>/ppk11<sup>PBac</sup>* and *ppk11<sup>Mi</sup>/+* have a reduction in mEPSP amplitude compared to wild type ( $p > 0.001$  and  $p > 0.01$ , respectively), and *PPK11<sup>PBac</sup>/+* does not ( $p = 0.101$ ). The EPSP amplitude is decreased in *ppk11<sup>Mi</sup>/ppk11<sup>PBac</sup>* ( $p < 0.001$ ), unchanged in *ppk11<sup>Mi</sup>/+* ( $p = 0.710$ ) and slightly increased in *ppk11<sup>PBac</sup>/+* ( $p < 0.05$ ). Quantal content is unchanged in all conditions ( $p = 0.086$ ,  $p = 0.139$ , and  $p = 0.366$ , for *ppk11<sup>Mi</sup>/ppk11<sup>PBac</sup>*, *ppk11<sup>Mi</sup>/+* and *ppk11<sup>PBac</sup>/+*, respectively). Muscle input resistance is decreased in *ppk11<sup>Mi</sup>/ppk11<sup>PBac</sup>*, *ppk11<sup>Mi</sup>/+* ( $p < 0.001$  and  $p < 0.01$ , respectively), and unchanged in *ppk11<sup>PBac</sup>/+* ( $p = 0.277$ ). Data for *PPK11<sup>PBac</sup>/+* are identical to that in Figure 2D.

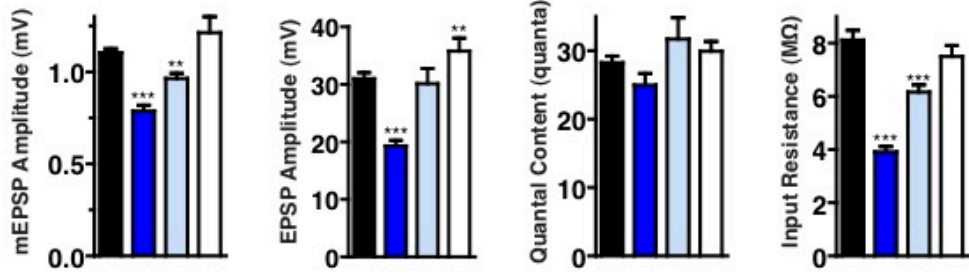


**Figure 10: The organization of the *ppk11/16* locus is conserved across multiple *Drosophila* species.**

The *ppk11* (blue) and *ppk16* (red) gene locus from *Drosophila melanogaster* is shown on top, with exons represented by solid blocks. Below are VISTA plots (Frazer et al., 2004) showing the % alignment across a 100 base pair window to different *Drosophila* species, where filled regions represent exons, and hollow regions represent introns.

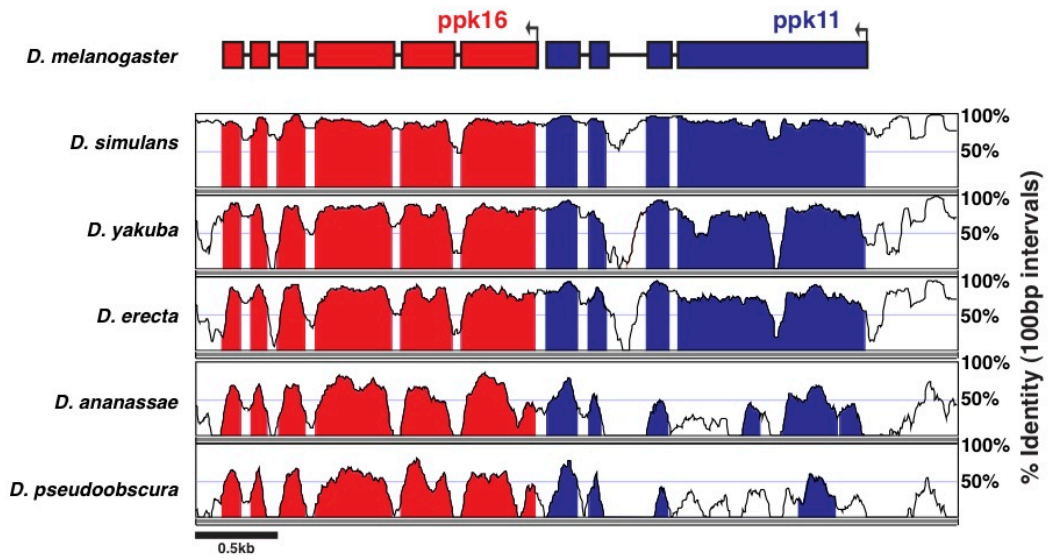


**Figure 11: Benzamil has separable effects on mEPSP amplitude and synaptic transmission.**

**A)** mEPSP amplitude and QC are expressed as % change from the baseline when treated with 50 $\mu$ M Benzamil. In all genotypes mEPSP amplitude is significantly decreased ( $p < 0.001$ ) and there is no change in QC in any condition.

**B)** Benzamil concentration is plotted on a semi-log plot against the % of the maximum block in PhTx induced homeostasis, as measured by % restoration of the baseline EPSP after the addition of PhTx (grey). EC50 value is 32  $\mu$ M.



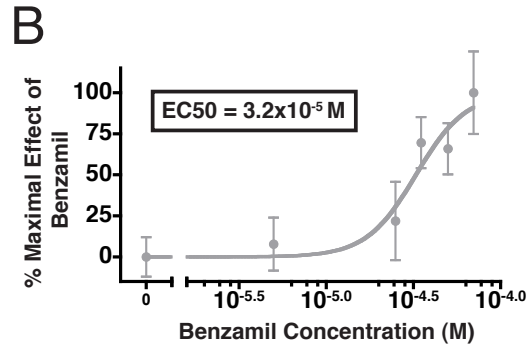
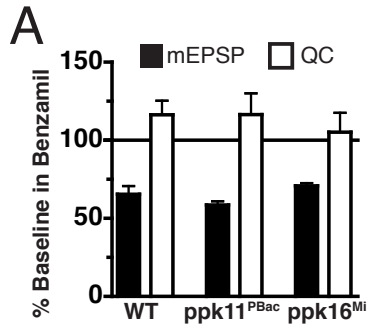


**Figure 12: EIPA blocks synaptic homeostasis.**

**A)** Percent change of mEPSP amplitude and quantal content (QC) in the presence of PhTx and varying concentrations of EIPA. mEPSP amplitude is decreased by PhTx in all conditions ( $p < 0.001$ ). QC is increased in WT and 10 $\mu$ M EIPA ( $p < 0.001$ ), but not in the presence of 20 $\mu$ M or 50 $\mu$ M EIPA ( $p = 0.606$  and  $p = 0.687$ , respectively).

**B)** mEPSP amplitude and QC are expressed as % change from the baseline when treated with 20 $\mu$ M EIPA. In both WT and *PPK11<sup>Mi</sup>* quantal content is significantly decreased ( $p < 0.01$ ) and there is no change in mEPSP amplitude ( $p = 0.157$  and  $p = 0.060$ . for WT and *PPK11<sup>Mi</sup>*, respectively).

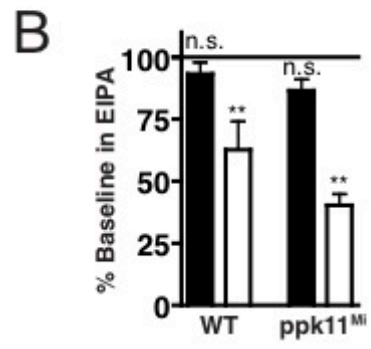
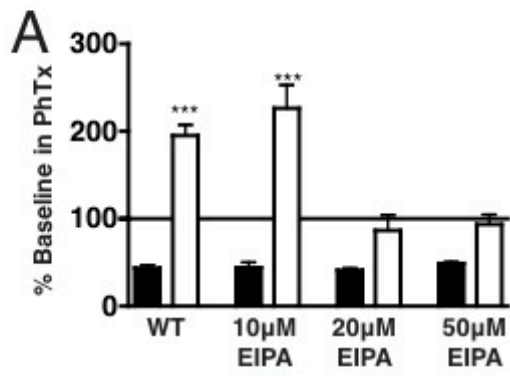


**Table 1. Specific mutations screened**

Gene Abbreviation	Gene Name	Stock Screened	N without PhTx	N with PhTx
CG32843	CG32843	PBac{WH}CG32843[f05546]	4	5
CcapR	Cardioacceleratory peptide receptor	PBac{WH}f01987	12	6
Rab3-GAP	Rab3 GTPase-activating protein	PBac{PB}rab3-GAP[c04953]	10	9
Syx17	syntaxin 17	w[1118]; PBac{w[+mC]=WH}Syx17[f01971]	3	6
CG1909	CG1909	y[1] w[1118]; PBac{y[+mDint]=3HPy[+]}C024	15	5
CG3885	CG3885	y[1] w[67c23]; P{w[+mC] y[+mDint2]=EPgy2}EY02200	10	5
lqf	liquid facets	y[1] w[67c23]; P{y[+mDint2] w[BR.E.BR]=SUPor- P}lqf[KG03016] ry[506]	9	11
ppk10	pickpocket10	PBac{RB}e00406	4	4
usnp	ubisnap	PBac{WH}usnp[f03352]	4	4
rab3	Rab-protein 3	PBac{PB}Rab3[c04828]	4	4
CG8743	CG8743	y[1]; P{y[+mDint2] w[BR.E.BR]=SUPor- P}LCBP1[KG07819] ry[506]/TM3, Sb[1] Ser[1]	9	3
Dat	dopamine N acetyltransferase	bw[1] Dat[lo]	14	7
ppk11	pickpocket11	w[1118]; PBac{w[+mC]=WH}ppk11[f02053]	11	14
CG10465	CG10465	w[1118]; P{w[+mC]=XP}CG10465[d00266]	3	4
CG12344	CG12344	w[1118]; PBac{w[+mC]=RB}CG12344[e040 18]	9	5
gad1	glutamic acid decarboxylase 1	y[1] w[67c23]; P{y[+mDint2] w[BR.E.BR]=SUPor- P}Gad1[KG01955] ry[506]	8	7
Dyb	dystrobrevin-like	y[1] w[67c23]; P{w[+mC] y[+mDint2]=EPgy2}Dyb[EY01099]	7	3
nAchRa-18c	nicotinic AChR alpha 18C	y[1] w[67c23] P{w[+mC] y[+mDint2]=EPgy2}nAcRalpha- 18C[EY10801]	6	4
arf51f	ADP ribosylation factor 51F	y[1] w[67c23]; P{y[+mDint2] w[BR.E.BR]=SUPor- P}Arf51F[KG02753]	13	8
CG32792	CG32792	y[1] P{y[+mDint2] w[BR.E.BR]=SUPor- P}CG32792[KG10039]	10	8
canB2	Calcineurin B2	w[1118]; P{w[+mC]=EP}CanB2[EP774]	12	6
CirI	CirI	y[1] w[67c23]; P{w[+mC] y[+mDint2]=EPgy2}CirI[EY12930]	8	4

**Table 2. Non-normalized values for electrophysiology measurements.**

Fig.	Genotype	[Ca <sup>2+</sup> ] <sub>e</sub> (mM)	PhTx	mEPSP (mV)	EPSP (mV)	Quantal Content	IR	n	mEPSP freq.
1d	WT	0.35	-	0.98±0.04	30.2±1.3	31.3±1.7	11.2±0.9	18	3.6±0.4
1c,d	PPK11 <sup>Mi</sup>	0.35	-	0.93±0.03	18.2±2.4	20.2±2.9	6.3±0.4	12	1.5±0.1
1c,d	PPK11 <sup>Precise</sup>	0.35	-	1.00±0.04	20.1±2.0	20.2±1.9	5.6±0.4	16	2.5±0.2
1d	WT	0.35	+	0.44±0.06	30.3±1.7	77.3±13.1	13.3±1.2	6	2.2±0.3
1c,d	PPK11 <sup>Mi</sup>	0.35	+	0.38±0.03	8.7±2.0	22.6±4.5	8.1±0.6	13	1.1±0.1
1c,d	PPK11 <sup>Precise</sup>	0.35	+	0.37±0.01	21.8±2.3	59.2±6.7	6.2±0.3	14	1.4±0.1
1d	WT	0.3	-	1.01±0.05	27.3±1.5	28.0±1.7	9.3±0.3	23	3.5±0.2
1d	PPK11 <sup>PBac</sup>	0.3	-	0.78±0.04	17.9±1.8	23.6±2.4	3.7±0.2	16	2.8±0.2
1d	PPK11 <sup>PBac</sup> / Df	0.3	-	0.78±0.05	14.3±1.4	19.2±2.1	4.4±0.3	14	2.3±0.2
1d	W118	0.3	+	0.51±0.02	24.4±1.6	49.1±3.4	9.5±0.4	18	3.5±0.2
1d	PPK11 <sup>PBac</sup>	0.3	+	0.41±0.03	8.1±1.3	19.5±2.6	3.7±0.4	12	2.0±0.1
1d	PPK11 <sup>PBac</sup> / Df	0.3	+	0.41±0.02	8.0±1.1	20.2±2.9	4.6±0.3	12	2.0±0.2
3a,b	WT	0.35	-	1.11±0.05	28.7±1.4	26.7±1.6	8.9±0.4	21	3.5±0.2
3a,b	PPK11 RNAi MN	0.35	-	1.06±0.07	30.8±2.8	29.9±2.6	7.9±0.5	11	3.4±0.3
3b	PPK11 RNAi Muscle	0.35	-	1.04±0.06	32.9±2.3	33.0±3.1	10.4±0.3	10	3.4±0.2
3b	dnPPK11 MN	0.35	-	0.96±0.03	33.7±1.7	35.5±2.1	8±0.3	12	3.0±0.1
3a,b	WT	0.35	+	0.48±0.02	29.6±1.3	65.1±4.5	8.6±0.3	27	3.3±0.2
3a,b	PPK11 RNAi MN	0.35	+	0.41±0.03	12.6±1.6	32.0±4.5	8.5±0.5	10	2.6±0.4
3b	PPK11 RNAi Muscle	0.35	+	0.44±0.03	27.9±2.3	63.0±5.0	10.4±0.4	9	3.0±0.2
3b	dnPPK11 MN	0.35	+	0.47±0.03	21.2±2.5	45.3±4.6	8.2±0.3	15	2.2±0.1
4a,b	WT	0.35	-	1.00±0.05	30.8±1.3	32.0±1.9	11.0±0.8	22	3.1±0.2
4a,b	PPK16 <sup>Mi</sup>	0.35	-	1.12±0.04	22.2±2.0	20.1±1.9	8.3±0.6	13	1.5±0.2
4b	PPK16 <sup>166</sup>	0.35	-	1.33±0.10	26.9±3.8	23.0±3.9	8.5±0.5	13	1.3±0.2
4a,b	WT	0.35	+	0.43±0.03	30.6±1.7	75±7.0	9.9±0.9	15	3.2±0.4
4a,b	PPK16 <sup>Mi</sup>	0.35	+	0.56±0.03	10.3±1.5	18.8±2.6	7.6±0.4	11	1.3±0.1
4b	PPK16 <sup>166</sup>	0.35	+	0.54±0.07	17.3±3.5	32.3±7.1	8.5±0.8	10	0.8±0.1
4d,e	WT	0.35	-	1.12±0.04	28.1±2.5	25.0±1.9	9.0±0.5	11	3.6±0.3
4d,e	PPK16 RNAi MN	0.35	-	0.89±0.04	24.3±2.6	28.0±3.2	5.4±0.3	12	2.6±0.3
4e	PPK16 RNAi Muscle	0.35	-	0.98±0.04	30.2±2.0	31.4±2.6	8.3±0.5	10	2.6±0.2
4e	PPK19 RNAi MN	0.35	-	1.11±0.03	36.6±1.9	33.2±2.1	8.3±0.2	10	4.5±0.2
4d,e	WT	0.35	+	0.49±0.02	29.2±1.6	63.1±5.4	9.2±0.5	18	3.1±0.3
4d,e	PPK16 RNAi MN	0.35	+	0.44±0.04	14.9±1.6	36.7±5.4	6.8±0.3	13	1.6±0.1
4e	PPK16 RNAi Muscle	0.35	+	0.41±0.02	22.3±2.2	55.5±5.6	9.4±0.5	11	1.9±0.2
4e	PPK19 RNAi MN	0.35	+	0.48±0.04	28.9±3.3	61.1±6.3	10.1±0.4	9	2.7±0.2
6a,b	WT	0.35	-	1.07±0.07	31.6±1.4	30.6±2.1	9.7±0.5	11	2.6±0.2
6a,b	GluRIIA <sup>SP16</sup>	0.35	-	0.32±0.01	16.5±1.4	53.1±5.2	10.6±0.4	20	2.5±0.2
6a,b	PPK11 <sup>PBac</sup>	0.35	-	0.87±0.03	26.5±1.5	30.7±1.8	5.3±0.3	14	2.7±0.2
6a,b	PPK11 <sup>PBac</sup> GluRIIA <sup>SP16</sup>	0.35	-	0.41±0.03	13.5±1.1	35.2±4.1	10.8±.6	13	1.8±0.2
6e	WT	0.35	-	1.06±0.07	32.9±2.2	32.3±2.9	8.7±0.5	14	3.4±0.3

6e	+, PPK11 <sup>PBac</sup> /+,+	0.35	-	1.21±0.09	35.8±2.3	29.9±1.4	7.5±0.4	10	4.3±0.3
6e	PPK16 <sup>Mi</sup> ,+,+,+	0.35	-	0.99±0.05	26.7±2.5	26.9±2.3	7.8±0.3	12	2.6±0.2
6e	+, PPK11 <sup>PBac</sup> / PPK16 <sup>Mi</sup> , +	0.35	-	0.88±0.04	26.7±1.9	31.7±2.8	4.7±0.5	18	2.8±0.2
6E,7 G	PPK16 <sup>Df</sup> , PPK11 <sup>Df</sup> / +,+	0.35	-	1.14±0.08	33.7±2.1	30.5±2.2	8.1±1.2	12	4.1±0.3
6e	WT	0.35	+	0.4±0.02	28.8±2.1	75.5±7.0	8.2±0.3	16	3.4±0.3
6e	+, PPK11 <sup>PBac</sup> /+,+	0.35	+	0.47±0.03	32.5±2.7	70.6±5.8	7.3±0.4	10	2.6±0.2
6e	PPK16 <sup>Mi</sup> ,+,+,+	0.35	+	0.46±0.03	21.0±3.1	45.1±6.0	8.6±0.3	13	1.7±0.1
6e	+, PPK11 <sup>PBac</sup> / PPK16 <sup>Mi</sup> , +	0.35	+	0.37±0.02	13.5±1.9	39.3±7.2	4.9±0.2	14	1.7±0.1
6E,7 G	PPK16 <sup>Df</sup> , PPK11 <sup>Df</sup> / +,+	0.35	+	0.42±0.03	25.3±3.4	60.7±7.6	5.7±0.2	10	2.9±0.3
7a,b	WT	0.35	-	1.11±0.06	34.3±1.7	31.0±1.0	8.8±0.3	7	3.9±0.2
7a,b	WT 50µM Benzamil	0.35	-	0.73±0.05	23.5±1.9	33.0±3.4	10.3±0.4	12	4.1±0.5
7a,b	WT 50µM Benzamil Washout	0.35	-	0.90±0.02	32.0±1.3	35.4±1.2	8.5±0.4	9	3.8±0.2
7a,b	WT	0.35	+	0.4±0.03	27.6±1.8	71.3±7.0	10.1±0.4	10	3.7±0.2
7a,b	WT 50µM Benzamil	0.35	+	0.33±0.02	13.7±1.8	42.1±5.1	11.7±0.3	12	3.5±0.3
7a,b	WT 50µM Benzamil Washout	0.35	+	0.44±0.03	27.3±3.2	66.5±9.1	9.5±0.3	12	3.3±0.2
7d	WT	0.35	-	1.06±0.05	30.5±2.3	28.8±1.9	11.2±0.2	9	2.5±0.1
7d	WT	0.35	+	0.56±0.03	26.9±1.8	49.2±4.9	11.0±0.9	9	2.9±0.4
7d	WT 50µM Benzamil	0.35	-	0.92±0.07	24.6±3.5	27.3±3.1	9.9±0.4	6	4.3±0.4
7d	WT PhTx 50µM Benzamil	0.35	+	0.38±0.03	9.3±1.1	25.0±2.8	9.6±0.5	11	2.7±0.2
7e	WT	0.5	-	1.13±0.05	40.2±0.8	36.4±1.6 (76.6±4.4)	9.8±0.3	12	3.9±0.4
7e	GluRIIA <sup>SP16</sup>	0.5	-	0.32±0.02	30.4±2.5	96.8±9.0 (163±22)	11.2±0.3	11	2.0±0.2
7e	WT 50µM Benzamil	0.5	-	0.70±0.03	34.9±1.0	50.5±2.1 (92.4±5.3)	8.8±0.4	15	4.9±0.3
7e	GluRIIA <sup>SP16</sup> 50µM Benzamil	0.5	-	0.26±0.01	18.3±1.3	70.8±4.9 (94.7±8.4)	12.3±0.5	15	2.4±0.3
7g	WT 25µM Benzamil	0.35	-	0.71±0.05	28.2±1.9	41.1±3.8	9.4±0.5	8	4.1±0.3
7g	WT 25µM Benzamil	0.35	+	0.33±0.02	22.5±3.3	68.5±10.4	10.5±0.6	7	2.5±0.3
7g	PPK16 <sup>Df</sup> , PPK11 <sup>Df</sup> / +,+ 25µM Benzamil	0.35	-	0.72±0.02	24.6±3.3	24.7±2.6	6.5±0.3	10	3.2±0.3
7g	PPK16 <sup>Df</sup> , PPK11 <sup>Df</sup> / +,+ 25µM Benzamil	0.35	+	0.35±0.03	14.1±2.7	38.1±5.9	8.8±1.0	13	2.6±0.2

**Abbreviations:** MN = motoneuron; IR = input resistance of muscle cell; n = sample size, number of recordings; Fig. = the figure panel to which the data refer; [Ca<sup>2+</sup>]<sub>e</sub> = extracellular calcium concentration in mM.

**Note:** In data sets where quantal content is corrected for non-linear summation the uncorrected data are reported and the corrected values appear parenthetically below.

### **Chapter 3:**

**Pickpocket18 does not contribute to NMJ growth or function.**

## SUMMARY

In the previous chapter we provided evidence that *ppk11* and *ppk16* encode two DEG/ENaC subunits that are necessary for synaptic homeostasis, and we presented a model for how they function at the synapse to potentiate release. Mammalian ENaCs are heterotrimeric channels. Since PPK11 participates in similar processes as mammalian ENaCs, we hypothesized that PPK11 would also share its subunit stoichiometry with mammalian ENaCs. We, therefore, sought a third DEG/ENaC subunit that could be part of a channel with PPK11 and PPK16. Here we examine the DEG/ENaC subunit gene, *pickpocket18* (*ppk18*). *ppk16* was identified as a gene required for synaptic homeostasis based on its proximity to *ppk11*. *ppk11*, *ppk16* and *ppk18* are located in series, making *ppk18* a likely third subunit of a channel with *ppk11* and *ppk16*. Surprisingly, we found that *ppk18* transcription is regulated independently from *ppk11* and *ppk16*, and that it is not necessary for the rapid induction of synaptic homeostasis, or for normal anatomical NMJ development. This indicates that PPK18 is not the third subunit of a PPK11 and PPK16 containing DEG/ENaC channel.



## INTRODUCTION

Homeostatic plasticity is believed to constrain changes that occur during learning, to create a plastic yet stable nervous system (Marder and Goaillard, 2006; Davis 2006). At the *Drosophila* NMJ, in response to a decrease in postsynaptic glutamate receptor sensitivity, there is an increase in neurotransmitter release that precisely offsets the change in receptor sensitivity, thereby restoring muscle activity (Petersen et al., 1997; Frank et al., 2006). The increase in release relies on an increase in action-potential evoked calcium influx (Müller and Davis, 2012). We have provided evidence in the previous chapter that DEG/ENaC channel subunits PPK11 and PPK16 are required for synaptic homeostasis at the *Drosophila* NMJ, and that they enhance presynaptic calcium influx by modulating the presynaptic resting potential.

DEG/ENaC channels are found in many species and are all predicted to be composed of three subunits (Jasti et al., 2007; Eastwood et al., 2012). Some DEG/ENaC channels subunits form homomeric channels, some form heteromeric channels, and others are capable of either. Mammalian ENaC channels preferentially form heteromers, demonstrated during their initial cloning and expression in oocytes (Canessa et al., 1994). It is unknown whether *Drosophila* PPK channel subunits form homomers or heteromers, since no members of this family have been successfully expressed in a heterologous system. There are 31 PPK genes in the *Drosophila* genome, and there is likely no single rule governing channel assembly (Zelle et al., 2013).

The possibility that PPK11 and PPK16 form heteromers with a third subunit is compelling because mammalian ENaCs are heteromers and PPK11 has ENaC-like functions (including salt taste, and airway fluid clearance; Liu et al., 2003a; Liu et al., 2003b). This scenario was supported by the genomic arrangement of *ppk11* and *ppk16*, which sit in the same locus as a third pickpocket subunit, *ppk18*. We have shown that *ppk11* and *ppk16* are transcribed as an operon-like unit that is upregulated during the sustained expression of synaptic homeostasis (see Chapter 2). It seemed likely that the transcriptional regulation of *ppk11* and *ppk16* would be shared with *ppk18*, and that PPK18 would be a third subunit of a DEG/ENaC channel.

*ppk18* has no known function, and has only been recently identified as a gene. We determined that despite the serial genomic arrangement of *ppk11*, *ppk16* and *ppk18*, *ppk18* is transcribed independently from the other two genes, and the transcription of *ppk18* is not upregulated during synaptic homeostasis. We also found that multiple different mutations in *ppk18* do not block synaptic homeostasis or disrupt normal NMJ development. These findings together support the conclusion that PPK18 does not form a channel with PPK11 and PPK16, and underscores the specificity of PPK11 and PPK16 regulation during synaptic homeostasis

## RESULTS

### ***ppk18* is regulated independently from *ppk11* and *ppk16*.**

We identified PPK18 as a possible third subunit of a DEG/ENaC channel with PPK11 and PPK16 due to its proximity within the genome (Figure 1). *ppk18* and *ppk16* are separated by only 158 basepairs. By comparing the sequences of *ppk18* across multiple *Drosophila* species, we see that the placement of these three genes in series is highly conserved across approximately 25 million years of evolutionary time (Figure 1). The serial placement of these three genes across multiple *Drosophila* species suggested that PPK18 might function together with PPK11 and PPK16.

Two genes are located within an intron of *ppk18*, and are predicted to be transcribed from the opposite DNA strand (Figure 1). These genes, *CG4017* and *CG17633*, currently have no known or predicted function. A *ppk18* transcript that spans these genes has been previously reported (Zelle et al., 2013). We were able to confirm this finding by generating primers targeted to the ends of *ppk18*, and running PCR with wild-type cDNA as a template (data not shown).

We previously saw that *ppk11* and *ppk16* are cotranscribed as a single mRNA that is upregulated during the sustained expression of synaptic homeostasis, induced by a mutation in the postsynaptic glutamate receptor subunit *GluRIIA* (see Chapter 2). By performing PCR using WT cDNA as a template, we were able to isolate individual *ppk11*, *ppk16*, and *ppk18* transcripts. However, we were unable to isolate a transcript that spanned *ppk18* and *ppk11*

or *ppk16* together (data not shown). This indicates that unlike *ppk11* and *ppk16*, which are cotranscribed, *ppk18* is transcribed independently from these other subunits.

We previously found that *ppk11* and *ppk16* are upregulated during the sustained expression of synaptic homeostasis, suggesting that they are not merely required for synaptic homeostasis, but likely contribute to the homeostatic potentiation of release. To determine if *ppk18* is also upregulated in *GluRIIA<sup>SP16</sup>* mutant animals, we performed QPCR using primers targeted against *ppk18*. We compared cDNA from the heads of wild type and *GluRIIA<sup>SP16</sup>* mutant larvae, and found no difference in transcript levels between the two genotypes (Figure 2a). Taken together, these findings indicate that *ppk18* is transcribed separately from *ppk11* and *ppk16* and, of the genes in this locus, only *ppk11* and *ppk16* are upregulated during the sustained expression of synaptic homeostasis.

### **Mutations in *ppk18* do not block synaptic homeostasis.**

In order to determine if *ppk18* is necessary for synaptic homeostasis we used multiple reagents that would be predicted to disrupt *ppk18* function (Figure 2b). These include: 1) A transposon in the fourth coding exon that is likely to be strong loss-of-function mutation. This transposon is a Minos-mediated integration cassette (MiMiC; Venken et al., 2011) transposon and will be called *PPK18<sup>MiMiC</sup>*. 2) A second transposon in the third coding exon. This transposon was a Minos(ET1; Metaxakis et al, 2005) line termed *PPK18<sup>Mi</sup>*. This line was outcrossed

to wild type ( $w^{1118}$ ) for 6 generations to create a comparable genetic background, and will be referred to as *PPK18<sup>Mi</sup> OutX6*. 3) An RNAi line targeted against *ppk18* (*UAS-PPK18-RNAi*). 4) A deficiency chromosome (Df) that uncovers the entire locus containing *ppk11*, *ppk16* and *ppk18*.

In order to assay for the rapid induction of synaptic homeostasis PhTx was applied for 10 minutes, as described in Chapter 2. We found that there was robust synaptic homeostasis after the addition of PhTx in both the homozygous *PPK18<sup>Mi</sup> OutX6* animals and the homozygous *PPK18<sup>MiMic</sup>* mutant animals, as indicated by an increase in quantal content (Figure 2C). We additionally tested an *UAS-PPK18-RNAi* line driven by the motorneuron specific driver *OK371-Gal4* (Mahr and Aberle, 2005) and did not observe a block in synaptic homeostasis. The effect on this RNAi line on *ppk18* transcript levels was not determined and we cannot rule out the possibility that the RNAi line is not effectively reducing *ppk18* RNA levels. However, taken together with the data from the two transposon insertions, we can conclude that the gene *ppk18* is dispensable in synaptic homeostasis.

We did not observe any major changes in baseline synaptic transmission in any of the *ppk18* mutations (Table 1). There was a small but significant increase in mEPSP amplitude in *PPK18<sup>Mi</sup> OutX6* and *OK371-Gal4 > UAS-PPK18-RNAi* ( $p < 0.05$  for both). Since this change is not consistent across all mutations we conclude that PPK18 does not contribute to baseline synaptic transmission.

***ppk18* does not participate in anatomical NMJ development.**

In order to determine if *ppk18* contributes to anatomical NMJ development we examined the NMJ of muscle 4, which is situated in the middle of the muscle making it ideal for visualizing all active zones within each NMJ by staining for the presynaptic active-zone associated protein Bruchpilot (Brp; Figure 3; Davis et al., 1997; Wagh et al., 2006). We examined animals homozygous for the *ppk18<sup>Mi</sup>* mutation as well as animals with *ppk18<sup>Mi</sup>* in *trans* to a deficiency chromosome that uncovers the *ppk18* locus (*ppk18<sup>Mi</sup>/Df*). There was no significant change in NMJ area (determined by staining for the PSD-95 homologue Discs Large; DLG), the number of active zones per NMJ, or the active zone density (calculated by dividing active zone number by NMJ area). We saw a small but significant reduction in bouton number at muscles 6/7, in segments 2 and 3, the muscles at which all of our recordings are made ( $p < 0.05$ ). Although significant, this is a relatively minor change. Taken together this data shows that *ppk18* does not play a major role in NMJ development.

## DISCUSSION

Due to its genomic location *ppk18* was an attractive candidate homeostasis gene and potential third subunit of a channel formed by PPK11 and PPK16. We found that despite the proximity to *ppk11* and *ppk16*, *ppk18* is transcribed separately from these other channel subunits and it is not upregulated during the sustained expression of synaptic homeostasis. Mutations in *ppk18* do not block the rapid induction of synaptic homeostasis, indicating that PPK18 does not function with PPK11 and PPK16 during synaptic homeostasis. The serial placement of *ppk11*, *ppk16* and *ppk18* made *ppk18* the best candidate homeostasis gene of the 31 members of the pickpocket family. However chemoreceptor subunits are commonly arranged in clusters such as the *ppk11/16/18* locus (Gardiner et al., 2008) and act in different processes despite genomic proximity.

It is possible that other pickpocket subunits are necessary for synaptic homeostasis. So far we have found that neither *ppk18* nor *ppk19* (see chapter 2) are necessary for synaptic homeostasis. While it is possible that a third subunit is required for PPK11 and PPK16 to form a channel and that assembly is similar to mammalian ENaC, it is equally likely that only *ppk11* and *ppk16* are necessary for channel assembly. There could be a PPK11 and PPK16 containing channel that includes only those two subunits, or PPK11 and PPK16 might form two homomeric channels with nonredundant functions in synaptic homeostasis. In order to determine the makeup of the DEG/ENaC that participates in synaptic

homeostasis we will need to screen through mutations in all 31 pickpocket subunit genes to determine if they are necessary for synaptic homeostasis. We will also need to use a heterologous expression system to determine the subunits required to form a functional channel. We have attempted to express these subunits in *Xenopus oocytes*, but were unable to isolate a Benzamil sensitive current (data not shown).

### **A Diversity of PPK gene function in *Drosophila***

Of the 31 pickpocket genes in *Drosophila*, most have not been characterized in detail (Ben-Shahar, 2011; Zelle et al., 2013). The pickpocket family was named for the putative role of these channels as mechanosensors. However, most characterized pickpocket family members are ascribed other functions. PPK1 is a potential exception, as it is expressed in class IV multidendritic sensory neurons and mutants in *ppk1* have altered locomotor patterns, indicating disrupted mechanosensation or proprioception (Ainsley et al, 2003). The *ppk1* mutants continue to respond to touch although mechanical nociception is impaired and a recent study identifies PPK1 as a pH-sensitive ASIC-like channel (Adams et al, 1998; Ainsley et al, 2003; Boiko et al., 2012; Kim et al., 2012). The idea that PPK11 and PPK16 could form a mechanosensitive channel is appealing, since the synaptic boutons are imbedded within muscle folds and the entire synapse moves when the muscle twitches after neurotransmission. Muscle movement could feedback into the homeostat through



mechanosensitive channels and could be a mechanism by which the efficacy of neurotransmitter release is sensed. It should be noted that evoked transmission is not required for the rapid induction of synaptic homeostasis, indicating that full muscle contraction cannot be the primary means to sense activity. Additionally our pharmacological data shows that PPK11 and PPK16 are not the primary "sensors" of activity (see Chapter 2). It remains possible that muscle movement could act as an added mechanism to sense and tune release by direct mechanical activation of PPK11 and PPK16. Although not essential to the rapid induction of synaptic homeostasis, this could contribute later in the maintenance of the homeostatic response, or it could provide the system with additional sensitivity.

Other members of the pickpocket family are chemosensory receptors. PPK28 has been identified as a water-sensing channel (Cameron et al, 2010; Chen et al, 2010). A series of recent papers describe a new role for pickpocket channels in courtship behavior, where PPK23, PPK25, and PPK29 function in sensory neurons that respond to cuticular hydrocarbons, which act as courtship pheromones (Lu et al, 2012, Thistle et al, 2012, Toda et al, 2012, Liu et al., 2012). These channels likely act directly as pheromone receptors. It is worth noting that there is a family of DEG/ENaCs that are directly gated by peptides. These include FaNaC in mollusks (Belkin and Abrams, 1993; Furukawa et al, 2006; Lingueglia et al, 2006) and HyNaC in Hydra (Golubovic et al, 2007), which are both gated by FMRFamide peptides. There has not been a channel found in

*Drosophila* that is directly peptide gated, although, its existence remains a possibility. There will likely be many more ligands and functions for DEG/ENaCs discovered as research on this large ion channel family progresses.

It is possible that PPK11 and PPK16 are ligand gated, or that they are modulated by ligands. We have provided a model in which they regulated by trafficking, based on their similarity to mammalian ENaCs. An alternative model is that they are ligand gated and only open after induction of synaptic homeostasis. They could respond to a novel ligand, or to one of the ligands that activates other pickpocket channels. They might also respond to neuropeptides such as FMRFamides, which would be in line with the function of neuropeptides as potent neuromodulators in other systems. This would not change the basic model for how PPK11 and PPK16 modulate resting membrane voltage to potentiate release during synaptic homeostasis.

Lastly, the DEG/ENaC superfamily is expanded in flies relative to mammals, and some of the pickpocket channels may not have direct functional orthologues in mammals. Some of the *Drosophila* ligands may not be used by mammals, while in other cases the varied functions of invertebrate DEG/ENaCs may have converged onto fewer mammalian DEG/ENaC channels. For example, mammalian ASIC channels can be modulated by RFamide peptides (Lingueglia, 2006). When looking into whether mammalian DEG/ENaCs contribute to similar processes in mammals, it may be worth studying multiple DEG/ENaC subfamilies.

## FIGURES AND TABLES

### **Figure 1: Conservation of the *ppk11/16/18* gene locus across multiple *Drosophila* species.**

Gene conservation map showing the locus containing *ppk11*, *ppk16*, and *ppk18* (green) from *Drosophila melanogaster* is shown on top, with exons represented by solid blocks. Below are VISTA plots (Frazer et al., 2004) showing the % alignment across a 100 base pair window to different *Drosophila* species, where filled regions represent exons, and hollow regions represent introns. Two genes run in the opposite direction of *ppk18*, dividing the coding region (pale grey). These genes are *CG4017* and *CG17633*.

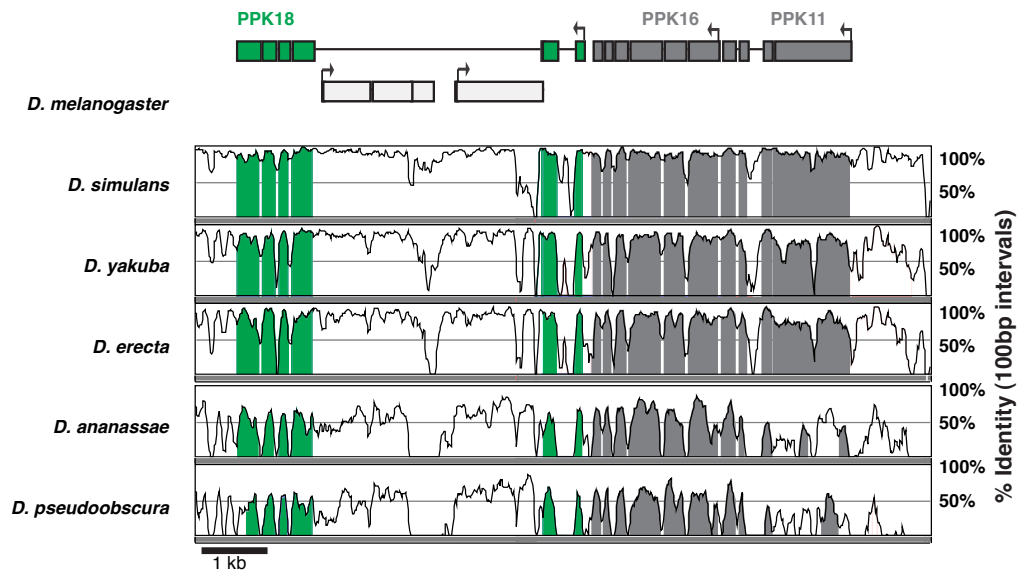


**Figure 2: *ppk18* mutations do not disrupt synaptic homeostasis.**

**A)** *ppk18* mRNA is unchanged in the *GluRIIA<sup>SP16</sup>* mutant. Experiment was performed in triplicate. **B)** A map of the *ppk18* gene locus, showing exons in green. Transposons are represented as arrowheads. The deficiency uncovering this region is shown in grey. **C)** The percent change in mEPSP (solid bars) and quantal content (QC; open bars) in the presence of PhTx relative to baseline for each genotype recorded in the absence of PhTx. All conditions show a significant decrease in mEPSP amplitude ( $p < 0.001$ ). *WT*, *ppk18<sup>MiMic</sup>*, *OK371-gal4/UAS-ppk18RNAi* (*OK371 > ppk18 RNAi*), and *ppk18<sup>Mi</sup> Out6X* all show an increase in quantal content after PhTx application ( $p < 0.001$ ). All data are recorded in 0.3-0.35mM extracellular calcium. Data are presented as average  $\pm$  SEM. Comparisons are made according to a Student's t-test. **D)** Sample mEPSP and EPSP traces for *WT* (top) and *ppk18<sup>Mi</sup> Outcrossed 6X* (bottom) with and without PhTx (right and left, respectively).

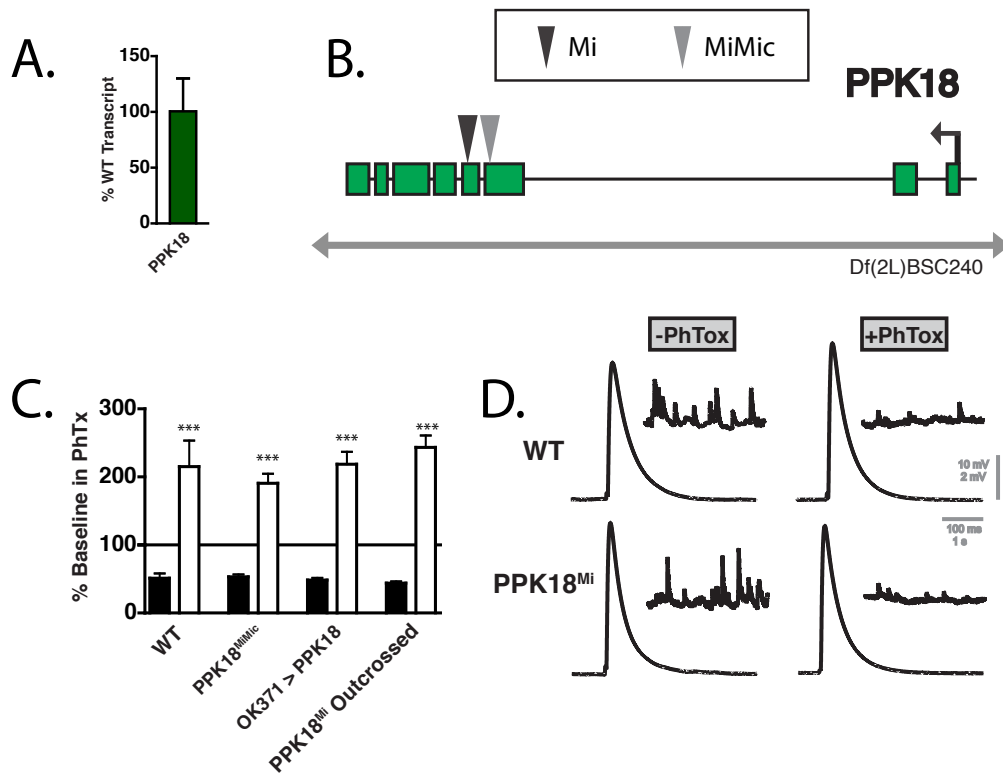


**Figure 3: *PPK18<sup>Mi</sup>* does not alter synapse gross morphology.**

**A)** Representative images of from muscle 4 of *WT*, *ppk18<sup>Mi</sup>*, and *PPK18<sup>Mi</sup>/Df* mutant animals stained for BRP (green), the DLG (red), and HRP (blue). **B)** The number of active zones per NMJ at muscle 4 is shown as the % *WT* active zones (measured as individual Brp puncta). Active zone number is not different from *WT* in either genotype. **C)** The area of the NMJ at muscle 4 is shown as %*WT* area, as measured by DLG staining. It is not significantly different from wild type in either genotype. **D)** The active zone density at muscle 4 is shown as % *WT* active zone density. There is no significant difference in either genotype. **E)** The number of boutons per NMJ at muscles 6/7 in segment 2 and segment 3 is expressed as percent %*WT* bouton number. There is a slight but significant decrease from wild type in both *PPK18<sup>Mi</sup>* and *PPK18<sup>Mi</sup>/Df* ( $p < 0.05$ ).

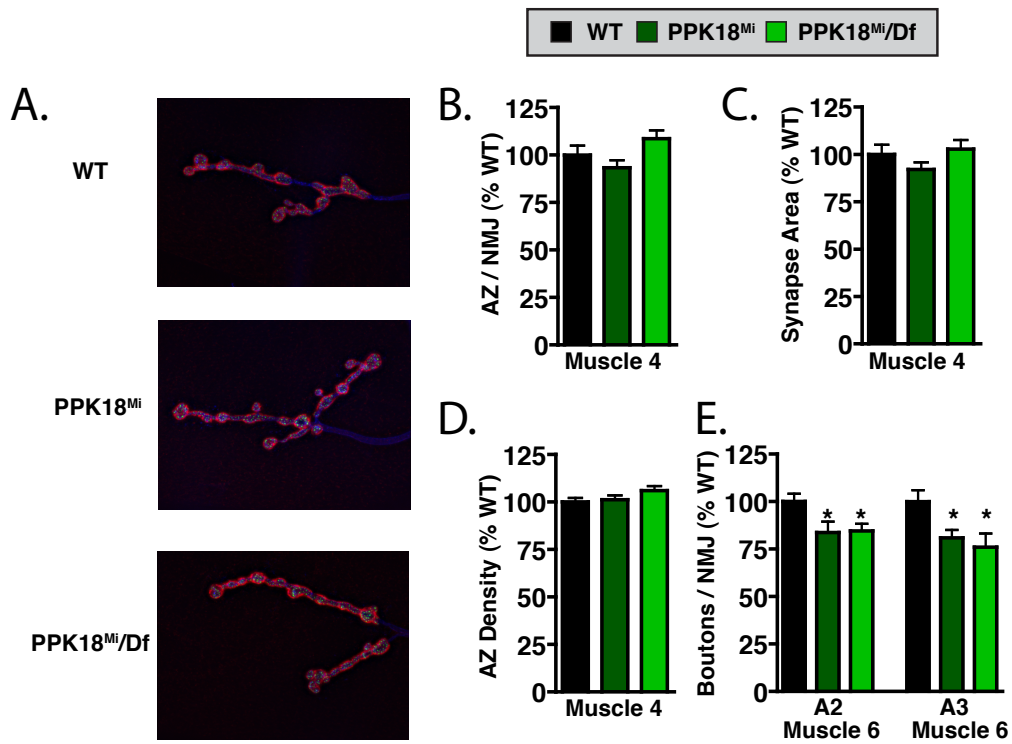




**Table 1: Non-normalized values for electrophysiology measurements.**

Fig.	Genotype	[Ca <sup>2+</sup> ] <sub>e</sub> (mM)	PhTx	mEPSP (mV)	EPSP (mV)	Quantal Content	IR	n	mEPSP freq.
1	WT	0.35	-	0.80±0.07	33.9±1.6	45.7±4.1	7.8±0.4	12	4.8±0.4
1	ppk18 <sup>MiMic</sup>	0.35	-	0.92±0.07	34.9±1.5	39.2±1.9	7.9±0.4	12	4.4±0.4
1	OK371/UAS-PPK18 RNAi	0.35	-	1.02±0.06	33.6±2.0	34.2±3.2	5.9±0.3	11	2.9±0.3
1	WT	0.35	+	0.41±0.06	37.2±2.1	98.3±17.5	8.4±0.8	4	3.8±0.3
1	ppk18 <sup>MiMic</sup>	0.35	+	0.49±0.03	35.1±1.5	74.9±5.5	8.5±0.4	13	2.9±0.4
1	OK371/UAS-PPK18 RNAi	0.35	+	0.50±0.03	36.5±2.9	74.9±6.2	7.9±0.4	11	1.4±0.1
1	WT	0.3	-	0.94±0.03	31.0±0.4	33.1±0.84	7.4±0.6	4	3.8±0.3
1	ppk18 <sup>Mi</sup> OutX6	0.3	-	1.20±0.06	45.8±2.7	28.0±2.5	6.7±0.3	13	3.0±0.2
1	ppk18 <sup>Mi</sup> OutX6	0.3	+	0.53±0.03	35.2±2.3	68.0±4.9	6.6±0.2	12	1.7±0.1

**Abbreviations:** IR = input resistance of muscle cell; n = sample size, number of recordings; Fig. = the figure panel to which the data refer; [Ca<sup>2+</sup>]<sub>e</sub> = extracellular calcium concentration in mM

## Chapter 4:

The *IR75/GRD* locus is required for synaptic homeostasis.

## SUMMARY

A transposon insertion mutation was identified in an ongoing forward genetic screen for mutations that block synaptic homeostasis. This transposon resides within a locus containing four ligand-gated ion channel subunits: *Ionotropic Receptor 75a (IR75a)*, *Ionotropic Receptor 75b (IR75b)*, *Ionotropic Receptor 75c (IR75c)* and *GABA and glycine-like receptor of Drosophila (GRD)*. We have combined electrophysiology, genetics, immunostaining, and quantitative PCR to explore the function of the genes in this locus during synaptic homeostasis and baseline synaptic transmission. We have found that multiple mutations within this locus block the rapid induction and sustained expression of synaptic homeostasis, but we are unable to isolate a single gene responsible for the block in synaptic homeostasis. The data suggests that *GRD* is the relevant gene and the experiments reported in this chapter lay the groundwork for future study of this locus.

## INTRODUCTION

In order to identify mutations that block synaptic homeostasis, an electrophysiology based forward genetic screen is ongoing (see Chapters 1 and 2; Dickman and Davis, 2009; Muller et al., 2011). One transposon insertion, *PBac(WH)f00655* was identified in the screen because it completely blocked the rapid induction of synaptic homeostasis in the presence of PhTx. The *PBac(WH)f00655* mutation will be referred to as "*Puny*" because of the reduced size of the EPSP in the presence of PhTx. This transposon resides on the third chromosome at the chromosomal location 3L(75A2). At the time it was isolated from the screen it was annotated as residing between two genes, *Ionotropic Receptor 75c (IR75c)* and *GABA and glycine-like receptor of Drosophila (GRD)*; Marygold et al., 2013). *IR75c* and *GRD* are transcribed in opposite directions, and the *Puny* transposon was situated in between, in a region that could have been important for the regulation of either gene. It was located ~1kb from *IR75c*, and ~5kb from *GRD*, and seemed more likely to disrupt *IR75c* based on proximity.

Recently additional data supports a *GRD* gene model that has a longer gene span. It now includes a short untranslated exon. The new gene span includes the *Puny* transposon. *Puny* now falls within the first intron of *GRD*, which is relatively large (~5kb). It is still unclear if this transposon disrupts the function of *GRD* or *IR75c* (Figure 1A), as this large intron could be a regulatory

element for either gene. In this chapter I discuss our efforts to define which gene is necessary for the homeostatic control of neurotransmitter release.

*IR75c* belongs to the Ionotropic Receptor (IR) family of olfactory receptors. Unlike mammalian olfactory receptors, which are G-protein-coupled receptors (GPCRs), *Drosophila* olfactory receptors are ligand-gated ion channels. These include the IRs and the Olfactory Receptors (ORs; Kaupp, 2010). The IRs are a family of approximately 60 genes that are evolutionarily related to ionotropic glutamate receptors (Benton et al, 2009). Each subunit has three transmembrane domains, a pore domain, and two extracellular ligand-binding domains. Due to the close relationship with ionotropic glutamate receptors, they likely form tetramers. The members of this family have divergent sequences, sharing the most similarity within the pore of the channel and the least in the ligand binding domains. These receptors respond to many different odorants, and despite the close evolutionary relationship to glutamate receptors, are unlikely to be responsive to glutamate (Benton et al, 2009; Abuin et al, 2010).

There are three predicted ionotropic GABA receptor subunits in *Drosophila*: *GRD*, *RDL* (*resistance to dieldrin*), and *LCCH3* (*ligand-gated chloride channel homologue 3*; Buckingham et al., 2005). *GRD* has no known *in vivo* function in *Drosophila* and it is unclear when in development and in what tissue it is expressed (Marygold et al., 2013). *GRD* can form GABA-gated channels when coexpressed in oocytes with *LCCH3*. Surprisingly, these channels were not Cl<sup>-</sup> permeable, but passed Na<sup>+</sup> and K<sup>+</sup> (Gisselmann et al, 2004).

Here we present evidence that the locus containing *GRD* and *IR75c* is required for synaptic homeostasis. We examined multiple mutations in and around the different genes in this locus, and found that many blocked synaptic homeostasis, although there was a high dependence on genetic background. We are unable to definitely state which gene in this locus is necessary for synaptic homeostasis, although further study of *GRD* is warranted. We also found that mutations in this locus do not alter the basic anatomy of the synapse, including synapse size and the number of active zones. However, there is a change in the size of the postsynaptic glutamate receptor fields. Further study is needed to determine which gene is necessary for synaptic homeostasis and if changes in glutamate receptor distribution are responsible for the block in synaptic homeostasis.

## RESULTS

In a forward genetic screen for mutations that block synaptic homeostasis we identified the transposon insertion *PBac(WH)f00655*, which we refer to here as *Puny*. The *Puny* transposon resides within a locus containing four genes *IR75a*, *IR75b*, *IR75c*, and *GRD* (listed by ascending sequence location; Figure 1A). To determine the requirement of these genes for synaptic homeostasis, we used mutations in and around different genes in this region that would be predicted to disrupt their function (Figure 1A). The eight reagents studied are detailed in the remainder of this paragraph. 1) A Minos(ET1) transposon insertion in a translated exon of *IR75a*, that will be referred to as *IR75a<sup>Mi</sup>* (Metaxakis et al, 2005). 2) A Minos(ET1) transposon insertion located in between *IR75c* and *GRD*, but closer to *IR75c* (43bp from the start site of *IR75c*). This will be referred to as *IR75c<sup>Mi</sup>*. 3) The original PiggyBac transposon identified in the screen, which resides within the first intron of *GRD*, and will be called *Puny* (Thibault et al, 2004). 4) A transposon in the third intron of *GRD*, that is a Minos-mediated integration cassette (MiMiC; Venken et al., 2011) transposon, referred to as *GRD<sup>MiMic</sup>*. 5) A deletion that we generated by imprecise excision of the *IR75c<sup>Mi</sup>* transposon. It removes 1533 bp in total, of which 1167 bp are in the *IR75c* gene. This deletion extends into the 5th translated exon of *IR75c*. This deletion will be referred to as *IR75c<sup>114</sup>* since it was the 114th line generated during transposon excision. 6) A small deficiency *DF(3L)Exel19006* that does not uncover any IR gene, but only removes *GRD* and one other gene (*CG5577*). This will be called

*GRD Df. 7*). A large deletion that uncovers this entire locus, and extends to other genes flanking this locus, *Df(3L)BSC415*. This is simply referred to as *Df. 8*) A previously uncharacterized RNAi line targeted to GRD, referred to as *UAS-GRD-RNAi*. These mutations were used to analyze the rapid induction of synaptic homeostasis, the sustained expression of synaptic homeostasis, baseline synaptic transmission, changes in transcript levels, and general NMJ morphology.

### **A deletion in GRD blocks synaptic homeostasis.**

In order to assay for the rapid induction of synaptic homeostasis, PhTx was applied for 10 minutes, as described in the previous chapters. In *WT* animals there was an increase in quantal content to offset the decrease in mEPSP amplitude, indicating normal synaptic homeostasis (Figure 1B,C; Table 1). In contrast, synaptic homeostasis was completely blocked in homozygous *GRD Df* mutant larvae, which are lacking the entire coding region for *GRD* and can therefore be assumed to be *GRD* null animals (Figure 1). It should be noted that *GRD Df* may alter *IR75a*, *IR75b*, or *IR75c* regulation as well, due to the proximity of these genes.

We then examined the sustained expression of synaptic homeostasis in the *GRD Df* mutant larvae by generating *GluRIIA<sup>SP16</sup>;GRD df* double mutant animals. Unlike *WT*, where we saw a robust increase in QC ( $p < 0.001$ ), we saw no change in QC between the *GRD Df* mutant larvae and the *GluRIIA<sup>SP16</sup>;GRD df*



double mutant ( $p = 0.21$ ; Figure 5C; Table 1), demonstrating that *GRD df* has a complete block in both the rapid induction and the sustained expression of synaptic homeostasis

However, two additional experiments failed to confirm a role for *GRD* in synaptic homeostasis. We tested a transposon insertion in an intron of *GRD*, *GRD<sup>MiMic</sup>*, for the rapid induction of synaptic homeostasis and found wild-type homeostasis (Figure 1C; Table 1). We also drove *UAS-GRD-RNAi* in muscle as well as pan neuronally with the driver combination *elav<sup>c155</sup>-gal4*, *Scabrous-Gal4*, and *BG57-Gal4* (referred to as *NMJ-Gal4*; Figure 1C). This did not block synaptic homeostasis. It should be noted that subsequent work from the laboratory has questioned the integrity of this triple Gal4 reagent (*NMJ-Gal4*) and I recommend that this experiment be repeated with individual Gal4 lines. It is possible that neither mutation disrupts *GRD*, as *GRD<sup>MiMic</sup>* is in an intron and the RNAi is uncharacterized. So it remains possible that *GRD* is the gene in this locus required for synaptic homeostasis.

In addition to homeostatic plasticity, we also analyzed baseline transmission in all conditions and found a trend towards an increase in mEPSP amplitude in the *GRD Df* mutant animals and a decrease in quantal content ( $p=0.075$  and  $p<0.01$ , respectively; Table 1). We also observed a slight increase in mEPSP amplitude in the *GRD<sup>MiMic</sup>* mutation ( $p<0.05$ ; Table 1) and a decrease in quantal content in the *NMJ-Gal4>GRD-RNAi* ( $p<0.001$ ; Table 1). Overall, there were no consistent changes in baseline synaptic transmission.

## **The Puny mutation blocks synaptic homeostasis in a background-dependent manner.**

We performed further analysis of the *Puny* mutation, that was originally identified in the screen. We confirmed the initial finding that this mutation completely blocked synaptic homeostasis (Figure 2A). We additionally performed complementation analysis, and found that the *Puny* mutation acted as a genetic loss-of-function mutation; synaptic homeostasis was blocked when the mutation was placed in *trans* to a Deficiency chromosome that uncovers this locus (*Puny/Df*) and synaptic homeostasis was restored when the mutation was placed in *trans* to a wild-type chromosome (*Puny/+*; Figure 2A).

We also assayed the sustained expression of synaptic homeostasis by placing the *Puny* mutation in the *GluRIIA*<sup>SP16</sup> mutant background. The sustained expression of synaptic homeostasis was completely blocked. There was a small though significant reduction in quantal content in the *GluRIIA*<sup>SP16</sup>;*Puny* mutant animals compared to *Puny* alone ( $p < 0.01$ ; Figure 2D), indicating that release is even lower than expected for a block of synaptic homeostasis and has been decreased from baseline.

Finally, we assayed baseline transmission in the *Puny* mutant animals as well as *Puny/Df* there was a reduction in baseline mEPSP amplitude and a corresponding reduction in EPSP amplitude ( $p < 0.001$  for all; Figure 2C). Otherwise, transmission was relatively normal. However, this reduction in

mEPSP amplitude prompted further analysis of the glutamate receptor subunit composition (see below).

At the time these experiments were conducted, the *GRD* gene span was annotated differently and the *Puny* mutation was closer to the IR75 gene cluster than to *GRD*. We, therefore, focused on the IR75 genes when looking at gene-expression changes in the *Puny* mutant background. We performed QPCR on wild type and *Puny* mutant animals, using primers targeted to *IR75a*, *IR75b*, and *IR75c* and were surprised to find an increase in transcript levels for all three genes (Figure 2E). This suggests that the expression of these genes is not disrupted by the *Puny* mutation but rather their levels are enhanced (see discussion). Lastly, in order to determine if the *Puny* mutation tracked to this genetic locus, we backcrossed this mutation 6X to *WT* ( $w^{1118}$ ). We were surprised to find that this restored the expression of synaptic homeostasis, confounding our previous results (Figure 2F; see discussion). The presence of the full-length transposon insertion in the outcrossed stock was confirmed by PCR (data not shown). Several possible explanations are discussed below, particularly given data that *GRD Df* blocks homeostasis.

### **The *Puny* mutation alters glutamate receptor clustering.**

Before discovering that the outcrossed stock restored the expression of synaptic homeostasis, we performed analysis of the anatomy of the synapse. It is worth reporting here, since it may be relevant to the future investigation of this

locus. First, we stained *wt* and *Puny* mutant synapses with antibodies to the presynaptic active-zone associated protein Bruchpilot (Brp) and the PSD-95 homologue Discs Large (DLG). We found no changes in the number of boutons per synapse at muscles 6/7, in segments 2 and 3, the muscles at which all of our recordings are made (Figure 3B). We also found no change in the active zone density at muscle 4 (Figure 3C).

*Puny* mutant synapses showed a reduction in mEPSP amplitude (Figure 2C). One likely change that could account for a reduction in quantal size is an alteration in the composition of the glutamate receptors (GluRs) at the NMJ. To this end, we performed immunostaining, using antibodies to three glutamate receptor subunits, GluRIIA, GluRIIB, and GluRIIC. These antibodies have been previously used for quantitative immunostaining (Albin and Davis, 2004, Hecksher et al., 2007). While we saw no reduction in overall GluRIIA intensity at the synapse (data not shown), we saw a decrease in the size of the individual GluRIIA puncta, indicating smaller receptor fields (Figure 4A,B). We saw a corresponding increase in the density of the puncta (Figure A,B). Together this indicates that there is a decrease in GluRIIA cluster size and there are more clusters of GluRIIA, but overall levels of GluRIIA at the synapse appear unchanged.

We also examined GluRIIB and GluRIIC, and found a similar reduction in GluR cluster size, and an increase in density, however the effect was most striking in GluRIIA (Figure 4C,D). There was also a slight decrease in overall

GluRIIB and C intensity (data not shown). The changes in GluR clustering could account for the decreased mEPSP amplitudes recorded in these mutants. The fragmented GluR clusters may not be properly aligned with the presynaptic active zones, which would decrease GluR activation during neurotransmission. Also, individual receptor fields may contain fewer receptors, leading to an overall reduction in quantal size.

### **IR75c mutations partially block synaptic homeostasis.**

In order to determine if *IR75c* is necessary for synaptic homeostasis, we first used a transposon insertion located in close proximity to *IR75c*, called *IR75c<sup>Mi</sup>*. We found that this mutation had a partial disruption of synaptic homeostasis (Figure 5A). When placed in trans to a deficiency chromosome that uncovers this entire locus (*IR75c<sup>Mi</sup>/Df*), the block in synaptic homeostasis was enhanced, and when placed in trans to a *wt* chromosome the block in synaptic homeostasis was abolished, consistent with this acting as a genetic loss of function mutation, but not a null mutation. Baseline synaptic transmission was not consistently changed (Table 1).

To test if *IR75c<sup>Mi</sup>* disrupts the sustained expression of synaptic homeostasis we generated a *GluRIIA<sup>SP16</sup>; IR75c<sup>Mi</sup>* double mutant. The double mutant shows a decrease in mEPSP amplitude without a homeostatic increase in presynaptic release ( $p = 0.82$ ; Figure 5C). This demonstrates that the *IR75c<sup>Mi</sup>*

mutation completely blocks the sustained expression of synaptic homeostasis, in contrast to the partial block of the rapid induction of synaptic homeostasis.

Because there were no mutations available that were clear null mutations in *IR75c*, we used the *IR75c<sup>Mi</sup>* transposon to generate a deletion in *IR75c*, through imprecise excision. We were able to generate a small deletion that removes about half of the coding region of the gene, including the start-site. We named this mutation *IR75<sup>114</sup>* because it was 114th excision line that was generated. We found that this mutation blocked the rapid induction of synaptic homeostasis (Figure 5A), although, there was a trend towards an increase in quantal content ( $p = 0.09$ ). We did not see any changes in baseline synaptic transmission in the *IR75<sup>114</sup>* mutation (Table 1). We also examined baseline at a low extracellular calcium concentration (0.2mM), to look for subtle changes in release, and saw no difference from *WT* (data not shown).

Overall, mutations in and around *IR75c* block synaptic homeostasis, without major changes in baseline synaptic transmission. As these mutations could be disrupting *GRD* expression as well, we cannot determine if *IR75c* is indeed necessary for synaptic homeostasis. To try to determine if *IR75a*, *IR75b*, and *IR75c* expression is disrupted by the *IR75c<sup>Mi</sup>* mutant, we performed QPCR on *WT* and *IR75c<sup>Mi</sup>* mutant animals, using primers targeted to *IR75a*, *IR75b*, and *IR75c*. We found an increase in transcript for all three genes (Figure 5D), similar to what was seen in the *Puny* mutation. This data suggests that *IR75a*, *IR75b*,

and *IR75c* are not disrupted by either the *Puny* or the *IR75c<sup>Mi</sup>* mutations, but rather that their transcription is enhanced (see discussion).

### ***IR75c<sup>114</sup>* mutations do not alter gross synapse morphology.**

To determine if *IR75c<sup>114</sup>* mutations alter anatomical NMJ development we quantified the number of synaptic boutons at muscle 6/7, the NMJ at which all of our electrophysiological recordings were performed. We saw no changes at either segment (Figure 6B). Next, we examined the NMJ of muscle 4 by staining for the presynaptic active-zone associated protein Bruchpilot (Brp). *IR75c<sup>114</sup>* mutations had no significant effect on NMJ area, determined by staining for the PSD-95 homologue Discs Large (DLG; Figure 6C), and no significant change in the number of active zones per NMJ (Figure 6D). When we calculated active zone density by dividing active zone number by NMJ area, we find a small ( $13.5\% \pm 4.1$ ,  $p < 0.05$  compared to wild type) decrease in *IR75c<sup>114</sup>* (Figure 6E). We have not quantified glutamate receptor clustering and cannot rule out a change in the postsynaptic receptor fields. However, this analysis indicated that the basic structure of the synapse is intact and unlikely to account for the block in synaptic homeostasis.

### **Mutations in *IR75a* do not block synaptic homeostasis.**

There were no mutations available that were predicted to disrupt *IR75b*, so we examined a mutation in *IR75a*. *IR75a<sup>Mi</sup>* is a transposon insertion in a coding

exon of *IR75a*. We examined baseline transmission and synaptic homeostasis in this mutant and found that synaptic homeostasis was mildly impaired but not blocked (Figure 7A; Table 1). The *IR75a<sup>Mi</sup>* mutation was generated in a background with *yellow* (*y*) and *white* (*w*) mutations on the X chromosome (*yw*). When baseline transmission was assayed in the genetic background, there was a large decrease in mEPSP amplitude, EPSP amplitude and quantal content (Figure 7C).

For consistency we exchanged the X chromosome with our *w<sup>1118</sup>* (*WT*) stock, which does not have a mutation in *y*. We were surprised to see that baseline transmission was completely restored to wild-type levels in *w<sup>1118</sup>;;IR75a<sup>Mi</sup>* animals (Figure 7C). The presence of the transposon insertion was confirmed by PCR (data not shown). It appears as though the defect in baseline transmission does not originate from the *IR75a<sup>Mi</sup>* insertion, but is rather the result of the genetic background. Since synaptic homeostasis was not blocked in either background, we conclude that *IR75a* is not necessary for synaptic homeostasis (Figure 7A).



## DISCUSSION

We have identified multiple mutations in the *IR75/GRD* locus that disrupt synaptic homeostasis. Due to the close placement of the genes in this region, we cannot conclude which gene (or genes) is necessary for synaptic homeostasis. Upon our initial investigation, the *IR75* genes seemed the most likely candidate homeostasis genes. However, due to both the new annotation of this locus and the data presented here, *GRD* has become a more likely possibility. A null mutation in *GRD* (*GRD<sup>df</sup>*) completely blocks the rapid induction and sustained expression of synaptic homeostasis. The question of whether or not *GRD* is indeed the gene responsible for the block in synaptic homeostasis could be easily resolved by restoring *GRD* expression in these animals, using the Gal4-UAS system. Gene specific rescue will be necessary to definitively determine if *GRD* is necessary for synaptic homeostasis.

If it is not possible to rescue synaptic homeostasis by replacing *GRD*, it may be the case that *IR75b* or *IR75c* are necessary for synaptic homeostasis. We have ruled out *IR75a*, since a mutation in the coding region does not disrupt synaptic homeostasis. Due to the complicated nature of this locus, gene specific rescue may not be the best strategy to determine if the *IR75* genes are required. Rather, there are two essential coreceptor subunits, *IR8a* and *IR25a*, which are necessary for the expression of all IR subunits in the antenna, including those in the *IR75* gene cluster (Abuin et al, 2011; Silbering et al., 2011). These genes are located in two distant loci, and mutations in *IR8a* and *IR25a* should have no

direct effect on the *IR75/GRD* locus. Confirmed null mutations in both of these subunits exist and if any members of the IR gene family were indeed components of the homeostatic machinery at the NMJ, it would be predicted that an *IR8a/IR25a* double mutant should disrupt synaptic homeostasis.

We examined transcript levels of the three *IR75* genes in the *Puny* and *IR75c<sup>Mi</sup>* mutants and found that levels of all three genes were increased. We never examined the expression of *GRD*, since at the time the experiments were conducted it was believed to reside farther from the site of the mutations. It is possible a reduction in *GRD* expression will correlate with the severity of the block in synaptic homeostasis in the different mutations, pointing towards *GRD* as the gene that is necessary for synaptic homeostasis. This could be resolved by QPCR.

Finally, in the *Puny* mutation we found that the block in synaptic homeostasis was dependent on genetic background (Figure 2F). Due to the high number of mutations that block synaptic homeostasis within this locus and the rare occurrence of mutations that block synaptic homeostasis, it seems an unlikely coincidence that a mutation in the genetic background of *Puny* blocks synaptic homeostasis. Further evidence that this mutation acts on this locus comes from the complementation analysis presented in Figure 2A, which rules out the possibility of a second site dominant or recessive mutation that falls outside the region uncovered by the deficiency chromosome (*Df*). It is possible that a nearby mutation that is not the *Puny* transposon, but still disrupts a gene in

this locus, causes the block in synaptic homeostasis. This could be something as small as a point mutation in this region. This hypothetical mutation would need to be close enough to be uncovered by the deficiency chromosome, but still could have been lost during backcrossing.

An alternative explanation could account for both the restoration of synaptic homeostasis in the backcrossed line and the results of the complementation analysis. If there is a mutation in the wild-type line that *Puny* was backcrossed to and this mutation is in the same pathway as the gene we are studying, then this background mutation could act as a "suppressor" of the phenotype. Alternatively, if there is a genetic modifier that acts more broadly to enhances synaptic homeostasis within the wild-type stock to which we outcrossed *Puny*, than the *Puny* mutation might not be penetrant in this background. Previous work indicates the existence of a repressor of synaptic homeostasis (Müller et al, 2011), highlighting that this process is subject to regulation. If the *WT* stock to which we outcrossed this line has enhanced synaptic homeostasis, and the genes in this locus are not core components of the homeostat, but rather peripheral components that modulate synaptic homeostasis, their contribution may be negligible under certain conditions imposed by genetic modifiers. Synaptic homeostasis is seen in many different wild-type stocks (data not shown). It would be worthwhile to outcross the *Puny* mutation to other wild-type backgrounds to see if the block in homeostasis

persists. This would indicate that there is something unique within the wild-type stock used here that would be worth exploring further.

### **GABA receptors and ion channel homeostasis.**

A mutation in the potassium channel gene *Shal* was shown to block synaptic homeostasis at the NMJ (Bergquist et al., 2010). The block in synaptic homeostasis was not because the core homeostatic machinery at the NMJ was broken, but rather due to a masking of synaptic homeostasis. In the *Shal* mutant there is upregulation of a second potassium channel gene, *Shaker* (*Sh*). *Sh* upregulation masks synaptic homeostasis by either changing the shape of the action potential or hyperpolarizing the terminal. In addition to upregulating *Sh* in the *Shal* mutant, *Shal* transcript itself is upregulated (unpublished data).

It is surprising to see an increase in *IR75a*, *IR75b*, and *IR75c* transcript in the *Puny* and *IR75c<sup>Mi</sup>* mutations. One possible hypothesis is that mutations in this region actually disrupt *GRD* expression, and that the loss of a GABA receptor alters excitation-inhibition balance throughout the nervous system. This could lead to feedback onto this locus to increase *GRD* transcript levels, as seen in the *Shal* mutants. Due to the close proximity of these genes and the mutations we have introduced, perhaps transcription of the *IR75* gene cluster is upregulated alongside *GRD*. The *GRD df* animals are homozygous viable, however there are only three GABA<sub>A</sub> receptor subunits found in *Drosophila*, and it is unknown how widely *GRD* contributes to overall inhibition in the nervous system.

Through immunostaining, we have observed a change in the size of the postsynaptic glutamate receptor clusters. Each puncta, which represents a receptor field for a single synaptic site, is smaller in the *Puny* mutant. The overall composition of the glutamate receptors across the synapse appears fragmented. It is possible that the increase in transcription of the IR75 gene cluster leads to ectopic IR75a, IR75b, and IR75c expression in the muscle. These channel subunits could compete for space with the normal complement of postsynaptic glutamate receptor subunits, considering the similar structure of the IRs and GluRs. The change in receptor clusters could cause the block in synaptic homeostasis.

Lastly, glutamic acid decarboxylase (GAD), which converts glutamate to GABA, is present at the NMJ. However, it has been proposed to act as a mechanism to break down glutamate in the synaptic cleft (Featherstone et al, 2000). There is no GABAergic input onto the NMJ and direct GABA application has no effect on muscle depolarization (Jan and Jan, 1976; Featherstone et al., 2000). If it turns out that *GRD* is indeed the gene within this locus that is disrupting synaptic homeostasis, it likely acts at a site other than the NMJ, and the disruption in synaptic homeostasis may be a secondary consequence of its role elsewhere in the nervous system.

## FIGURES AND TABLES

### Figure 1: Mutations in *GRD* disrupt synaptic homeostasis.

**A)** The locus containing *IR75a*, *IR75b*, *IR75c* and *GRD*. The gene span is indicated as a solid bar, and arrows represent the start site of translation. Transposon insertions are shown as arrowheads and deletions are shown as colored lines with arrows representing a continuation beyond the genomic region shown (see results for details on each reagent). **B)** Sample mEPSP and EPSP traces for *WT* (top) and *GRD df* (bottom) with and without PhTx (right and left, respectively). **C)** The percent change in mEPSP (solid bars) and quantal content (QC; open bars) in the presence of PhTx relative to baseline for each genotype recorded in the absence of PhTx. All conditions show a significant decrease in mEPSP amplitude ( $p < 0.001$ ). All conditions have an increase in quantal content ( $p < 0.001$ ) except *GRD df*, which shows no significant change in quantal content ( $p = 0.15$ ). All data are recorded in 0.3-0.35mM extracellular calcium. Data are presented as average  $\pm$  SEM. Comparisons are made according to a Student's t-test.

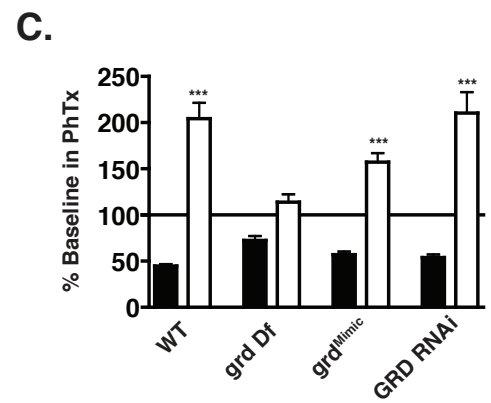
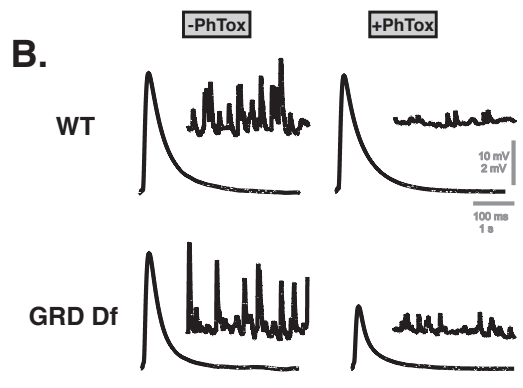
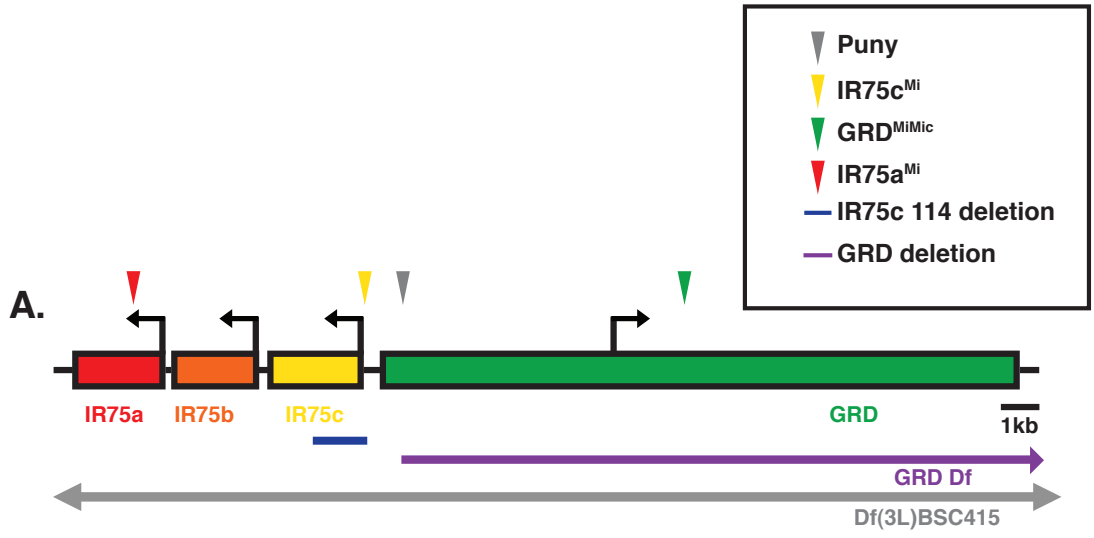


**Figure 2: *Puny* mutations disrupt synaptic homeostasis in a background dependent manner.**

**A)** The percent change in mEPSP (solid bars) and quantal content (QC; open bars) in the presence of PhTx relative to baseline for each genotype recorded in the absence of PhTx. All conditions show a significant decrease in mEPSP amplitude ( $p < 0.001$ ). All conditions have an increase in quantal content ( $p < 0.001$ ) except *Puny* and *Puny/Df*, which shows no significant change in quantal content ( $p = 0.45$  and  $p = 0.83$ , respectively). All data are recorded in 0.3mM extracellular calcium. Data are presented as average  $\pm$  SEM. Comparisons are made according to a Student's t-test. **B)** Sample mEPSP and EPSP traces for *WT* (top) and *Puny* (bottom) with and without PhTx (right and left, respectively). **C)** mEPSP Amplitude, EPSP Amplitude, and quantal content, shown for *WT*, *Puny*, *Puny/Df*, *Puny/+*, and *Df/+* at 0.3mM external  $Ca^{2+}$ . Significance is indicated. **D)** mEPSP amplitude and quantal content (QC) are shown as percent baseline for each genotype. *GluRIIA<sup>SP16</sup>* is shown as percent change relative to wild type. The *GluRIIA<sup>SP16</sup>;Puny;GluRIIA<sup>SP16</sup>* double mutant is normalized to *Puny* alone. mEPSP amplitudes are decreased ( $p < 0.001$ ) in genotypes that include the *GluRIIA<sup>SP16</sup>* mutation. *GluRIIA<sup>SP16</sup>* shows an increase in QC ( $p < 0.001$ ), while *GluRIIA<sup>SP16</sup>;Puny;GluRIIA<sup>SP16</sup>* has a decrease in QC ( $p < 0.01$ ). **E)** QPCR comparing wt and *Puny* mutant animals. *IR75a*, *IR75b* and *IR75c* mRNA are increased in the *Puny* mutant. Experiment was performed in triplicate. **F)** Data is



presented as in **A** for *wt* and *Puny OutX6*. Both conditions have an increase in mEPSP amplitude and QC ( $p < 0.001$  for all).

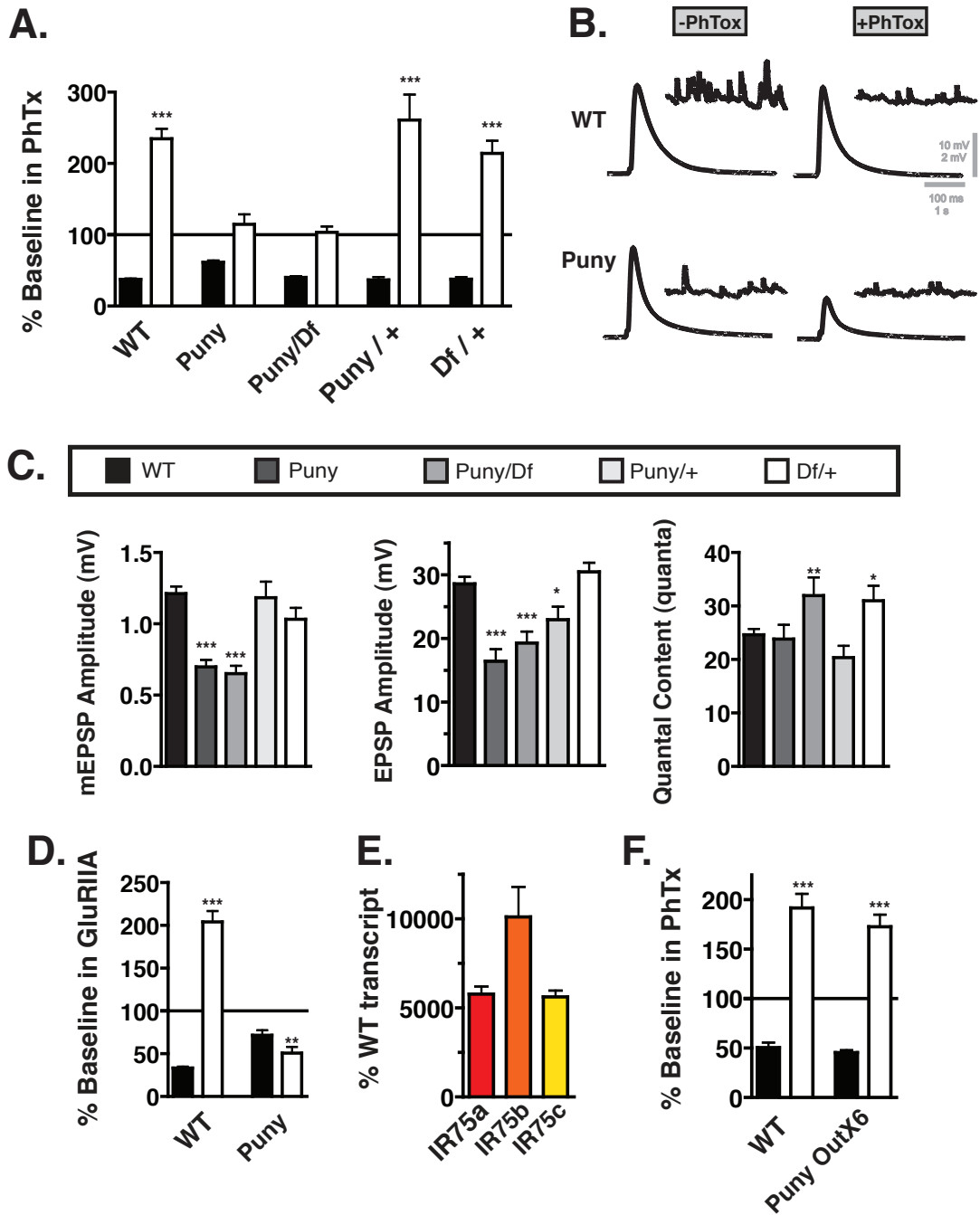


**Figure 3: Puny mutations do not alter NMJ size or active zone density.**

**A)** Representative images of from muscle 4 of *WT*, and *puny* mutant animals stained for BRP (green) and the DLG (red). **B)** The number of boutons per NMJ at muscles 6/7 in segment A2 and A3 is expressed as percent wild type (% WT) bouton number. No significant changes were observed. **C)** The active zone density at muscle 4 is shown as % WT active zone density. There is no significant difference.

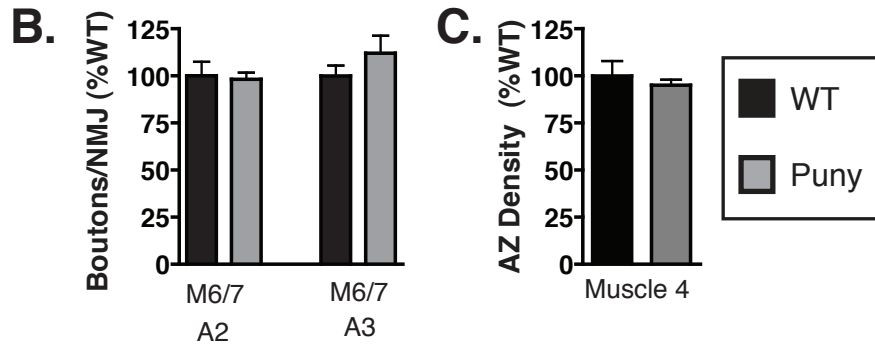
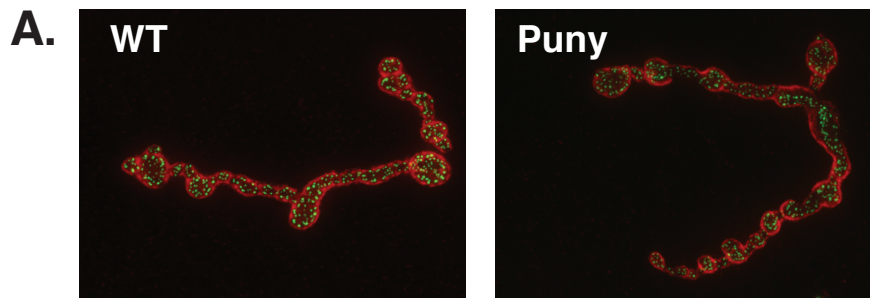


**Figure 4: *Puny* mutations have altered glutamate receptor distribution.**

**A)** Representative images from muscle 4 for *WT* and *Puny* mutant animals stained for GluRIIA (left). Sections of each image are magnified 5X (right). **B)** GluRIIA density is plotted for the synapse (left; calculated by dividing the puncta number by the HRP area). The area of all the individual GluRIIA puncta is plotted (GluRIIA area) as an average (middle) and a cumulative frequency plot (left) **C)** GluRIIB data is plotted as in B. **D)** GluRIIC data is plotted as in B.

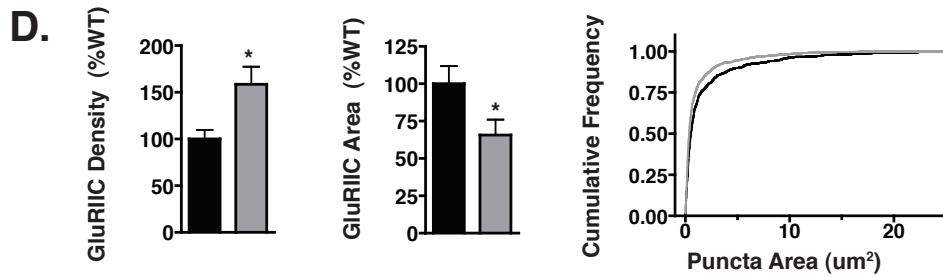
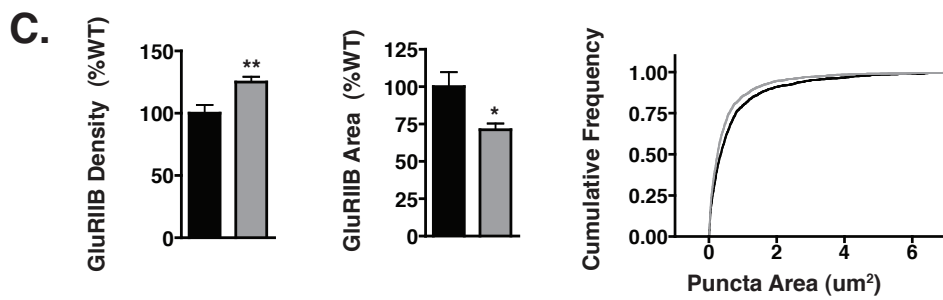
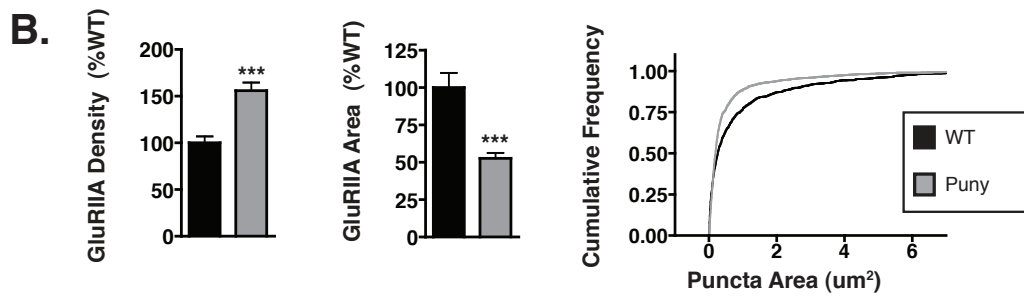
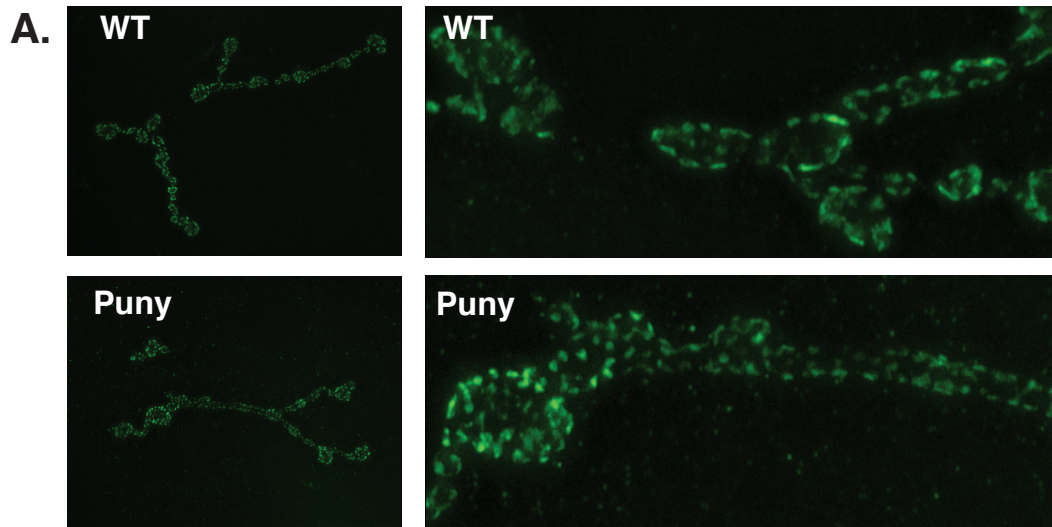


**Figure 5: Mutations in *IR75c* block synaptic homeostasis.**

**A)** The percent change in mEPSP (solid bars) and quantal content (QC; open bars) in the presence of PhTx relative to baseline for WT, *IR75c<sup>Mi</sup>*, *IR75c<sup>Mi</sup>/Df*, *IR75c<sup>Mi</sup>/+*, and *IR75c<sup>114</sup>* recorded in the absence of PhTx. All conditions show a significant decrease in mEPSP amplitude ( $p < 0.001$ ). WT, *IR75c<sup>Mi</sup>*, and *IR75c<sup>Mi</sup>/+* all show an increase in quantal content after PhTx application ( $p < 0.001$ ,  $P < 0.05$ , and  $p < 0.001$ , respectively). All data are recorded in 0.3-0.35mM extracellular calcium. Data are presented as average  $\pm$  SEM. Comparisons are made according to a Student's t-test. **B)** Sample mEPSP and EPSP traces for *WT* (top) and *IR75c<sup>114</sup>* (bottom) with and without PhTx (right and left, respectively). **C)** mEPSP amplitude and quantal content (QC) are shown as percent baseline for each genotype. *GluRIIA<sup>SP16</sup>* is shown as percent change relative to wild type. The *GluRIIA<sup>SP16</sup>;GRD df* double mutant is normalized to *Grd df* alone. The *GluRIIA<sup>SP16</sup>;IR75c<sup>Mi</sup>* double mutant is normalized to *IR75c<sup>Mi</sup>* alone. mEPSP amplitudes are decreased ( $p < 0.001$ ) in genotypes that include the *GluRIIA<sup>SP16</sup>* mutation. *GluRIIA<sup>SP16</sup>* shows an increase in QC ( $p < 0.001$ ). **D)** QPCR comparing wt and *IR75c<sup>Mi</sup>* mutant animals. *IR75a*, *IR75b* and *IR75c* mRNA are increased in the *IR75c<sup>Mi</sup>* mutant. Experiment was performed in triplicate.

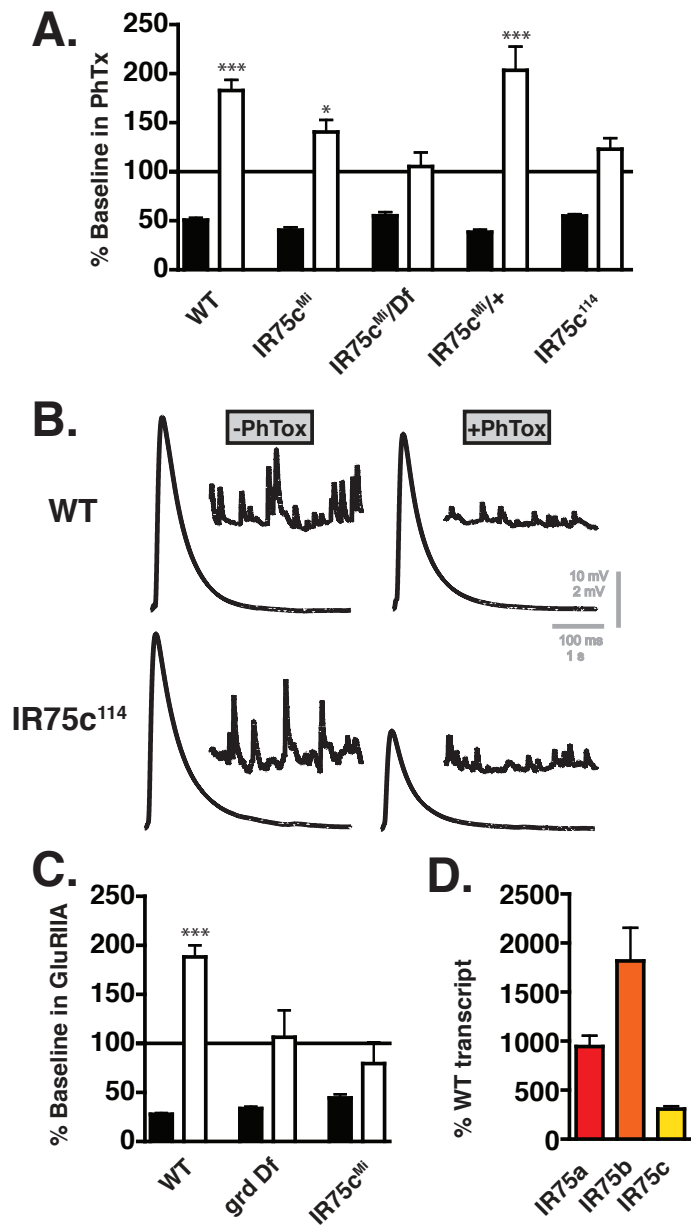




**Figure 6: *IR75c*<sup>114</sup> mutations do not alter synapse morphology.**

**A)** Representative images of from muscle 4 of *wild type* (*WT*) and *IR75c*<sup>114</sup> mutant animals stained for BRP (green), the DLG (red), and HRP (blue). **B)** The number of boutons per NMJ at muscles 6/7 in segment 2 and segment 3 is expressed as percent wild type (% WT) bouton number, and is not significantly different from *WT*. **C)** The area of the NMJ at muscle 4 is shown as %WT area, as measured by DLG staining. It is not significantly different from wild type. **D)** The number of active zones per NMJ at muscle 4 is shown as the % WT active zones (measured as individual Brp puncta). Active zone number is not different from *WT* in either genotype. **E)** The active zone density at muscle 4 is shown as % WT active zone density. There is a significant decrease in *IR75c*<sup>114</sup> compared to *WT* ( $p < 0.05$ ).

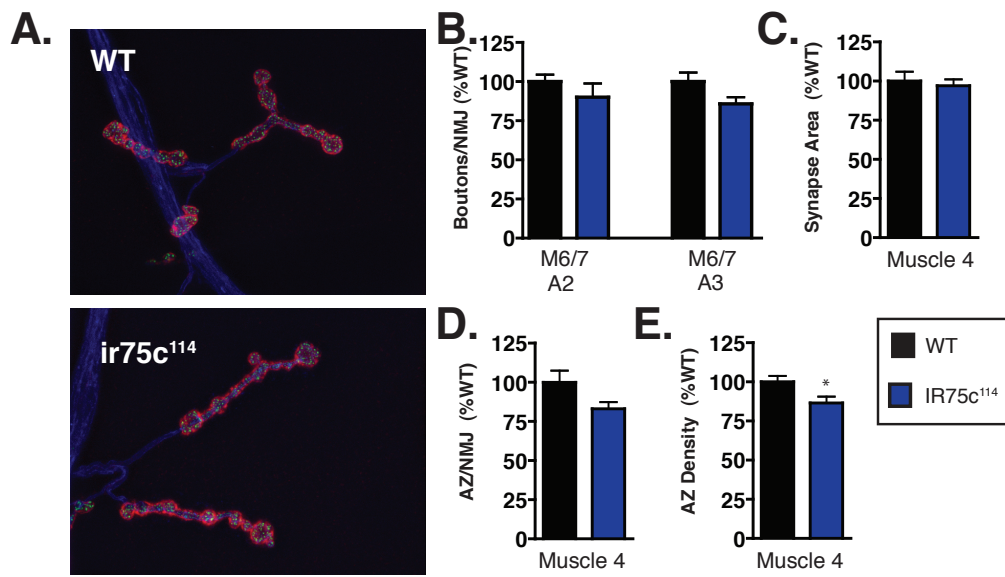


**Figure 7: *IR75a* mutations do not block synaptic homeostasis.**

**A)** The percent change in mEPSP (solid bars) and quantal content (QC; open bars) in the presence of PhTx relative to baseline for *WT* ( $w^{1118}$ ),  $w^{1118}; IR75a^{Mi}$ , and  $yw;;IR75a^{Mi}$  recorded in the absence of PhTx. All conditions show a significant decrease in mEPSP amplitude ( $p < 0.001$ ). All conditions show an increase in quantal content after PhTx application ( $p < 0.001$ ,  $P < 0.05$ , and  $p < 0.01$ , respectively). All data are recorded in 0.3mM extracellular calcium. Data are presented as average  $\pm$  SEM. Comparisons are made according to a Student's t-test. **B)** Sample mEPSP and EPSP traces for *WT* (left) and  $yw;;IR75a^{Mi}$  (middle), and  $w^{1118}; IR75a^{Mi}$  (right). **C)** mEPSP Amplitude, EPSP Amplitude, and quantal content, shown for *WT* ( $w^{1118}$ ),  $w^{1118}; IR75a^{Mi}$ , and  $yw;;IR75a^{Mi}$  at 0.3mM external  $Ca^{2+}$ . Significance is indicated.

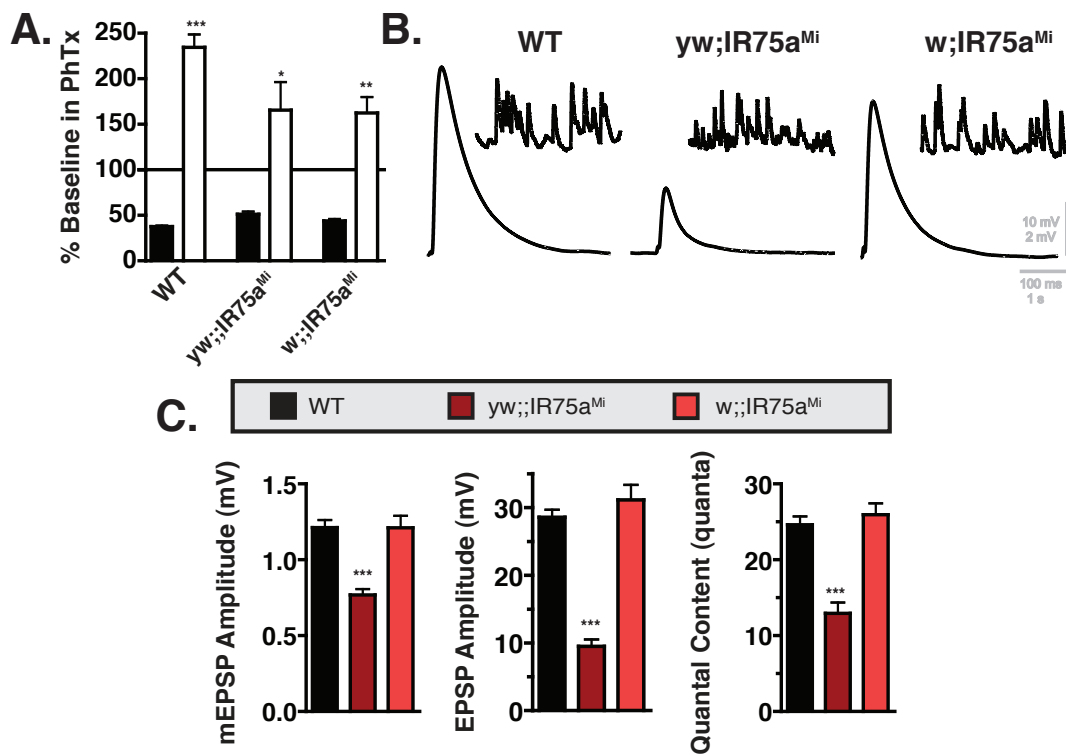


**Table 1: Non-normalized values for electrophysiology measurements.**

Fig.	Genotype	[Ca <sup>2+</sup> ] <sub>e</sub> (mM)	PhTx	mEPSP (mV)	EPSP (mV)	Quantal Content	IR	n
1	WT	0.3	-	1.2±0.06	28.5±1.9	23.7±2.2	9.8±0.8	8
1	WT	0.3	+	0.5±0.04	25.3±2.2	60.8±8.0	9.2±0.7	13
1	GRD Df	0.3	-	1.5±0.01	25.7±1.8	17.1±0.8	6.0±0.6	18
1	GRD Df	0.3	+	1.1±0.07	20.6±1.2	19.4±1.5	6.4±0.6	15
1	WT	0.35	-	1.0±0.06	31.1±1.9	32.8±2.3	9.7±0.7	13
1	WT	0.35	+	0.5±0.04	31.4±1.9	74.4±7.2	9.2±0.4	10
1	GRD <sup>MiMic</sup>	0.35	-	1.3±0.08	35.2±0.6	29.3±1.8	10.3±0.6	12
1	GRD <sup>Mimic</sup>	0.35	+	0.7±0.04	31.9±1.7	46.1±2.9	11.3±0.6	16
1	WT	0.3	-	1.0±0.08	28.7±1.7	31.6±3.3	9.1±0.5	13
1	WT	0.3	+	0.5±0.03	20.7±1.7	42.7±4.9	10.3±0.6	13
1	NMJ-Gal4>UAS-GRD-RNAi	0.3	-	1.1±0.04	15.8±1.5	13.9±1.3	10.2±0.3	14
1	NMJ-Gal4>UAS-GRD-RNAi	0.3	+	0.6±0.04	17.8±2.2	29.3±3.1	10.4±0.5	16
2	WT	0.3	-	1.2±0.05	28.6±1.1	24.6±1.1	9.2±0.3	40
2	WT	0.3	+	0.5±0.01	26.1±1.6	57.7±3.4	8.6±0.3	24
2	Puny	0.3	-	0.7±0.05	16.4±1.9	23.8±2.7	3.8±0.3	11
2	Puny	0.3	+	0.4±0.02	11.1±0.9	27.2±3.3	4.7±0.5	14
2	Puny/Df	0.3	-	0.7±0.05	19.3±1.8	31.9±3.4	4.3±0.2	16
2	Puny/Df	0.3	+	0.3±0.01	8.6±0.7	33.1±2.6	4.1±0.2	9
2	Puny/+	0.3	-	1.2±0.11	23.0±2.0	20.3±2.2	6.7±0.7	11
2	Puny/+	0.3	+	0.4±0.05	21.5±2.5	52.1±7.3	6.5±0.8	10
2	Df/+	0.3	-	1.0±0.08	30.5±1.4	31.0±2.8	7.6±0.6	9
2	Df/+	0.3	+	0.4±0.03	25.0±1.3	66.3±5.5	7.0±0.3	8
2	WT	0.3	-	1.1±0.11	29.0±2.9	27.0±2.0	8.5±0.4	8
2	GluRIIA <sup>SP16</sup>	0.3	-	0.4±0.02	20.1±1.4	55.1±3.4	14.4±1.0	7
2	Puny	0.3	-	0.6±0.03	13.7±1.6	22.1±3.5	3.8±0.3	8
2	GluRIIA <sup>SP16</sup> ; Puny	0.3	-	0.5±0.04	5.02±0.7	11.2±1.6	13.6±0.9	9
2	Puny OutX6	0.3	-	1.1±0.06	34.5±2.2	31.8±1.5	8.5±0.4	12
2	Puny OutX6	0.3	+	0.5±0.03	26.4±1.6	55.0±3.9	8.0±0.3	15
5	WT	0.3	-	0.9±0.06	27.6±2.1	30.9±2.2	9.5±0.3	14
5	WT	0.3	+	0.5±0.02	24.7±1.9	49.6±3.9	9.5±0.5	15
5	IR75c <sup>Mi</sup>	0.3	-	1.0±0.03	19.7±1.4	20.7±1.7	5.5±0.2	15
5	IR75c <sup>Mi</sup>	0.3	+	0.4±0.03	11.1±1.0	29.1±2.6	5.8±0.3	14
5	IR75c <sup>Mi</sup> /Df	0.3	-	0.8±0.04	25.2±1.8	31.1±1.9	6.7±0.4	11
5	IR75c <sup>Mi</sup> /Df	0.3	+	0.5±0.03	13.4±1.4	32.7±4.5	7.9±0.3	16
5	IR75c <sup>Mi</sup> /+	0.3	-	1.1±0.03	26.5±1.6	25.3±1.5	9.4±0.4	16
5	IR75c <sup>Mi</sup> /+	0.3	+	0.4±0.03	21.0±2.6	51.6±6.1	8.2±0.6	15
5	WT	0.35	-	0.9±0.04	33.0±1.8	38.3±2.6	8.3±0.3	20
5	WT	0.35	+	0.4±0.03	30.5±1.5	80.8±5.8	8.6±0.5	12
5	IR75c <sup>114</sup>	0.35	-	0.9±0.05	31.1±0.9	26.9±2.7	6.0±0.4	18

5	IR75c <sup>114</sup>	0.35	+	0.5±0.02	22.0±1.8	45.2±4.2	7.6±0.4	15
5	WT	0.3	-	1.2±0.06	29.0±1.4	24.7±1.4	8.9±0.3	28
5	GluRIIA <sup>SP16</sup>	0.3	-	0.3±0.01	15.8±1.3	47.7±3.0	12.8±0.6	16
5	GRD df	0.3	-	1.5±0.09	24.3±1.6	16.2±0.9	6.0±0.5	23
5	GluRIIA <sup>SP16</sup> ;GRD df	0.3	-	0.7±0.06	8.1±1.9	12.8±3.5	8.4±1.6	9
5	IR75c <sup>Mi</sup>	0.3	-	1.0±0.03	18.2±1.4	18.9±1.8	5.8±0.3	18
5	IR75c <sup>Mi</sup> ;GluRIIA	0.3	-	0.3±0.02	6.7±2.0	20.0±5.2	8.6±0.8	14
7	WT	0.3	-	1.2±0.05	28.6±1.1	24.6±1.1	9.2±0.2	40
7	WT	0.3	+	0.5±0.01	26.1±1.6	57.7±3.4	8.6±0.3	24
7	yw;;IR75a <sup>Mi</sup>	0.3	-	0.8±0.04	9.5±1.0	12.9±1.4	5.8±0.4	18
7	yw;;IR75a <sup>Mi</sup>	0.3	+	0.4±0.02	8.3±1.4	21.5±1.5	6.4±0.3	11
7	w;;IR75a <sup>Mi</sup>	0.3	-	1.2±0.08	31.1±2.2	25.9±1.5	9.8±0.6	13
7	w;;IR75a <sup>Mi</sup>	0.3	+	0.5±0.03	22.2±1.7	42.6±4.6	8.9±0.2	16

**Abbreviations:** IR = input resistance of muscle cell; n = sample size, number of recordings; Fig. = the figure panel to which the data refer; [Ca<sup>2+</sup>]<sub>e</sub> = extracellular calcium concentration in mM.

## **Chapter 5:**

### **General Discussion**

## **Gene Identification: From Screen to Function.**

The brain is astounding in its complexity and its capacity for change. The stimuli we are confronted within our daily lives and the memories we create have far ranging consequences within the nervous system. Homeostatic mechanisms are necessary to constrain change and keep neuronal systems functional. Altered homeostatic signaling is hypothesized to contribute to the cause or progression of neurological disease. For example, impaired or maladaptive homeostatic signaling may participate in the progression of autism-spectrum disorders (Ramocki and Zohngbi, 2008), Alzheimer's Disease (Kamenetz et al., 2003), post-traumatic epilepsy (Davis and Bezprozvanny, 2000; Houweling et al., 2005) and epilepsy (Bernard et al., 2004; Jakubs et al., 2006).

We are only beginning to understand the molecular mechanisms that underlie any form of homeostatic plasticity. Forward genetic screening has been an essential tool in gene discovery in many different processes (St Johnston, 2002) and applying this technique to the homeostatic potentiation of presynaptic release at the NMJ has been instrumental in identifying genes required for synaptic homeostasis. The work presented in this thesis has focused specifically on mutations in ligand-gated ion channel subunit genes identified in a genetic screen because they block synaptic homeostasis.

It is currently unknown how activity is sensed in the muscle and how it is relayed back to the presynaptic terminal. In other words, what is the sensor and what is the retrograde signal? At the outset of these projects, ionotropic receptors



seemed like plausible components of either the sensor or the retrograde signaling pathway. The evidence presented in chapter 2 shows that, surprisingly, two DEG/ENaC channel subunits, PPK11 and PPK16, do not act as we hypothesized, but rather that they are a part of the presynaptic machinery that enhances release during synaptic homeostasis. DEG/ENaC channel activity is continuously required during the homeostatic potentiation of release and serves to enhance action-potential evoked presynaptic calcium influx. Furthermore, *ppk11* and *ppk16* transcription is increased during the sustained expression of synaptic homeostasis. These findings provide a mechanism through which DEG/ENaC channels function during synaptic homeostasis and point to PPK11 and PPK16 as core components of the synaptic homeostasis machinery.

We cannot conclude on the function of any of the genes in the *IR75/GRD* locus, presented in chapter 4, and it remains possible that they will be components of either the sensory apparatus or retrograde signaling machinery, as hypothesized at the onset of their study. This locus is clearly important for NMJ function and worthy of further study into what role these genes play at the synapse or elsewhere in the nervous system (see chapter 4).

### **ENaCs as homeostatic effector proteins**

PPK11 acts in similar processes as mammalian ENaCs, including salt taste and airway fluid clearance. Examining the regulation of mammalian ENaCs in other homeostatic systems could inform future study at the *Drosophila* NMJ. Homeostatic systems require effector mechanisms to implement change in the

parameter under regulation. Mammalian ENaCs can be seen as homeostatic effectors in systemic sodium homeostasis and the regulation of airway fluid levels. While ENaCs can be modulated in many ways, they are not ligand gated in the classical manner; they are constitutively active channels and their surface abundance is highly regulated by trafficking to and from the plasma membrane.

***Taste Cells:*** While mammalian ENaCs have been studied in many tissues outside the nervous system, their primary neuronal function is as taste receptors in the tongue. They are responsible for a component of salt taste, in particular, the response to low-salt concentrations (Chandrasekhar, et al., 2010; Yarmolinsky et al., 2009). Low-salt taste is inhibited by Amiloride compounds and in ENaC mutant animals (Halpern 1998; Chandrasekhar, et al., 2010).

The homeostatic regulation of systemic salt balance is a process that is vital to the survival of any organism. The regulation of salt intake can be seen as an initial coarse modulation of input into the homeostatic system that regulates salt balance. This is particularly important during restricted salt availability. Feedback regulating salt taste, and thereby salt input, acts via ENaCs. ENaCs are trafficked to the sensory (apical) surface in response Aldosterone and Angiotensin II, both of which are regulated by low salt or fluid levels. This has been confirmed by an increase in amiloride sensitive currents as well as ENaC immunostaining in taste cells (Lin et al, 1999; Herness, 1992; Shigemura et al, 2013). ENaCs can be considered as homeostatic effector proteins that drive salt intake.

One intriguing possibility based on the work presented in this thesis, is that in addition to the documented increase in ENaC at the sensory (apical) surface of the taste receptors, there could also be an increase towards the basal (presynaptic) side of the cell. This could depolarize the presynaptic terminal and facilitate transmission in a manner similar to what is seen that the *Drosophila* NMJ. An enhancement in transmission on top on an enhancement in salt perception could greatly strengthen an organism's ability to detect even very low concentrations of salt when salt deprived. This hypothesis remains to be tested.

***Kidney Cells:*** ENaCs function in salt homeostasis and blood pressure regulation by acting as Na<sup>+</sup> transport proteins in the kidney. Salt is reabsorbed at many sites along the length of the nephron. However, the cortical collecting duct (CCD) is the primary site where Na<sup>+</sup> reabsorption is regulated (Hamm et al, 2010; Lifton, 2001). After dehydration or salt-deprivation, aldosterone is released from the adrenal cortex, which acts on the mineralocorticoid receptor (MR) in the CCD, leading to a number of direct and transcriptional changes that together result in enhanced ENaC channel abundance on the apical membrane. The increase in ENaC surface abundance causes an increase in Na<sup>+</sup> diffusion through ENaC channels and into the principle cells lining the CCD. Na<sup>+</sup> is pumped out the basolateral membrane by the Na/K-ATPase, leading to Na<sup>+</sup> reabsorption. The K<sup>+</sup> buildup caused by the pump is relieved by K<sup>+</sup> diffusion through the ROMK potassium channel (Schild, 2010; Hamm et al., 2010).

There are many sites of short- and long-term regulation that converge on ENaC abundance and function at the cell surface, including the enhanced transcription of ENaC and the Na/K-ATPase (Schild, 2010). One of the best-studied methods of ENaC regulation is the ubiquitination of ENaC by Nedd4-2 and subsequent internalization by clathrin mediated endocytosis. This removal pathway is highly regulated by phosphorylation at several steps and likely to be rapidly engaged (Balla and Hallows, 2008; Hamm et al, 2010; Verrey et al, 2008). *Drosophila* Nedd4 family members include *dNedd4*, *dSmurf*, and *Su(Dx)Itch*. *dNedd4* mutations alter *Drosophila* NMJ morphology (Myat et al., 2002; Sakata et al., 2004), and *dSmurf* acts on the BMP signaling pathway (Podos et al., 2001). Since the BMP signaling pathway is permissive in synaptic homeostasis, it may not be possible to distinguish between an effect on BMP signaling and on PPK11 and PPK16 surface abundance. It is also worth noting that the Nedd4 scaffolding proteins in *Drosophila*, *14-3-3epsilon* and *14-3-3zeta* (also called *Leonardo*), alter synaptic transmission and short-term plasticity at the NMJ (Broadie et al., 1997). The best strategy to test the relevance of ubiquitin-mediated internalization of a DEG/ENaC at the NMJ would be to mutate potential ubiquitination sites on PPK11 and PPK16.

The data from the kidney and from taste cells highlight two areas where ENaCs act as homeostatic effector proteins within a single process. ENaCs participate in salt homeostasis in other tissues as well, including in sweat glands and the colon (Butterworth, 2010). Diseases of blood-pressure dysregulation

highlight the importance of ENaC as a homeostatic effector protein in the regulation of salt homeostasis and blood pressure. Liddle Syndrome is an autosomal dominant form of hypertension in which the ENaCs cannot be ubiquitinated and internalized and, therefore, remain at the surface to promote excess  $\text{Na}^+$  reabsorption. In contrast, a recessive form of Pseudohypoaldosteronism Type 1 (PHA1) causes hypotension and salt-wasting and is caused by loss-of-function mutations in ENaC subunits (Lifton, 2001). Neither of these diseases is associated with any neurological issues that cannot be traced directly to blood pressure dysregulation. ENaC is, however, enriched in the mouse and human dentate gyrus and cerebellum, as seen through *in situ* and microarray analysis, respectively (Hawrylycz et al., 2012; Lein et al., 2007). This suggests that ENaC may function in the central nervous system, although not in a manner essential to prevent neurological disorders.

***Lung fluid homeostasis:*** ENaCs also participate as homeostatic effector proteins in a separate system, the regulation of lung fluid levels. Fluid accumulation in the lungs is highly regulated, as some fluid is necessary for efficient gas exchange, however, too much fluid accumulation is inhibitory to this process. The regulation of fluid level in the airways can be considered a homeostatic process, with proper fluid level as the set point. Fluid is continuously secreted through the airway epithelia and rates can vary with blood-pressure changes and after injury. Fluid removal from the lungs is accomplished through  $\text{Na}^+$  and  $\text{Cl}^-$  absorption that is dependent on ENaC channels and cystic fibrosis

transmembrane conductance regulator (CFTR) proteins, respectively. ENaC channels function in the lung in a manner similar to their role in the kidney; ENaC channels allow  $\text{Na}^+$  to passively flow from the airspace across the apical surface and into lung epithelial cells.  $\text{Na}^+$  is then pumped out the basal side by the  $\text{Na}^+$ - $\text{K}^+$ -ATPase. Water removal is accomplished by passive reabsorption that follows the movement of salt (Eaton et al, 2009; Sartori et al, 2010). ENaC mutant mice die after birth from not clearing lungs and ENaC hypomorphic mice have enhanced susceptibility to pulmonary edema (fluid accumulation in the airspaces; Egli et al., 2004).

**Common Features:** There are common themes that emerge by comparing these different systems in which ENaC acts as a homeostatic effector protein. In both the kidney and the lung ENaC is trafficked to the apical membrane and transports  $\text{Na}^+$  passively into the cell.  $\text{Na}^+$  is pumped out the basal side by the  $\text{Na}^+$ - $\text{K}^+$ -ATPase and a  $\text{K}^+$  Channel relieves excess potassium buildup. It is tempting to speculate that this regulatory unit may be utilized at the *Drosophila* NMJ as well. However, there is a fundamental difference in the role of ENaC in these systems. ENaCs transport  $\text{Na}^+$  in the lung and kidney, with the epithelial cell acting as a way station.  $\text{Na}^+$  levels within the epithelial cell need not be strictly regulated although the amount transported must be. In contrast, at the NMJ, internal  $\text{Na}^+$  concentration must be closely controlled to allow analog modulation of resting potential. It is possible that ratio of the  $\text{Na}^+$ - $\text{K}^+$ -ATPase to PPK11 and PPK16 is highly regulated at the NMJ and that this coupling creates

graded changes in internal  $\text{Na}^+$  concentrations. It will be challenging to directly test the role of the  $\text{Na}^+\text{-K}^+\text{-ATPase}$  in synaptic homeostasis, due to the important role it plays in regulating the resting potential at the NMJ. However, it would be worth examining transcriptional changes during synaptic homeostasis to see if they track those of *ppk11* and *ppk16*.

In both the kidney and at the NMJ there is an initial increase in ENaC activity that is independent of transcription and a longer-term increase in ENaC transcription. This likely replenishes the available pool of ENaC channels by transcription of new channels. This would enable the rapid engagement of a homeostatic process that is initiated through trafficking and a replenishment of channels accounting for protein turnover. It could also create an upper limit on the initial response of the system, preventing aberrant excitation at the NMJ or excess salt reabsorption in the kidney. There is recent evidence that this may not be the way ENaC is regulated in rat taste cells, where it was seen that animals on a low salt diet do not upregulated ENaC expression (Huang and Stähler, 2009). Since transcriptional upregulation was only examined at a single time point, 15 days after the initiation of salt deprivation, this warrants further study.

Lastly, It is worth noting that certain neurotransmitters regulate ENaC channels in the lungs. Epinephrine acts through the  $\beta_2$ -receptor to increase ENaC surface expression, and there is evidence that dopamine acts through D1 and D2 receptors to increase ENaC activity (Matthay et al., 2005; Eaton et al.,

2009). Both neurotransmitters act directly on receptors in the epithelial cells, highlighting a potential site of overlap between neuronal and non-neuronal ENaC regulation. Additionally, a recent study has also shown direct allosteric modulation of an ASIC channel by the neurotransmitter serotonin (Wang et al., 2013). It remains to be seen if other members of the DEG/ENaC superfamily can be modulated directly by neurotransmitters.

Monoamine neurotransmitters act as potent neuromodulators in many systems (Marder, 2012) and could potentiate release via ENaC at the NMJ. Components of the dopamine-signaling pathway were identified through microarray analysis comparing wild-type and *GluRIIA* mutant animals (unpublished data), and it is possible that dopamine could be the retrograde signal, leading to ENaC translocation to the presynaptic terminal and synaptic potentiation.



## **EXPERIMENTAL PROCEDURES**

### **Electrophysiology**

Recordings were made from muscle 6 in abdominal segments 2 and 3 from third instar larvae, as previously described (Frank et al., 2006, 2009, Müller et al, 2012). Recordings were made in HL3 saline containing (in mM): 70 NaCl, 5 KCl, 10 MgCl<sub>2</sub>, 10NaHCO<sub>3</sub>, 115 Sucrose, 4.2 trehalose, 5 HEPES, and 0.35 CaCl<sub>2</sub>, unless otherwise specified. Quantal content was calculated by dividing the average EPSP amplitude by the average mEPSP amplitude, for each muscle recording. Where specified, quantal content was corrected for nonlinear summation (NLS), according to established methods (Martin et al., 1955; Davis and Goodman, 1998) For acute pharmacological homeostatic challenge, larvae were incubated in Philanthotoxin-433 (PhTx; 10-20μM; Sigma-Aldrich) for 10 minutes (Frank et al., 2006). Benzamil hydrochloride hydrate (Sigma-Aldrich) was prepared as a stock in H<sub>2</sub>O, and diluted to the desired concentration in HL3 saline. EIPA (5-(n-ethyl-n-isopropyl)amiloride; Sigma-Aldrich) was prepared as a stock in DMSO, then diluted 1:1000 in HL3 for to a concentration of EIPA of 20μM. A 1:1000 dilution of DMSO is without effect on synaptic transmission (Frank et al., 2006).

Two-electrode voltage clamp recordings were done as previously described (Müller et al, 2012). All recordings were made from muscle 6 in

abdominal segments 2 and 3 from third instar larvae in HL3 saline with 1mM CaCl<sub>2</sub>. mEPSPs were recorded with the amplifier in bridge mode before switching to TEVC mode. mEPSPs were analyzed rather than mEPSCs, because of the low signal to noise ratio for mEPSCs. EPSC analysis was conducted using custom-written routines for Igor Pro 5.0 (wavemetrics), and mEPSPs were analyzed using Mini Analysis 6.0.0.7 (Synaptosoft).

### **Fly Stocks and Genetics**

In all experiments, the *w*<sup>1118</sup> strain was used at the wild-type control, and animals were raised at 22°C, unless otherwise noted. *Drosophila melanogaster* stocks with the following mutations, *UAS*-transgenes, or *GAL4* drivers were used in the course of chapter 2: *UAS-ppk11-RNAi*, *UAS-ppk11-dn*, and *UAS-ppk19-RNAi*, were the kind gifts of Lei Liu. *ppk11*<sup>Mi</sup>, *ppk11*<sup>PBac</sup>, *ppk16*<sup>Mi</sup>, and *Df(2l)BSC240* (PPK deficiency) were acquired from the Bloomington stock center. *UAS-ppk16-RNAi* was acquired from the Vienna Stock Center (VDRC transformant ID 22990). The *GluRIIA*<sup>SP16</sup> null mutation (Petersen et al., 1997), the *OK371-GAL4* driver (Mahr and Aberle, 2005), and the *MHC-Gal4* driver (Schuster et al., 1996) have all been previously reported on. The precise excision, *ppk11*<sup>Precise</sup>, and the imprecise excision, *ppk16*<sup>166</sup>, were generated according to standard procedures (See Below; Metaxakis et al., 2005).

Deletions were identified by PCR, and all results were verified through sequencing.

*Drosophila melanogaster* stocks with the following mutations, *UAS*-transgenes, or *GAL4* drivers were used in the course of chapter 3: *ppk18<sup>Mi</sup>*, *ppk18<sup>MiMic</sup>*, *UAS-PPK18-RNAi* and *Df(2l)BSC240* (PPK deficiency) were acquired from the Bloomington stock center.

*Drosophila melanogaster* stocks with the following mutations, *UAS*-transgenes, or *GAL4* drivers were used in the course of chapter 4: *IR75a<sup>Mi</sup>*, *IR75c<sup>Mi</sup>*, *Puny* (*PBacWHf00655*), and *GRD<sup>Mimic</sup>*, *GRD Df* (*DF(3L)Exel19009*) were acquired from the Bloomington stock center. *UAS-GRD-RNAi* was acquired from the Vienna Stock Center (VDRC transformant ID 5329). For driving expression in all neurons and muscles (here called *NMJ-gal4*) we used the driver combination *elav<sup>C155</sup>-Gal4* on the X, *Scabrous-gal4* on the second chromosome, and the muscle driver *BG57-Gal4* on the third chromosome.

The imprecise excision, *IR75c<sup>114</sup>*, was generated according to standard procedures (Metaxakis et al., 2005). Before beginning the excision the stock was isogenized to ensure that all third chromosomes were identical (to avoid possible PCR artifacts during excision verification). Double balanced flies containing the Minos Transposase (*MT*) driven off the heat-shock promoter (*w;CyO-MT/If; TM6b/TM3Sb*) were crossed to isogenized homozygous *IR75c<sup>Mi</sup>* flies. The cross was flipped daily so that

all eggs were at the same stage. All eggs were heat-shocked in a water bath at 37 °C for 1 hour from the 2nd to 5th day after the cross was made. Single male flies containing markers for the transposase (*CyO*), for the *IR75c<sup>Mi</sup>* insertion (GFP in the eye), and the third chromosome balancer *TM6B* were chosen (*w; CyO-MT/+; IR75c<sup>Mi</sup>/TM6B*) and crossed to the third chromosome balancer stock *w;; TM3Sb/TM6B*. A single male was chosen from each cross that had no markers on the second chromosome, indicating the absence of *CyO-MT*, and that did not contain GFP in the eye but did have the third chromosome balancer *TM3Sb*, indicating that the Minos Transposase had been excised, (*w;+; IR75c\*/TM3Sb*). This single male was crossed to the large deficiency that uncovers this region in *trans* to the balancer *TM6B* (*w;+; Df/TM6B*). From this cross, a stable line was made from *w;+; IR75c\*/TM6B* flies, and *w;+; IR75c\*/Df* flies were isolated for PCR from the same cross. Approximately 300 lines per transposon were generated this way, and we found the rate of imprecise excision to be similar to what has been reported (1:50). For *ppk11<sup>Mi</sup>* and *ppk16<sup>Mi</sup>* this procedure was modified to include second chromosome balancers. All deletions were identified by PCR, and all results were verified through sequencing.

## **Anatomical Analysis**

In chapters 2, 3 and 4, third-instar larval preparations were fixed in Bouin's fixative, washed, and incubated overnight at 4°C in primary antibodies. Secondary antibodies were applied at room temperature for 2hrs. The following antibodies were used: anti-NC82 (1:100; mouse; Developmental Studies Hybridoma Bank), and anti-DLG (1:10,000; rabbit). Alexa conjugated secondary antibodies and Cy5-conjugated goat anti-HRP were used at 1:250 (Jackson ImmunoResearch Laboratories; Molecular Probes). Larval preparations were mounted in Vectashield (Vector) and imaged at room temperature using an Axiovert 200 (Zeiss) inverted microscope, a 100X Plan Aplanachromat objective (1.4NA), and a cooled CCD camera (Coolsnap HQ, Roper). Intelligent Imaging Innovations (3I) software was used to capture, process, and analyze images.

In chapter 4, the following antibodies were used: anti-GluRIIA (1:10 mouse; Developmental Studies Hybridoma Bank 8B4D2), anti-GluRIIB (1:2500, rabbit; gift of Aaron DiAntonio), and anti-GluRIIC (1:5000, rabbit; gift of Aaron DiAntonio).

### **CNS Quantitative RT-PCR**

RT-PCR was performed as previously described (Bergquist et al., 2010). In chapters 2 and 3, primer-probes specific for real-time PCR detection of *ppk11*, *ppk16*, *ppk18* and *Ribosomal protein L32 (RpL32)* were designed and developed by Applied Biosystems. The CNS was

removed from 25 third-instar larvae per sample (3 samples/genotype). Total RNA was isolated from each sample using the standard Trizol protocol. A DNase digestion removed potential DNA contamination (RQ1 RNase-free DNase Promega).

In chapter 4, primer-probes specific for real-time PCR detection of *IR75a*, *IR75b*, and *IR75c* and Ribosomal protein L32 (*RpL32*) were designed and developed by Applied Biosystems. The head and body were separated for 25 third-instar larvae per sample (3 samples/genotype). The head tissue was not analyzed, since the signal was below detection. Instead the body tissue was used in all data presented here. Total RNA was isolated from each sample using the standard Trizol protocol. A DNase digestion removed potential DNA contamination (RQ1 RNase-free DNase Promega).

#### **cDNA extraction and amplification**

cDNA libraries were generated using the SMARTer RACE cDNA Amplification Kit (Clontech). Primers used for PPK11 and PPK16 amplification were as follows: ppk11 forward, atgtccgacgttccaggag; ppk11 reverse, attagccggccctaatgacc; ppk16 forward, atggcttcaagaagcggcg; ppk16 reverse, ctactcccggttgatgtatt. PCR was done using TAQ polymerase, according to standard procedures.

## Calcium Imaging

Third instar larvae were dissected and incubated in ice cold,  $\text{Ca}^{2+}$ -free HL3 containing 5mM Oregon-Green 488 BAPTA-1 (hexapotassium salt, Invitrogen) and 1 mM Alexa 568 (Invitrogen). After incubation for 10 minutes, the preparation was washed with ice cold HL3 for 10 – 15 minutes. Single action-potential evoked spatially-averaged  $\text{Ca}^{2+}$  transients were measured in type-1b boutons synapsing onto muscle 6/7 of abdominal segments A2/A3 at an extracellular  $[\text{Ca}^{2+}]$  of 0.5 mM using a confocal laser-scanning system (Ultima, Prairie Technologies) at room temperature. Excitation light (488 nm) from an air-cooled krypton-argon laser was focused onto the specimen using a 60X objective (1.0 NA, Olympus), and emitted light was detected with a gallium arsenide phosphide-based photocathode photomultiplier tube (Hamamatsu). Line scans across single boutons were made at a frequency of 313 Hz. Fluorescence changes were quantified as  $\Delta F/F = (F(t) - F_{\text{baseline}}) / (F_{\text{baseline}} - F_{\text{background}})$ , where  $F(t)$  is the fluorescence in a region of interest (ROI) containing a bouton at any given time,  $F_{\text{baseline}}$  is the mean fluorescence from a 300-ms period preceding the stimulus, and  $F_{\text{background}}$  is the background fluorescence from an adjacent ROI without any indicator-containing cellular structures. One synapse (3 – 6 boutons) was imaged per preparation. The average  $\text{Ca}^{2+}$  transient of a

single bouton is based on 7 – 11 line scans. Experiments in which the resting fluorescence decreased by >15 % within an individual transient, and/or which had a Fbaseline > 800 a.u. were excluded from analysis. There was no significant difference in Alexa 568 fluorescence intensity between wild-type synapses (724±83 a.u.) and *GluRIIA*<sup>SP16</sup>-mutant synapses (1007±151 a.u.; p=0.12) indicating similar dye loading in both genotypes. The time interval between each action potential stimulus was at least 15 seconds. The same boutons were imaged in the absence and presence of 75 μM Benzamil. For further details see Müller and Davis (2012).



## REFERENCES:

- Abuin, L., Bargeton, B., Ulbrich, M.H., Isacoff, E.Y., Kellenberger, S., and Benton, R. (2011). Functional Architecture of Olfactory Ionotropic Glutamate Receptors. *Neuron* 69, 44-60.
- Adams, C.M., Anderson, M.G., Motto, D.G., Price, M.P., Johnson, W.A., and Welsh, M.J. (1998). Ripped pocket and pickpocket, novel *Drosophila* DEG/ENaC subunits expressed in early development and in mechanosensory neurons. *The Journal of Cell Biology* 140, 143-152.
- Ainsley, J.A., Pettus, J.M., Bosenko, D., Gerstein, C.E., Zinkevich, N., Anderson, M.G., Adams, C.M., Welsh, M.J., and Johnson, W.A. (2003). Enhanced locomotion caused by loss of the *Drosophila* DEG/ENaC protein Pickpocket1. *Current Biology* 13, 1557-1563.
- Albin, S.D., and Davis, G.W. (2004). Coordinating structural and functional synapse development: postsynaptic p21-activated kinase independently specifies glutamate receptor abundance and postsynaptic morphology. *The Journal of Neuroscience* 24, 6871-6879.
- Alle, H., and Geiger, J.R.P. (2006). Combined analog and action potential coding in hippocampal mossy fibers. *Science* 311, 1290-1293.
- Arnadóttir, J., O'Hagan, R., Chen, Y., Goodman, M.B., and Chalfie, M. (2011). The DEG/ENaC protein MEC-10 regulates the transduction channel complex in *Caenorhabditis elegans* touch receptor neurons. *The Journal of neuroscience* 31, 12695-12704.
- Awatramani, G.B., Price, G.D., and Trussell, L.O. (2005). Modulation of Transmitter Release by Presynaptic Resting Potential and Background Calcium Levels. *Neuron* 48, 109-121.
- Belkin, K.J., and Abrams, T.W. (1993). FMRFamide produces biphasic modulation of the LFS motor neurons in the neural circuit of the siphon withdrawal reflex of *Aplysia* by activating Na<sup>+</sup> and K<sup>+</sup> currents. *The Journal of neuroscience* 13, 5139-5152.
- Ben-Shahar, Y. (2011). Chapter 1 - Sensory Functions for Degenerin/Epithelial Sodium Channels (DEG/ENaC), Vol 76, 1 edn (Elsevier Inc.).
- Benson, C.J., Xie, J., Wemmie, J.A., Price, M.P., Henss, J.M., Welsh, M.J., and Snyder, P.M. (2002). Heteromultimers of DEG/ENaC subunits form H<sup>+</sup>-gated channels in mouse sensory neurons. *Proceedings of the National Academy of Sciences* 99, 2338-2343.

Benton, R., Vannice, K.S., Gomez-Diaz, C., and Vosshall, L.B. (2009). Variant Ionotropic Glutamate Receptors as Chemosensory Receptors in *Drosophila*. *Cell* 136, 149-162.

Bergquist, S., Dickman, D.K., and Davis, G.W. (2010). A Hierarchy of Cell Intrinsic and Target-Derived Homeostatic Signaling. *Neuron* 66, 220-234.

Bernard, C., Anderson, A., Becker, A., Poolos, N.P., Beck, H., and Johnston, D. (2004). Acquired dendritic channelopathy in temporal lobe epilepsy. *Science* 305, 532-535.

Bhalla, V., and Hallows, K.R. (2008). Mechanisms of ENaC regulation and clinical implications. *Journal of the American Society of Nephrology : JASN* 19, 1845-1854.

Bianchi, L., and Driscoll, M. (2002). Protons at the gate: DEG/ENaC ion channels help us feel and remember. *Neuron* 34, 337-340.

Blumenthal, T. (2004). Operons in eukaryotes. *Briefings in functional genomics & proteomics* 3, 199-211.

Boiko, N., Kucher, V., Stockand, J.D., and Eaton, B.A. (2012). Pickpocket1 is an ionotropic molecular sensory transducer. *The Journal of biological chemistry* 287, 39878-39886.

Bollmann, J.H., Sakmann, B., and Borst, J.G. (2000). Calcium sensitivity of glutamate release in a calyx-type terminal. *Science* 289, 953-957.

Borst, J.G., and Sakmann, B. (1998). Facilitation of presynaptic calcium currents in the rat brainstem. *The Journal of Physiology* 513 ( Pt 1), 149-155.

Bouhours, B., Trigo, F.F., and Marty, A. (2011). Somatic depolarization enhances GABA release in cerebellar interneurons via a calcium/protein kinase C pathway. *The Journal of neuroscience* 31, 5804-5815.

Branco, T., Staras, K., Darcy, K.J., and Goda, Y. (2008). Local Dendritic Activity Sets Release Probability at Hippocampal Synapses. *Neuron* 59, 475-485.

Broadie, K., Rushton, E., Skoulakis, E.M., and Davis, R.L. (1997). Leonardo, a *Drosophila* 14-3-3 protein involved in learning, regulates presynaptic function. *Neuron* 19, 391-402.

Buckingham, S.D., Biggin, P.C., Sattelle, B.M., Brown, L.A., and Sattelle, D.B. (2005). Insect GABA receptors: splicing, editing, and targeting by antiparasitics and insecticides. *Molecular Pharmacology* 68, 942-951.

Butterworth, M.B. (2010). Regulation of the epithelial sodium channel (ENaC) by membrane trafficking. *BBA - Molecular Basis of Disease* 1802, 1166-1177.

- Cameron, P., Hiroi, M., Ngai, J., and Scott, K. (2010). The molecular basis for water taste in *Drosophila*. *Nature* 465, 91-95.
- Canessa, C.M., Schild, L., Buell, G., Thorens, B., Gautschi, I., Horisberger, J.D., and Rossier, B.C. (1994). Amiloride-sensitive epithelial Na<sup>+</sup> channel is made of three homologous subunits. *Nature* 367, 463-467.
- Chalfie, M. (2009). Neurosensory mechanotransduction. *Nature Reviews Molecular Cell Biology* 10, 44-52.
- Chandrashekar, J., Hoon, M.A., Ryba, N.J.P., and Zuker, C.S. (2006). The receptors and cells for mammalian taste. *Nature* 444, 288-294.
- Chandrashekar, J., Kuhn, C., Oka, Y., Yarmolinsky, D.A., Hummler, E., Ryba, N.J.P., and Zuker, C.S. (2010). The cells and peripheral representation of sodium taste in mice. *Nature* 464, 297-301.
- Chen, Z., Wang, Q., and Wang, Z. (2010). The Amiloride-Sensitive Epithelial Na<sup>+</sup> Channel PPK28 Is Essential for *Drosophila* Gustatory Water Reception. *The Journal of neuroscience : the official journal of the Society for Neuroscience* 30, 6247-6252.
- Christie, J.M., Chiu, D.N., and Jahr, C.E. (2010). Ca<sup>2+</sup>-dependent enhancement of release by subthreshold somatic depolarization. *Nature Neuroscience* 14, 62-68.
- Chu, Y., Fioravante, D., Thanawala, M., Leitges, M., and Regehr, W.G. (2012). Calcium-dependent isoforms of protein kinase C mediate glycine-induced synaptic enhancement at the calyx of Held. *The Journal of neuroscience* 32, 13796-13804.
- Cull-Candy, S.G., Miledi, R., Trautmann, A., and Uchitel, O.D. (1980). On the release of transmitter at normal, myasthenia gravis and myasthenic syndrome affected human end-plates. *The Journal of Physiology* 299, 621-638.
- Cuthbert, A.W., and Fanelli, G.M. (1978). Effects of some pyrazinecarboxamides on sodium transport in frog skin. *British Journal of Pharmacology* 63, 139-149.
- Cuttle, M.F., Tsujimoto, T., Forsythe, I.D., and Takahashi, T. (1998). Facilitation of the presynaptic calcium current at an auditory synapse in rat brainstem. *The Journal of Physiology* 512 ( Pt 3), 723-729.
- Daniels, R.W., Collins, C.A., Gelfand, M.D., Dant, J., Brooks, E., Krantz, D.E., and DiAntonio, A. (2004). Increased Expression of the *Drosophila* Vesicular Glutamate Transporter Leads to Excess Glutamate Release and a Compensatory Decrease in Quantal Content. *The Journal of neuroscience* 24, 10466-10474.

Davis, G.W. (2006). Homeostatic control of neural activity: from phenomenology to molecular design. *Annu Rev Neurosci*.

Davis, G.W. (2013). Homeostatic Signaling and the Stabilization of Neural Function. *Neuron* 80, 718-728.

Davis, G.W., and Bezprozvanny, I. (2001). Maintaining the stability of neural function: a homeostatic hypothesis. *Annual review of physiology* 63, 847-869.

Davis, G.W., and Goodman, C.S. (1998). Synapse-specific control of synaptic efficacy at the terminals of a single neuron. *Nature* 392, 82-86.

Davis, G.W., Schuster, C.M., and Goodman, C.S. (1997). Genetic analysis of the mechanisms controlling target selection: target-derived Fasciclin II regulates the pattern of synapse formation. *Neuron* 19, 561-573.

Deeg, K.E., and Aizenman, C.D. (2011). Sensory modality-specific homeostatic plasticity in the developing optic tectum. *Nature Neuroscience* 14, 548-550.

DiAntonio, A., Petersen, S.A., Heckmann, M., and Goodman, C.S. (1999). Glutamate receptor expression regulates quantal size and quantal content at the *Drosophila* neuromuscular junction. *The Journal of neuroscience* 19, 3023-3032.

Dickman, D.K., and Davis, G.W. (2009). The schizophrenia susceptibility gene dysbindin controls synaptic homeostasis. *Science* 326, 1127-1130.

Dickman, D.K., Tong, A., and Davis, G.W. (2012). Snapin is critical for presynaptic homeostatic plasticity. *The Journal of neuroscience* 32, 8716-8724.

Drummond, H.A., Price, M.P., Welsh, M.J., and Abboud, F.M. (1998). *ScienceDirect.com - Neuron - A Molecular Component of the Arterial Baroreceptor Mechanotransducer. Neuron*.

Eastwood, A.L., and Goodman, M.B. (2012). Insight into DEG/ENaC channel gating from genetics and structure. *Physiology* 27, 282-290.

Eaton, D.C., Helms, M.N., Koval, M., Bao, H.F., and Jain, L. (2009). The contribution of epithelial sodium channels to alveolar function in health and disease. *Annual review of physiology* 71, 403-423.

Egli, M., Duplain, H., Lepori, M., Cook, S., Nicod, P., Hummler, E., Sartori, C., and Scherrer, U. (2004). Defective respiratory amiloride-sensitive sodium transport predisposes to pulmonary oedema and delays its resolution in mice. *The Journal of Physiology* 560, 857-865.

Featherstone, D.E., Rushton, E., Rohrbough, J., Liebl, F., Karr, J., Sheng, Q., Rodesch, C.K., and Broadie, K. (2005). An essential *Drosophila* glutamate receptor subunit that functions in both central neuropil and neuromuscular junction. *The Journal of neuroscience* 25, 3199-3208.

Featherstone, D.E., Rushton, E.M., Hilderbrand-Chae, M., Phillips, A.M., Jackson, F.R., and Broadie, K. (2000). Presynaptic glutamic acid decarboxylase is required for induction of the postsynaptic receptor field at a glutamatergic synapse. *Neuron* 27, 71-84.

Frank, C.A., Kennedy, M.J., Goold, C.P., Marek, K.W., and Davis, G.W. (2006). Mechanisms Underlying the Rapid Induction and Sustained Expression of Synaptic Homeostasis. *Neuron* 52, 663-677.

Frank, C.A., Pielage, J., and Davis, G.W. (2009). A presynaptic homeostatic signaling system composed of the Eph receptor, ephexin, Cdc42, and CaV2.1 calcium channels. *Neuron* 61, 556-569.

Frazer, K.A., Pachter, L., Poliakov, A., Rubin, E.M., and Dubchak, I. (2004). VISTA: computational tools for comparative genomics. *Nucleic acids research* 32, W273-279.

Furukawa, Y., Miyawaki, Y., and Abe, G. (2006). Molecular cloning and functional characterization of the *Aplysia* FMRamide-gated Na<sup>+</sup> channel. *Eur J Physiol* 451, 646-656.

Gardiner, A., Barker, D., Butlin, R.K., Jordan, W.C., and Ritchie, M.G. (2008). *Drosophila* chemoreceptor gene evolution: selection, specialization and genome size. *Molecular ecology* 17, 1648-1657.

Garty, H., and Palmer, L.G. (1997). Epithelial sodium channels: function, structure, and regulation. *Physiological Reviews*.

Gisselmann, G., Plonka, J., Pusch, H., and Hatt, H. (2004). *Drosophila melanogaster* GRD and LCCH3 subunits form heteromultimeric GABA-gated cation channels. *British Journal of Pharmacology* 142, 409-413.

Golubovic, A., Kuhn, A., Williamson, M., Kalbacher, H., Holstein, T.W., Grimmlikhuijzen, C.J.P., and Gründer, S. (2007). A peptide-gated ion channel from the freshwater polyp *Hydra*. *Journal of Biological Chemistry* 282, 35098-35103.

Gonzalez-Islas, C., Chub, N., Garcia-Bereguian, M.A., and Wenner, P. (2010). GABAergic synaptic scaling in embryonic motoneurons is mediated by a shift in the chloride reversal potential. *The Journal of neuroscience* 30, 13016-13020.

Goold, C.P., and Davis, G.W. (2007). The BMP ligand Gbb gates the expression of synaptic homeostasis independent of synaptic growth control. *Neuron* 56, 109-123.

Halpern, B.P. (1998). Amiloride and vertebrate gustatory responses to NaCl. *Neuroscience and biobehavioral reviews* 23, 5-47.

Hamm, L.L., Feng, Z., and Hering-Smith, K.S. (2010). Regulation of sodium transport by ENaC in the kidney. *Current opinion in nephrology and hypertension* 19, 98-105.

Hawrylycz, M.J., Lein, E.S., Guillozet-Bongaarts, A.L., Shen, E.H., Ng, L., Miller, J.A., van de Lagemaat, L.N., Smith, K.A., Ebbert, A., Riley, Z.L., et al. (2012). An anatomically comprehensive atlas of the adult human brain transcriptome. *Nature* 489, 391-399.

Heckscher, E.S., Fetter, R.D., Marek, K.W., Albin, S.D., and Davis, G.W. (2007). NF- $\kappa$ B, I $\kappa$ B, and IRAK Control Glutamate Receptor Density at the *Drosophila* NMJ. *Neuron* 55, 859-873.

Herness, M.S. (1992). Aldosterone increases the amiloride-sensitivity of the rat gustatory neural response to NaCl. *Comparative biochemistry and physiology Comparative physiology* 103, 269-273.

Houweling, A.R., Bazhenov, M., Timofeev, I., Steriade, M., and Sejnowski, T.J. (2005). Homeostatic synaptic plasticity can explain post-traumatic epileptogenesis in chronically isolated neocortex. *Cerebral cortex* 15, 834-845.

Huang, T., and Stähler, F. (2009). Effects of dietary Na<sup>+</sup> deprivation on epithelial Na<sup>+</sup> channel (ENaC), BDNF, and TrkB mRNA expression in the rat tongue. *BMC neuroscience* 10, 19.

Hummler, E., Barker, P., Gatzky, J., Beermann, F., Verdumo, C., Schmidt, A., Boucher, R., and Rossier, B.C. (1996). Early death due to defective neonatal lung liquid clearance in  $\alpha$ ENaC-deficient mice. *Nature Genetics* 12, 325-328.

Hummler, E., and Planès, C. (2010). Importance of ENaC-mediated sodium transport in alveolar fluid clearance using genetically-engineered mice. *Cellular physiology and biochemistry : international journal of experimental cellular physiology, biochemistry, and pharmacology* 25, 63-70.

Jakubs, K., Nanobashvili, A., Bonde, S., Ekdahl, C.T., Kokaia, Z., Kokaia, M., and Lindvall, O. (2006). Environment matters: synaptic properties of neurons born in the epileptic adult brain develop to reduce excitability. *Neuron* 52, 1047-1059.

Jan, L.Y., and Jan, Y.N. (1976). Properties of the larval neuromuscular junction in *Drosophila melanogaster*. *The Journal of Physiology* 262, 189-214.

Jan, L.Y., and Jan, Y.N. (1976). L-glutamate as an excitatory transmitter at the *Drosophila* larval neuromuscular junction. *The Journal of Physiology* 262, 215-236.

Jasti, J., Furukawa, H., Gonzales, E.B., and Gouaux, E. (2007). Structure of acid-sensing ion channel 1 at 1.9 Å resolution and low pH. *Nature* 449, 316-323.

Kamenetz, F., Tomita, T., Hsieh, H., Seabrook, G., Borchelt, D., Iwatsubo, T., Sisodia, S., and Malinow, R. (2003). APP Processing and Synaptic Function. *Neuron* 37, 925-937.

Katz, B., and Miledi, R. (1970). Further study of the role of calcium in synaptic transmission. *The Journal of Physiology* 207, 789-801.

Kaupp, U.B. (2010). Olfactory signalling in vertebrates and insects: differences and commonalities. 1-13.

Keck, T., Keller, G.B., Jacobsen, R.I., Eysel, U.T., Bonhoeffer, T., and Hübener, M. (2013). Synaptic Scaling and Homeostatic Plasticity in the Mouse Visual Cortex In Vivo. *Neuron* 80, 327-334.

Keshishian, H., Broadie, K., Chiba, A., and Bate, M. (1996). The *drosophila* neuromuscular junction: a model system for studying synaptic development and function. *Annu Rev Neurosci* 19, 545-575.

Khorkova, O., and Golowasch, J. (2007). Neuromodulators, not activity, control coordinated expression of ionic currents. *The Journal of neuroscience* 27, 8709-8718.

Kim, S.E., Coste, B., Chadha, A., Cook, B., and Patapoutian, A. (2012). The role of *Drosophila* Piezo in mechanical nociception. *Nature* 483, 209-212.

Kim, S.H., and Ryan, T.A. (2010). CDK5 serves as a major control point in neurotransmitter release. *Neuron* 67, 797-809.

Kleyman, T.R., and Cragoe, E.J. (1988). Amiloride and its analogs as tools in the study of ion transport. *The Journal of membrane biology* 105, 1-21.

Lifton, R.P., Gharavi, A.G., and Geller, D.S. (2001). Molecular mechanisms of human hypertension. *Cell* 104, 545.

Lin, W., Finger, T.E., Rossier, B.C., and Kinnamon, S.C. (1999). Epithelial Na<sup>+</sup> channel subunits in rat taste cells: localization and regulation by aldosterone. *The Journal of comparative neurology* 405, 406-420.

Lingueglia, E., Deval, E., and Lazdunski, M. (2006). FMRamide-gated sodium channel and ASIC channels: A new class of ionotropic receptors for FMRamide and related peptides. *Peptides* 27, 1138-1152.

Liu, L., Johnson, W.A., and Welsh, M.J. (2003). *Drosophila* DEG/ENaC pickpocket genes are expressed in the tracheal system, where they may be involved in liquid clearance. *Proceedings of the National Academy* 100, 2128-2133.

Liu, L., Leonard, A.S., Motto, D.G., Feller, M.A., Price, M.P., Johnson, W.A., and Welsh, M.J. (2003). Contribution of *Drosophila* DEG/ENaC Genes to Salt Taste. *Neuron* 39, 133-146.

Liu, T., Starostina, E., Vijayan, V., and Pikielny, C.W. (2012). Two *Drosophila* DEG/ENaC Channel Subunits Have Distinct Functions in Gustatory Neurons That Activate Male Courtship. *The Journal of neuroscience* 32, 11879-11889.

Lu, B., LaMora, A., Sun, Y., Welsh, M.J., and Ben-Shahar, Y. (2012). ppk23-Dependent chemosensory functions contribute to courtship behavior in *Drosophila melanogaster*. *PLoS Genetics* 8, e1002587.

Mahr, A., and Aberle, H. (2006). The expression pattern of the *Drosophila* vesicular glutamate transporter: A marker protein for motoneurons and glutamatergic centers in the brain. *Gene Expression Patterns* 6, 299-309.

Marder, E. (2012). Neuromodulation of neuronal circuits: back to the future. *Neuron* 76, 1-11.

Marder, E., and Goaillard, J.-M. (2006). Variability, compensation and homeostasis in neuron and network function. *Nature Reviews Neuroscience* 7, 563-574.

Marie, B., Pym, E., Bergquist, S., and Davis, G.W. (2010). Synaptic Homeostasis Is Consolidated by the Cell Fate Gene *gooseberry*, a *Drosophila* pax3/7 Homolog. *The Journal of neuroscience : the official journal of the Society for Neuroscience* 30, 8071-8082.

Marrus, S.B., Portman, S.L., Allen, M.J., Moffat, K.G., and DiAntonio, A. (2004). Differential localization of glutamate receptor subunits at the *Drosophila* neuromuscular junction. *The Journal of neuroscience* 24, 1406-1415.

MARTIN, A.R. (1955). A further study of the statistical composition on the end-plate potential. *The Journal of Physiology* 130, 114-122.

Marygold, S.J., Leyland, P.C., Seal, R.L., Goodman, J.L., Thurmond, J., Strelets, V.B., Wilson, R.J., and consortium, F. (2013). FlyBase: improvements to the bibliography. *Nucleic acids research* 41, D751-757.

Matthay, M.A., Robriquet, L., and Fang, X. (2005). Alveolar Epithelium. *Proceedings of the American Thoracic Society* 2, 206-213.



- Menon, K.P., Carrillo, R.A., and Zinn, K. (2013). Development and plasticity of the *Drosophila* larval neuromuscular junction. *Wiley interdisciplinary reviews Developmental biology* 2, 647-670.
- Metaxakis, A., Oehler, S., Klinakis, A., and Savakis, C. (2005). Minos as a genetic and genomic tool in *Drosophila melanogaster*. *Genetics* 171, 571-581.
- Mochida, S., Few, A.P., Scheuer, T., and Catterall, W.A. (2008). Regulation of presynaptic Ca<sub>v</sub>2.1 channels by Ca<sup>2+</sup> sensor proteins mediates short-term synaptic plasticity. *Neuron* 57, 210-216.
- Müller, M., and Davis, G.W. (2012). Transsynaptic control of presynaptic Ca<sup>2+</sup> influx achieves homeostatic potentiation of neurotransmitter release. *Current biology : CB* 22, 1102-1108.
- Müller, M., Liu, K.S.Y., Sigrist, S.J., and Davis, G.W. (2012). RIM Controls Homeostatic Plasticity through Modulation of the Readily-Releasable Vesicle Pool. *The Journal of neuroscience* 32, 16574-16585.
- Müller, M., Pym, E.C.G., Tong, A., and Davis, G.W. (2011). Rab3-GAP Controls the Progression of Synaptic Homeostasis at a Late Stage of Vesicle Release. *Neuron* 69, 749-762.
- Myat, A., Henry, P., McCabe, V., Flintoft, L., Rotin, D., and Tear, G. (2002). *Drosophila* Nedd4, a ubiquitin ligase, is recruited by Commissureless to control cell surface levels of the roundabout receptor. *Neuron* 35, 447-459.
- Nelson, A.M., Marshall, K.L., and Lumpkin, E.A. (2011). DEG/ENaCs lead by a nose: mechanotransduction in a polymodal sensory neuron. *Neuron* 71, 763-765.
- Nerbonne, J.M., Gerber, B.R., Norris, A., and Burkhalter, A. (2008). Electrical remodelling maintains firing properties in cortical pyramidal neurons lacking KCND2-encoded A-type K<sup>+</sup> currents. *The Journal of Physiology* 586, 1565-1579.
- O'Brien, R.J., Kamboj, S., Ehlers, M.D., Rosen, K.R., Fischbach, G.D., and Huganir, R.L. (1998). Activity-Dependent Modulation of Synaptic AMPA Receptor Accumulation. *Neuron* 21, 1067-1078.
- Paradis, S., Sweeney, S.T., and Davis, G.W. (2001). Homeostatic control of presynaptic release is triggered by postsynaptic membrane depolarization. *Neuron* 30, 737-749.
- Penney, J., Tsurudome, K., Liao, E.H., Elazzouzi, F., Livingstone, M., Gonzalez, M., Sonenberg, N., and Haghghi, A.P. (2012). TOR Is Required for the Retrograde Regulation of Synaptic Homeostasis at the *Drosophila* Neuromuscular Junction. *Neuron* 74, 166-178.

Petersen, S.A., Fetter, R.D., Noordermeer, J.N., Goodman, C.S., and DiAntonio, A. (1997). Genetic Analysis of Glutamate Receptors in *Drosophila* Reveals a Retrograde Signal Regulating Presynaptic Transmitter Release. *Neuron* 19, 1237-1248.

Piedras-Rentería, E.S., Pyle, J.L., Diehn, M., Glickfeld, L.L., Harata, N.C., Cao, Y., Kavalali, E.T., Brown, P.O., and Tsien, R.W. (2004). Presynaptic homeostasis at CNS nerve terminals compensates for lack of a key Ca<sup>2+</sup> entry pathway. *Proceedings of the National Academy of Sciences* 101, 3609-3614.

Plomp, J.J., van Kempen, G.T., and Molenaar, P.C. (1992). Adaptation of quantal content to decreased postsynaptic sensitivity at single endplates in alpha-bungarotoxin-treated rats. *The Journal of Physiology* 458, 487-499.

Plomp, J.J., van Kempen, G.T., and Molenaar, P.C. (1994). The upregulation of acetylcholine release at endplates of alpha-bungarotoxin-treated rats: its dependency on calcium. *The Journal of Physiology* 478 ( Pt 1), 125-136.

Podos, S.D., Hanson, K.K., Wang, Y.C., and Ferguson, E.L. (2001). The DSmurf ubiquitin-protein ligase restricts BMP signaling spatially and temporally during *Drosophila* embryogenesis. *Developmental cell* 1, 567-578.

Qin, G., Schwarz, T., Kittel, R.J., Schmid, A., Rasse, T.M., Kappei, D., Ponimaskin, E., Heckmann, M., and Sigrist, S.J. (2005). Four different subunits are essential for expressing the synaptic glutamate receptor at neuromuscular junctions of *Drosophila*. *The Journal of neuroscience* 25, 3209-3218.

Ramocki, M.B., and Zoghbi, H.Y. (2008). Failure of neuronal homeostasis results in common neuropsychiatric phenotypes. *Nature* 455, 912-918.

Sakaba, T., and Neher, E. (2001). Quantitative relationship between transmitter release and calcium current at the calyx of held synapse. *The Journal of neuroscience* 21, 462-476.

Sakata, T., Sakaguchi, H., Tsuda, L., and Higashitani, A. (2004). *Drosophila* Nedd4 Regulates Endocytosis of Notch and Suppresses Its Ligand-Independent Activation. *Current Biology*.

Sandrock, A.W., Dryer, S.E., Rosen, K.M., Gozani, S.N., Kramer, R., Theill, L.E., and Fischbach, G.D. (1997). Maintenance of acetylcholine receptor number by neuregulins at the neuromuscular junction in vivo. *Science* 276, 599-603.

Sartori, C., Rimoldi, S.F., and Scherrer, U. (2010). Lung fluid movements in hypoxia. *Progress in cardiovascular diseases* 52, 493-499.

Schild, L. (2010). The epithelial sodium channel and the control of sodium balance. *Biochimica et Biophysica Acta (BBA) - Molecular Basis of Disease* 1802, 1159-1165.

Schneck, D.J. (1987). Feedback control and the concept of homeostasis. *Mathematical Modelling* 9, 889-900.

Schneggenburger, R., and Neher, E. (2000). Intracellular calcium dependence of transmitter release rates at a fast central synapse. *Nature* 406, 889-893.

Schuster, C.M., Davis, G.W., Fetter, R.D., and Goodman, C.S. (1996). Genetic dissection of structural and functional components of synaptic plasticity. II. Fasciclin II controls presynaptic structural plasticity. *Neuron* 17, 655-667.

Shigemura, N., Iwata, S., Yasumatsu, K., Ohkuri, T., Horio, N., Sanematsu, K., Yoshida, R., Margolskee, R.F., and Ninomiya, Y. (2013). Angiotensin II modulates salty and sweet taste sensitivities. *The Journal of neuroscience* 33, 6267-6277.

Shu, Y., Hasenstaub, A., Duque, A., Yu, Y., and McCormick, D.A. (2006). Modulation of intracortical synaptic potentials by presynaptic somatic membrane potential. *Nature* 441, 761-765.

Silbering, A.F., Rytz, R., Grosjean, Y., Abuin, L., Ramdya, P., Jefferis, G.S.X.E., and Benton, R. (2011). Complementary Function and Integrated Wiring of the Evolutionarily Distinct *Drosophila* Olfactory Subsystems. *The Journal of neuroscience : the official journal of the Society for Neuroscience* 31, 13357-13375.

St Johnston, D. (2002). The art and design of genetic screens: *Drosophila melanogaster*. *Nature Reviews Genetics* 3, 176-188.

Swensen, A.M., and Bean, B.P. (2003). Ionic mechanisms of burst firing in dissociated Purkinje neurons. *The Journal of neuroscience* 23, 9650-9663.

Thiagarajan, T.C., Lindskog, M., Malgaroli, A., and Tsien, R.W. (2007). LTP and adaptation to inactivity: overlapping mechanisms and implications for metaplasticity. *Neuropharmacology* 52, 156-175.

Thibault, S.T., Singer, M.A., Miyazaki, W.Y., Milash, B., Dompe, N.A., Singh, C.M., Buchholz, R., Demsky, M., Fawcett, R., Francis-Lang, H.L., et al. (2004). A complementary transposon tool kit for *Drosophila melanogaster* using P and piggyBac. *Nature Genetics* 36, 283-287.

Thistle, R., Cameron, P., Ghorayshi, A., Dennison, L., and Scott, K. (2012). Contact Chemoreceptors Mediate Male-Male Repulsion and Male-Female Attraction during *Drosophila* Courtship. *Cell* 149, 1140-1151.

- Toda, H., Zhao, X., and Dickson, B.J. (2012). The *Drosophila* Female Aphrodisiac Pheromone Activates ppk23+ Sensory Neurons to Elicit Male Courtship Behavior. *Cell Reports* 1, 599-607.
- Tsurudome, K., Tsang, K., Liao, E.H., Ball, R., Penney, J., Yang, J.-S., Elazzouzi, F., He, T., Chishti, A., Lnenicka, G., et al. (2010). The *Drosophila* miR-310 Cluster Negatively Regulates Synaptic Strength at the Neuromuscular Junction. *Neuron* 68, 879-893.
- Turrigiano, G. Homeostatic Synaptic Plasticity: Local and Global Mechanisms for Stabilizing Neuronal Function.
- Turrigiano, G. (2012). Homeostatic synaptic plasticity: local and global mechanisms for stabilizing neuronal function. *Cold Spring Harbor perspectives in biology* 4, a005736.
- Turrigiano, G., Abbott, L.F., and Marder, E. (1994). Activity-dependent changes in the intrinsic properties of cultured neurons. *Science* 264, 974-977.
- Turrigiano, G.G. (2008). The self-tuning neuron: synaptic scaling of excitatory synapses. *Cell* 135, 422-435.
- Turrigiano, G.G., Leslie, K.R., Desai, N.S., Rutherford, L.C., and Nelson, S.B. (1998). Activity-dependent scaling of quantal amplitude in neocortical neurons. *Nature* 391, 892-896.
- Venken, K.J.T., Simpson, J.H., and Bellen, H.J. (2011). Genetic manipulation of genes and cells in the nervous system of the fruit fly. *Neuron* 72, 202-230.
- Verrey, F., Fakitsas, P., Adam, G., and Staub, O. (2008). Early transcriptional control of ENaC (de)ubiquitylation by aldosterone. *Kidney international* 73, 691-696.
- Wagh, D.A., Rasse, T.M., Asan, E., Hofbauer, A., Schwenkert, I., Dürrbeck, H., Buchner, S., Dabauvalle, M.-C., Schmidt, M., Qin, G., et al. (2006). Bruchpilot, a protein with homology to ELKS/CAST, is required for structural integrity and function of synaptic active zones in *Drosophila*. *Neuron* 49, 833-844.
- Waldmann, R., Champigny, G., Bassilana, F., Heurteaux, C., and Lazdunski, M. (1997). A proton-gated cation channel involved in acid-sensing. *Nature* 386, 173-177.
- Wang, X., Li, W.G., Yu, Y., Xiao, X., Cheng, J., Zeng, W.Z., Peng, Z., Xi Zhu, M., and Xu, T.L. (2013). Serotonin Facilitates Peripheral Pain Sensitivity in a Manner That Depends on the Nonproton Ligand Sensing Domain of ASIC3 Channel. *The Journal of neuroscience* 33, 4265-4279.

Wemmie, J.A., Price, M.P., and Welsh, M.J. (2006). Acid-sensing ion channels: advances, questions and therapeutic opportunities. *Trends in Neurosciences* 29, 578-586.

Weyhersmüller, A., Hallermann, S., Wagner, N., and Eilers, J. (2011). Rapid active zone remodeling during synaptic plasticity. *The Journal of neuroscience* 31, 6041-6052.

Yarmolinsky, D.A., Zuker, C.S., and Ryba, N. (2009). Common Sense about Taste: From Mammals to Insects. *Cell* 139, 234-244.

Zelle, K.M., Lu, B., Pyfrom, S.C., and Ben-Shahar, Y. (2013). The Genetic Architecture of Degenerin/Epithelial Sodium Channels in *Drosophila*. *G3: Genes| Genomes| Genetics* 3, 441-450.

Zhao, C., Dreosti, E., and Lagnado, L. (2011). Homeostatic synaptic plasticity through changes in presynaptic calcium influx. *The Journal of neuroscience* 31, 7492-7496.

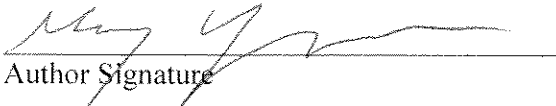
Ziemann, A.E., Schnizler, M.K., Albert, G.W., Severson, M.A., Howard III, M.A., Welsh, M.J., and Wemmie, J.A. (2008). Seizure termination by acidosis depends on ASIC1a. *Nature Neuroscience* 11, 816-822.

**Publishing Agreement**

*It is the policy of the University to encourage the distribution of all theses, dissertations, and manuscripts. Copies of all UCSF theses, dissertations, and manuscripts will be routed to the library via the Graduate Division. The library will make all theses, dissertations, and manuscripts accessible to the public and will preserve these to the best of their abilities, in perpetuity.*

***Please sign the following statement:***

*I hereby grant permission to the Graduate Division of the University of California, San Francisco to release copies of my thesis, dissertation, or manuscript to the Campus Library to provide access and preservation, in whole or in part, in perpetuity.*

  
\_\_\_\_\_  
Author Signature

12-13-13  
Date